HIGHLY EMISSIVE CdTe QUANTUM DOTS PASSIVATED WITH NOVEL BRANCHED LIGANDS AS FLUORESCENT SENSORS

A thesis submitted

in partial fulfilment for the Degree of

Doctor of Philosophy

By

Yogesh Sanjay Choudhary

SC15D008

Department of Chemistry

INDIAN INSTITUTE OF SPACE SCIENCE AND TECHNOLOGY

THIRUVANANTHAPURAM

DECEMBER 2021

CERTIFICATE

This is to certify that the thesis entitled **'HIGHLY EMISSIVE CdTe QUANTUM DOTS PASSIVATED WITH NOVEL BRANCHED LIGANDS AS FLUORESCENT SENSORS'** submitted by **Yogesh Sanjay Choudhary** (SC15D008) to the Indian Institute of Space Science and Technology Thiruvananthapuram, in partial fulfillment for the award of the degree of **Doctor of Philosophy** is a *bonafide* record of research work carried out by him under my supervision. The contents of this thesis, in full or in parts, have not been submitted to any other Institution or University for the award of any degree or diploma.

Dr. Gomathi. N.
Supervisor
Associate Professor
Department of Chemistry

Thiruvananthapuram
December 2021

Countersignature of the HOD with seal

DECLARATION

I declare that this thesis entitled '**Highly Emissive CdTe Quantum Dots Passivated with Novel Branched Ligands as Fluorescent Sensors'** submitted in partial fulfillment of the degree of **Doctor of Philosophy** is a record of original work carried out by me under the supervision of **Dr. Gomathi N.** and has not formed the basis for the award of any other degree or diploma, in this or any other Institution or University. In keeping with the ethical practice in reporting scientific information, due acknowledgments have been made wherever the finding of others have been cited.

Yogesh S. Choudhary
SC15D008

Thiruvananthapuram-695547

December 2021

ACKNOWLEDGEMENT

I am extremely grateful for reaching at this stage where I could formally thank each one of them who contributed significantly during my research endeavor. There are numerous people who worked and supported me directly or indirectly without whom this thesis would not have been possible. I am extremely thankful to all of them.

First, I would like to extend my deepest and sincere gratitude to my guide and mentor, Dr. Gomathi N, without whom the Ph.D. journey was impossible. During last six years, she was there with me from the time I joined PhD, with fruitful discussions, critical comments and immense support. I am extremely thankful for her patience and trust in me and the kind of freedom she offered me to carry out my research, which instill me a sense of deep satisfaction and independence. I had great time with her, discussing the various aspects of my work and the way it led the Ph.D. to move ahead.

Another major contribution in shaping this thesis goes to my doctoral committee members whose constructive and critical comments in all the doctoral committee meetings have proved adequately useful to configure the contents of the thesis. So, I am sincerely thankful to all my doctoral committee members; Prof. C. Vijayan from IIT Madras, Dr. Biswapriya Deb from NIIST Trivandrum, Dr. K. B. Jinesh and Dr. Jobin Cyriac from IIST for their valuable comments and support.

I am extremely thankful to the previous HODs of dept, of Chemistry, Prof. Kuruvilla Joseph, Prof. Nirmala Rachel James and current HOD Prof. K. Prabhakaran for their immense support in all aspects of my Ph.D. journey. My sincere thanks to all the other faculty members of Dept. of Chemistry, IIST, Dr. K G Sreejalekshmi, Dr. K Y Sandhya, Dr. Mary. J. Gladis, Dr. Mahesh S for their friendly and warm engagements during various academic and non-academic departmental activities.

I am thankful to all my lab mates who played a significant contribution in making this journey worth pursuing. Their presence in my life in this wonderful journey will always be remembered. I am grateful to my present and past colleagues Dr. Manjunath, Dr. Mukhtar Ali, Dr. Reneesh, Dr. Sarah, Dr. Narasimman, Dr. Jalaja, Dr.

Rakesh, Dr. Lavanya, Dr. Sujith, Dr. Reshma, Dr. Aswathi, Dr. Meegle, Dr. Devi Renuka, Dr. Haritha. I also cherish some wonderful memories with Dr. Linsha, Dr. Roymon and others. I cannot forget the valuable help provided to me during my early phase of PhD career by Dr. Manjunath and Dr. Kiran. I am pleased to spend some quality time with my current labmates, Varsha, Chitra, Deeraj, Sanu, Arya, Saisree, Ann, Bhasha, Govind, Sreekala. I am extremely contented to my colleague Dr. Neema for her immense help throughout my PhD journey. The acknowledgement of this work is incomplete without the staff members of the dept of chemistry. They all helped in all the possible ways at all the moments. I am extremely thankful to all of them. Mrs. Rehna, Mrs. Jayshree L, Mrs. Jayshree R, Mrs. Bindu, Mrs. Bindu PC, Mr. Loveson, Mr. Muraleedharan, Mr. Sreekumaran Nair.

I would also like to take this opportunity to thank the persons without whom many of the characterization works would not have been possible. Dr. K. Shibu and the staff at STIC, CUSAT, Cochin, Dr. Vijayaraghavan from PSGIAS, Coimbatore, Dr. Saju Pillai from NIIST Trivandrum.

I would like to thank the IIST administration, academic section, finance section, transport section and others invisible players in my PhD journey at IIST. I also would like to express my sincere gratitude to the canteen service of IIST. Also, I would like to take this opportunity to thanks all those persons staying in the IIST vicinity but contributed significantly by saving me in those hunger moments. I cherished my bond with them.

The journey of PhD was not possible without fun and excitement offered by my friends. I am very much thankful to all my friends Dr. Shashank, Dr. Preetam, Dr. Pramod, Dr. Darshika, Dr. Praveen, Dr. Surya. I will always cherish the memories I shared with all of them.

At last, I would like to thank almighty, my parents and my family members who were in my constant support throughout. Without their blessings, this would not have been a reality. Words fail me completely, in thanking my mother Ratna Choudhary, without whose constant prayer and ceaseless love, my ambition of pursuing PhD wouldn’t have been fulfilled; my father Sanjay Choudhary, the strong pillar of my

life and my sister Surabhi Choudhary for being with me in all the ups and downs of my life, and my late grandmother Shalini Choudhary, who would have been most proud about this success. My special thanks to all my close relatives too who were directly or indirectly connected to me, deeply across this journey.

There are many more names which become the pillars of my survival at IIST. Mentioning here everyone may not be possible, but I would like to thank all those unnamed people who were somehow connected with me. I am thankful to all those because of whom I could acquire the strength to carry out this work to reach this concluding point. Thank You all.

Yogesh

ABSTRACT

Nano scale materials are the most crucial in the present era of bio and nano technology. They stand as a basic building block for the medical electronic, and various other useful applications. The nano materials can be tuned to obtain various nano scale structures or shapes. The basic significance of nano sized organic or inorganic material is that its properties vary significantly compared to its bulk counterparts. These changes in the optical and the electronic properties of the nano materials compared to its bulk counterpart could be easily noticed. These nano materials can be of metals, non-metals, alloys, polymers or so. As the bulk semiconductor material is shrunken down to its nano scale, widening of its bandgap energy happens and the phenomenon can be termed as a quantum confinement phenomenon. The confinement of materials in all the three dimensions is termed as quantum dots (QDs). Recently, nanotechnology exclusively based on QDs has successfully entered numerous electronic and biomedical industries. QDs can also act as a fluorescent probe for variety of applications. In the present study, the optical properties of the quantum dots were utilized for the sensing applications. The quantum dots are synthesized with the help of different organic ligands. The ligands stabilize the quantum dots by encapsulating it, resulting in effectively exhibiting of the quantum phenomenon. Although there was a substantial number of applications, where these nanomaterials have employed, there is still room for exploration, in terms of understanding the fundamentals, their intriguing physical and chemical nature, and fabrication of these materials on accordance with the current needs. We have synthesized a range of nanoparticles based on CdTe QDs, performed a comprehensive morphological and photophysical characterizations and demonstrated their chemical sensor applications for the detection of biological, environmental and industrially significant molecules. The studies conducted using various CdTe QDs given in this thesis is briefed below.

In the present thesis, we tried to synthesize the quantum dots using various novel ligands. The purpose of the study was to understand the significance of the branched chain ligands, where one methyl group is present in one of the branches of the ligand. This makes the ligand bulkier than the conventional linear chain ligands. For the synthesis of the quantum dots, we preferred a colloidal synthetic route over the other available methods due to the ease of its synthesis. We have made use of the three novel ligands, using which we have synthesized the CdTe quantum dots and the same quantum dots has been studied for fluorescence sensing applications.

In the first work we synthesized CdTe quantum dots using 3MIBA ligand and studied the properties of the quantum dots using various characterization techniques like TEM, XRD, XPS, UV-VIS spectroscopy and Fluorescence spectroscopy. The lifetime studies and zeta potential studies were also conducted to get more insights into

our system. The as synthesized 3-MIBA capped CdTe quantum dot (CdTe@3-MIBA) was found out to be highly fluorescent and was successfully used to detect the mercury ions at the nano-molar concentration. The performance of the sensor was found out to be linear in the range of 1.5–100 nM with an excellent detection limit of 1.5 nM. The mechanism of sensing was decoded using various studies and it was concluded that the quenching behavior of the sensor was due to the electron transfer and aggregation.

We explored the possibility of using another novel branched chain ligand namely ethyl 2-mercaptopropionate for the synthesis of CdTe quantum dots. Extensive microscopic and photo physical characterizations revealed the behavior of the synthesized QD's. In the present case, the QDs, were found out to be highly sensitive for Cu^{2+} ions. A detailed studies were performed to unearth the mechanism of quenching of the QD's in the presence of Cu^{2+} ions. The sensor was linearly responding in the range of 0.5 nM to 129.5 nM with a detection limit (LOD) of 0.5 nM, providing a pathway for the QDs based Cu^{2+} probe.

The synthesis of highly fluorescent water soluble CdTe QDs using a novel branched ligand 3-Methoxybutyl 3-mercaptopropionate (3MB3MP), by facile colloidal synthesis method. The synthesized QD shows excitation independent high fluorescent emission at 590 nm upon exciting at 360 nm wavelength. The QDs shows excellent temporal stability and a typical phenomenon of photo-brightening/photo activation effect, up to 190 minutes of continuous irradiation of UV rays. The fluorescence is then found to quench suddenly, under further irradiation. We have proposed a model for this photoactivation effect, by conducting thorough investigation. We hypothesize that, the in-situ formed ROS species may be interacting with the surface of QDs and satisfying the dangling bonds present on the surface of QDs. This can ultimately reduce the sites for non-radiative decay, and thus enhancing the fluorescence emission. The results obtained from photoactivation studies motivated us to investigate the effects of ROS, in laboratory condition as well. For this purpose, we have chosen, one of the typical ROS, H_2O_2, which is the most stable among ROS. We have observed that, in the presence of H_2O_2, even in the absence of UV radiation, the fluorescence emission of CdTe@3MB3MP QDs are found to be enhanced. Therefore, a novel label free fluorescence-based detection of H_2O_2 has been demonstrated using CdTe@3MB3MP QDs. The fluorescent emission is found to be enhanced in linear fashion within a range of 10- 250 nM concentration of H_2O_2, which then found to collapse significantly upon concentrations higher than 300 nM. A thorough photophysical and microscopic characterizations has been carried out in order to unveil the mechanism of H_2O_2 detection, including UV-Vis absorption spectral studies, FTIR, XPS, time resolved fluorescence decay studies etc.

TABLE OF CONTENTS

LIST OF FIGURES

LIST OF TABLES

ABBREVIATIONS

CB	Conduction band
CdTe QDs	Cadmium Telluride Quantum Dots
CdTe@3-MIBA	Cadmium Telluride Quantum Dots capped with the ligand 3-MIBA
CdTe@E2MP	Cadmium Telluride Quantum Dots capped with the ligand E2MP
CdTe@3MB3MP	Cadmium Telluride Quantum Dots capped with the ligand 3MB3MP
EDS	Energy-dispersive X-ray spectroscopy
E2MP	Ethyl-2-mercaptopropionate
ET	Electron transfer
PET	Photoinduced electron transfer
FRET	Förster (fluorescence) resonance energy transfer
FTIR	Fourier transform infrared spectroscopy
FWHM	Full width at half maximum
H_2O_2	Hydrogen peroxide
HRXPS	High resolution X-ray photoelectron spectroscopy
IFE	Inner filter effect
LOD	Limit of detection
LUMO	Lowest unoccupied molecular orbital
3-MIBA	3-Mercaptoisobutyric acid
3MB3MP	3- Methoxy Butyl 3 Mercapto Propionate
MPA	Mercaptopropionic acid
NPs	Nanoparticles
PL	Photoluminescence

QDs	Quantum dots
QY	Quantum yield
SAED	Selected area electron diffraction
TCSPC	Time-correlated single-photon counting
TEM	Transmission electron microscopy
TMDs	Transition metal dichalcogenides
TGA	Thioglycolic acid
VB	Valence band
XPS	X-ray photoelectron spectroscopy
XRD	X-ray crystallography

NOTATIONS

Φ	Quantum yield
E	FRET efficiency
ε	Dielectric constant
η	Refractive index
A	Absorbance
I	Intensity
λ	Wavelength
τ	Lifetime
χ^2	Chi-square
T	Temperature
t	Time
s	Standard deviation of blank
k	Slope
F	Fluorescence intensity
C	Concentration

CHAPTER 1

INTRODUCTION

This chapter highlights the scope of this thesis and the introduction to the topic. It discusses the different synthetic strategies, significance of ligands, relaxation strategies followed by the fluorescence-based sensing and its aspects with a brief touch on the mechanisms involved. Finally, it concludes with the possible scope and the structure of the thesis.

1.1 Quantum Dots

Nano scale materials are the most crucial in the present era of bio and nano technology. They stand as a basic building block for the medical, electronic, and various other useful applications. The nano materials can be tuned to obtain various nano scale structures or shapes. The basic significance of nano sized organic or inorganic material is that its properties vary significantly compared to its bulk counterparts. These changes in the optical and the electronic properties of the nano materials compared to its bulk counterpart could be easily noticed. These nano materials can be of metals, nonmetals, alloys, polymers or so. Each have its own advantages, though we tried to focus our attention on the metallic nano materials.

The nano materials can be of various sizes and shapes. The change in the material properties with the size was spotted very early and various works were carried out to synthesize nano materials of different sizes and shapes. In case of nano particles, mostly spherical, the commonly reported range was 1 to 100 nm. These size dependent properties proved extremely crucial and opened the new dimension of the nano science and nano technology.

When the size of the material is constrained into these nano dimensions, several amazing properties of the material turn up. And so, the researchers across the world were behind exploring those. As the bulk semiconductor material is shrunken

down to its nano scale, widening of its bandgap energy happens and the phenomenon can be termed as a quantum confinement phenomenon. The confinement of materials in a single dimension is termed as quantum wells, while two-dimensional confinement is termed as quantum wires and the confinement in all the three dimensions is termed as quantum dots (QDs). The peculiar condition for the quantum confinement phenomenon to occur is that the size of the material should be less than its excitonic Bohr radii (Alivisatos, 1996). The exciton Bohr radius (rB) can be simply quoted as the distance between the electron and hole. If, we consider, m_e and m_h as the effective masses of electrons and holes, respectively, then, exciton Bohr radius can be expressed by

$$r_B = \frac{\hbar\hat{}2\varepsilon}{e^2}\left(\frac{1}{m_e} + \frac{1}{m_h}\right)$$

where, ħ, ε and e are reduced Planck constant, dielectric constant, and the charge of an electron respectively (Enright & Fitzmaurice, 1996).When the Bohr radius is comparable to the wavelength of an electron, quantum confinement phenomenon becomes dominant. This thus changes the optical and the electronic properties of the materials. The same phenomenon could not be observed in the bulk materials.

Of these nanomaterials, QDs are ultra-small, and the size range typically falling in between 1.5 and 10.0 nm. In the QDs, we can expect the presence of hundreds to tens of thousands of atoms per crystallite according to the size of QDs. Recently, nanotechnology exclusively based on QDs has successfully entered numerous electronic and biomedical industries. Therefore, we focus our studies pertaining to the synthesis, properties and applications of QDs, in this thesis. QDs are semiconductor nanocrystals often termed as ‘artificial atom’, owing to its discrete energy levels. QDs were first recognized by Ekimov and Onushenko (1981), and its quantum confinement effects, and subsequent optical and optoelectronic properties were postulated by Efros and Efros (1982). Subsequently, the first colloidal semiconductor nanocrystals were created by Louis Brus (1984).

Generally, QDs are synthesized from group II- VI (eg: CdSe, ZnS etc.), III-V (eg: GaP, InP etc.), and IV-VI (eg: PbSe, PbS etc.) in the periodic table, because of their semiconductor properties. QDs are having high surface to volume ratio. Therefore, large percentage of atoms can be found at the surface of QDs. This high surface to volume ratio, combined with extremely small size, renders their properties highly different from bulk materials. However, if the size of QDs exceeds exciton Bohr radius, it generates both the free and bound electron–hole pairs, and its optical properties are not much different from their bulk counterpart (Gaponenko & Demir, 2018). Hence, the excitonic Bohr radii condition is crucial in identifying the QDs.

1.2 General Properties of QDs

The research in the QDs across the decades points towards the size dependent material properties. The size of the materials also controls the electronic states. For the typical QDs, the electronic energy states are discrete, whereas the same is continuous for the bulk materials.

The three-dimensional confinement of QDs indicates the confinement of electron-hole pair in all the three dimensions. The quantum confinement results in the creation of discrete energy bands with an intrinsic bandgap. Therefore, by absorbing incident light, the electrons in the materials can be excited from low lying valence band (VB) to the higher energy conduction bands (CB), leaving a hole in VB. This electron and hole can bind to each other, which is widely known as excitons. When the excited electron returns to its ground state, the excitonic recombination happens, with the emission of a photon of longer wavelength, which is known as fluorescence. By changing the size of the QDs, the bandgap of the material can be tuned, which in turn can change the wavelength of emission. Thus, by manipulating the size of the QDs, we can achieve the desired emission wavelength across the visible spectrum. The existence of quantum confinement is responsible for blue shift in the emission spectrum of the QDs, as the excitonic transition energy and the bandgap energy increases.

The QDs are usually compared with the fluorescent dye molecules owing to its several advantages over the later one, such as wide excitation and narrow emission spectra. Generally, QDs in a colloidal solution shows polydispersity. Therefore, the emission spectra of the QD solution consists as a sum of the spectra of many individual QDs of varying sizes. Thus, the nature of the emission spectra is a direct indication of size distribution of the sample. Typically, an emission width of 20-35 nm is observed for a solution of homogeneous QDs, which is narrow compared to many of the fluorescent dyes. Another important aspect of QDs is its large Stokes shifts. Most of the QDs absorb light at wavelengths shorter than the emission. The optical property of the QDs is strongly welcomed by the researchers across the globe for exploring different applications. In a nutshell, QDs belongs to the category of materials which are highly resistant to photobleaching, exhibits better fluorescence compared to traditional organic dyes, covering a wide spectrum from UV to IR with extremely narrow and mostly symmetrical emission. This is accompanied by the wide absorption spectra.

Stabilization of QDs using proper ligands is significant, as it can tune the properties of QDs to large extent. Hence, in the present study, we focused on this parameter and tried to explore the different ways by which QDs can be effectively stabilized. We also noticed the change in the optical and the sensing properties of the QDs stabilized with different ligands.

The QDs are usually stabilized using the organic layer mostly made up of some mercapto salt. The passivation of the surface sites of QDs plays a critical role in increasing the fluorescence efficiency and the quantum yield of QDs. The loss of fluorescence efficiency and the quantum yield of QDs is mainly attributed to the inefficient surface passivation which results in several non-radiative decay pathways. This passivating layer stabilizes the QDs, while preserving its discrete electronic structures.

Hence, ligands play a crucial role in the synthesis of the QDs. We cannot expect the QDs synthesis without the appropriate ligand to wrap it up. The ligand protects the external surface of the QDs from any kind of erosion and also provides stability to it.

The quantity of the ligand reacted and used for the synthesis, matters the size of the QDs, as, lack of ligands in enough quantity may prove responsible for the increased size of the QDs and the wide size distribution. The length of the ligands, selected for stabilizing the QDs, also plays a notifying role. The longer ligand is supposed to have better stability over the shorter ligand (Weidman et al., 2018). The ligands which are mostly used for the synthesis of the QDs are the mercapto salts, usually having the linear mercapto chains. But in the present thesis, we tried to synthesize the QDs using various non-linear mercapto ligands, having a methyl group as a side chain. So, these side chains can improve the quantum yield and sensitivity of the QDs and make them highly photoactive. These advantages offer enhanced selectivity and sensitivity for the sensing of various heavy metal ions such as Hg^{2+} and Cu^{2+}. The position of these side chain is also crucial to further shape the optical as well as physicochemical properties of the QDs (K. Ma et al., 2013a). A representative schematic diagram of QDs is shown in Figure 1.1.

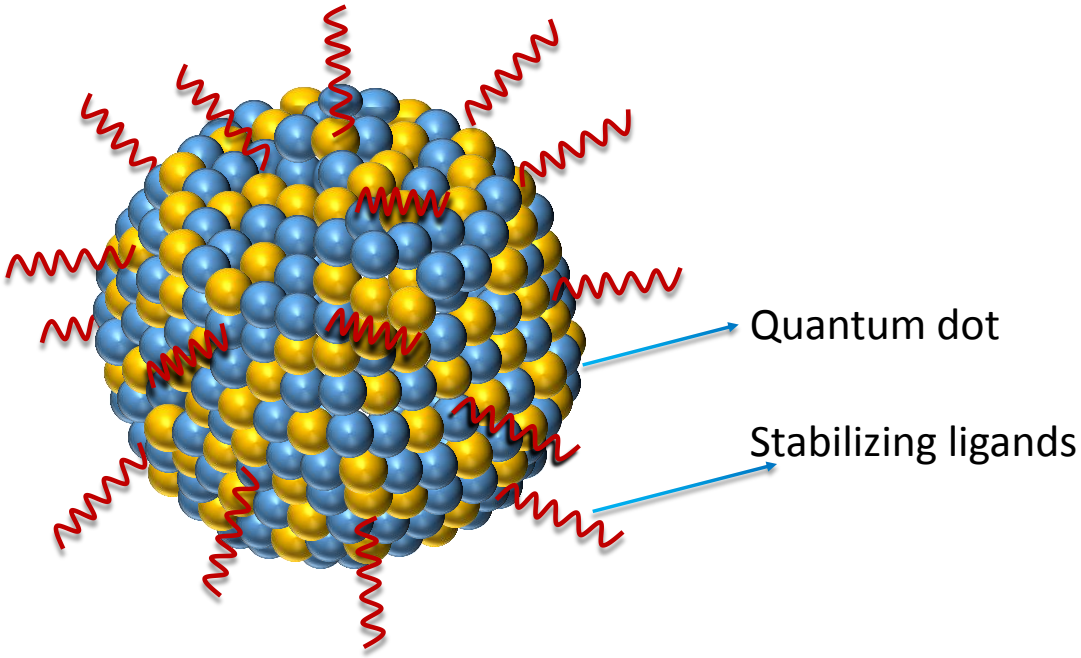

Figure 1.1. Schematic representation of a typical quantum dot

1.3 Various Methods of Synthesis of QDs

Quantum dots, thanks to their remarkable characteristics, such as being highly efficient multi-photon absorbers, possibility for surface modification to conjugate biomolecules in order to achieve selective targeting, excellent chemical sensing abilities and unique optical properties; brought them in the limelight of the scientific community, especially last decade or two. This significantly led to development of the plenty of methods for the synthesis of semiconductor based QDs with desired size and shape. Synthesis of QDs were first accomplished by precipitation method of metal ion (Ag, Hg, Pb, Zn, Cd, In) solution by a hydroxide of S, Se, or Te (Farkhani & Valizadeh, 2014). The two popular strategies reported to synthesize QDs are top-down and bottom-up approach. We will discuss about these two methods in general followed by a brief literature review of various methods employed by different research groups.

1.3.1 Top-down approaches

In the top-down approach, bulk semiconductor is crushed down to the nano dimension to form QDs. This can be achieved using several high end techniques such as electron beam lithography (Gourgon et al., 1994), reactive-ion etching (Lee & Ku, 2012), focused ion beams (FIB) (Bacher et al., 1999) and dip pen lithography (Biswas et al., 2015). For obtaining QDs of size around 30 nm, electron beam lithography, etching methods such as reactive ion or wet chemical methods are generally used. This is achieved by using desired packing geometries, which can provide controlled size and shapes. Many reports are available on these strategies for the fabrication of high precision nanostructures on suitable substrate for various applications such as photodetectors, photovoltaic cells, novel multiplexed biological sensors, etc. For example, Bacher et al. (1999) fabricated single CdTe/CdMnTe quantum dots by focused ion beam lithography. They made use of selective intermixing using focused ion beam lithography and subsequent rapid thermal annealing to realize single CdTe/CdMnTe quantum dots. They reported the usage of gallium ion as source ion beam system, with a diameter of about 30 nm, providing the high spatial resolution

required for the fabrication of lateral nanostructures. The samples were annealed at a temperature of 390 °C in N_2 atmosphere in order to facilitate the intermixing between Cd and Mn atoms at the heterointerface and the recurrence of quantum efficiency of the implanted areas. On the other side, Lin et al. (2006) demonstrated the application of photolithography patterning in conjunction with layer by-layer assembly technique to fabricate QD micro-structured patterns on indium tin oxide (ITO) glass. Five kinds of fluorescent thin films were fabricated using poly(diallyldimethylammonium chloride) (PDDA) such as (PDDA–CdSe@CdS)n, (PDDA–CdTe)n, (PDDA–CdSe@CdS–PDDA–CdTe)n, [(PDDA–CdSe@CdS)2–(PDDA–CdTe)]n, and [(PDDA–CdSe@CdS)–(PDDA–CdTe)2]n, where n represents the number of preparation cycles. The authors demonstrated that the colors and emissions of QD films can be tuned by controlling the order of deposition and number of bilayers in $(PDDA–CdSe@CdS)_n$ and $(PDDA–CdTe)_n$ films. These multiple-color microstructures can find an easy application in LEDs and biosensors.

A simple method for marking the position of individual self-assembled CdTe/ZnTe QDs were reported by Sawicki et al. (2015), employing photolithography, with a single Mn^{2+} ion. Samples containing self-assembled CdTe QDs embedded in a ZnTe barrier are grown on a GaAs substrate by molecular beam epitaxy. The QD layer with a planar QD density of $5x10^9/cm^2$ was doped with a very low density of Mn^{2+} ions, kept 100 nm below the sample surface. As synthesized QDs are used as solid state nano-emitters, like N-V centers in diamond or colloidal QDs, facilitating their advanced implementations as in quantum communication schemes involving networks of distant emitters coupled through an optical cavity mode. Despite high performance of the devices made by these methods, the scope for further exploration of precise control over the coverage of QDs and the film thickness can still be an active research area.

For applications like nanoscale sensors, molecular electronic and quantum optics applications, where accurate positioning of the quantum dots on the specific substrates or photonic structures are required, high precision techniques like dip pen nanolithography (DPN) is more suitable (Pankiewicz et al., 2015). Water soluble QDs

are more appropriate for this technique, as it involves deposition via water meniscus on an atomic force microscope tip. Roy et. al (2007), made use of CdSe/ZnS quantum dots dispersed in toluene and $CoFe_2O_4$ cobalt ferrite particles to write nanoscale structures. For this purpose, an autoprobe was used in ambient conditions with a humidity level around 30–35% and the temperature around 30 °C using Si_3N_4 cantilevers for writing these structures. Another example of utilization of DPN technique for the fabrication of protein microarrays and nanoarrays, tagged by using colloidal CdSe/ZnS QDs was demonstrated by Gokarna et al. (2008), as an optical readout of biochips. According to the literature, the real potential of DNP lies in writing with macromolecules and nanoparticles for applications such as nanoscale sensors, molecular electronic, photonic devices etc.

Even though, these top-down methods are highly popular, these methods create several hindrance to the synthesis of QDs such as incorporation of impurities into the QDs, structural imperfections by patterning etc., therefore not as effective as the other approaches.

1.3.2 Bottom-up approaches

In bottom-up synthesis of QDs, nano materials are synthesized using the chemical approaches and the QDs are grown atom by atom or molecules by molecules via nucleation. It can be broadly subdivided into wet chemical methods and vapor phase methods.

1.3.2.1 Vapor-phase Methods

In vapor phase methods, layers are grown atom-by-atom, leading to the self-assembly of QDs on a substrate without any patterning. Low temperature atomic layer epitaxy (LT-ALE), for example, has been proven to be a very reliable technique for the controlled formation of CdSe based, self-assembled quantum dot (SQD) type nanostructures embedded in ZnSe at a lower substrate temperature of 230 °C. (Kurtz et al., 2000). Small dots with a lateral diameter of 5±6 nm, corresponding to the bulk exciton Bohr radius, and a height of 5±6 monolayer (ML) can be obtained by this

method. Xin et al. (1996), alternatively reports the formation of CdSe dots on ZnSe and ZnSe-based alloy buffers using a Riber 32 R&D molecular beam epitaxy (MBE) machine equipped with elemental sources. In this procedure, a ZnSe buffer was first grown on (100) GaAs substrates at 300 °C to a thickness of approximately 2 μm. Then the substrate temperature was increased to 350 °C, for the growth of CdSe dots. The dots were typically grown at a growth rate of 0.4 ML/s. Whereas, transition from two- to three-dimensional growth during migration enhanced epitaxy (MEE) of CdSe on ZnSe by systematically varying the CdSe thickness were studied by Leonardi et al. (1998). Structures that contain islands within the quantum well (QW) region were obtained, when the CdSe exceeds a critical thickness. Photoluminescence (PL) shows emission energies up to 2.7 eV for flat QWs while samples with CdSe layers above the critical thickness show a broad emission around 2.3 eV.

1.3.2.2 Wet Chemical Methods

It follows conventional precipitation method, involving nucleation (homogeneous and heterogeneous) and limited growth of nanoparticles. Examples of wet chemical synthesis (Pottathara et al., 2019; Majid & Bibi, 2018) are micro emulsion (J. Liu et al., 2004), sol-gel (Arachchige & Brock, 2007), hot-solution decomposition (Murray et al., 1993), sonic wave (Junjie Zhu et al., 2000), etc. For example, highly luminescent CdTe QDs in sol-gel-derived composite silica spheres coated with 5,11,17,23-tetra-tert-butyl-25,27-diethoxy-26,28-dihydroxycalix[4]arene (C[4]/SiO2/CdTe) are prepared by Haibing Li and Qu (2007) via the sol-gel technique in aqueous media.

The initial efforts for the synthesis of the QDs was mainly focused on the organic phase synthesis. Hence, most of the reported works on the QDs synthesis was based on the organometallic synthetic routes. Synthesizing the QDs by this route comes with its own drawbacks. This synthesis route requires high temperature (approx. 250-300 °C) for the QDs to form. Further, the typical output of the reaction yields a hydrophobic QDs, as it gets coated with a hydrophobic surfactant. As the obtained QDs are hydrophobic in nature, it cannot be used for water-based applications. To use these

QDs for bio applications, the hydrophobic ligand must be first replaced with hydrophilic one. Though it can be performed using ligand exchange strategy, it decreases the fluorescence quantum yield of the QDs significantly. This largely generates a need for the synthesis of the QDs in the aqueous medium having a hydrophilic ligand attached to its surface in an in-situ manner. Further, the water phase synthesis of the QDs is quite favorable over the organic phase because of its several advantages especially for biological applications. The two most used methods for synthesizing the water soluble QDs are hydrothermal method and the colloidal synthetic route. Both the methods offer an advantage of simplicity, reproducibility and scaling. Though, the initial reports on the synthesis of water phase colloidal QDs were based on ligand exchange techniques, it was soon replaced by the aqueous phase synthesis of the colloidal QDs , to achieve an enhanced quantum yield (Yanjie Zhang & Clapp, 2011). For example, Q. Zhao et al. (2013) synthesized the core CdSe QDs of dithizone functionalized CdSe/CdS quantum dots in organic phase, and CdS shells were grown epitaxially using H_2S as S precursor. The lipophilic CdSe/CdS was modified by mercaptoacetic acid to enable water solubility and was precipitated from the organic phase. This QDs were then dissolved in p^H 7.17 PBS and stored at 4 °C and found to be stable for nearly 6 months, with the maximum emission wavelength at 545 nm. Another report focuses on the synthesis of highly luminescent CdTe QDs in a mixture of trioctylphosphine/dodecylamine (TOP/DDA) and transferred into water by using amino-ethanethiol.HCl (AET) or mercaptopropionic acid (MPA)(Sander F. Wuister et al., 2003).

Rogach et al. (2007), devised a pioneering work for the synthesis of CdTe QDs in aqueous phase using short chain thiols. In a typical procedure, mixing of tellurium and cadmium precursors in the presence of a thiolated capping agent resulted in the formation of highly luminescent CdTe QDs in an aqueous phase, upon heating at 100 °C. Upon keeping the reaction time longer, QDs with higher size can be obtained. The advantages of this method include safe, easy, and highly reproducible results. Ung et al., (2012), synthesized CdTe and CdSe QDs using 3-mercaptopropionic acid (MPA, 99%), and mercapto succinic acid (MSA) as stabilizers, with a luminescence quantum

yield of 30–85%. In another study, CdTe QDs were synthesized in aqueous phases by using the reaction between Cd^{2+} ions and NaHTe in solution in the presence of thiopropionic acid (TPA) as a stabilizer with a quantum yield of 40–50% (Qian et al., 2006; He et al., 2006). The major advantage of these QDs is their non-blinking nature, due to the coating of TPA. S. Y. Choi et al. (2012), otherwise, synthesized water soluble CdTe nanocrystals by using dithiol-functionalized ionic liquids (dTFILs) consisting of dithiol and vinylimidazolium coupled with chloride using a direct aqueous synthetic route. This approach utilizes the bidendate chelate interaction offered by the dithiol groups and the aqueous solubility as well as possible post-polymerization reactions by the hydrophilic vinylimidazolium groups. To exert the advantages of simplicity, high reproducibility of aqueous synthesis, and low cost, D. Zhou et al. (2011) demonstrated a one pot approach for synthesis of aqueous CdTe QDs through a room-temperature N_2H_4-promoted strategy. The advantage of this method is that, besides conventional thiol-ligands, such as thioglycolic acid, 3-mercaptopropionic acid, 1-thioglycerol, 2-mercaptoethylamine, glutathione, and L-cysteine, special ligands like 4-mercaptobenzoic acid, per-6-thio-α-cyclodextrin, and per-7-thio-β-cyclodextrin can also be used in this strategy.

1.4 Applications of QDs

1.4.1 Optoelectronic devices

1.4.1.1 Solar Cells

The demand for the optoelectronic devices is in rising trend as the devices hold strong potential in several fields. One of the significant devices constructed and operated efficiently using the fluorescent materials like QDs, is no doubt, a solar cell. Further, the solar cell holds an advantage of being a renewable and green energy source. Several cadmium based QDs are being used for the fabrication of solar cells to exploit their quantum phenomenon. For the fabrication of QD based solar cells, it is necessary to incorporate the QDs in polymeric matrix. One of the major hurdles in the field of solar energy conversion is to improve the power conversion efficiency (PCE). Various

ways and methods have been adopted to achieve the same and efforts could be visible by looking towards the papers reporting the increased PCE along the way (Kuddus et al., 2021). Type of polymers and QDs are two of the parameters to be considered for improving PCE. Since the NIR spectrum covers almost 50% of the solar spectrum, NIR wavelength have a significant contribution to the solar cells, altogether. Hence it becomes a smart choice to consider the QDs having a wide absorption spectrum all the way from UV to NIR. This can be well achieved by selecting a CdHgTe QDs as reported (Haotong Wei et al., 2012). The overall point of continuing this rush towards the better and effective solar cell, all consolidate to a point where highly effective transport of free carriers takes place provided by an extremely high charge carrier mobility. One of the significant advantages of using the QDs for fabricating the solar cells, is the provision of a wide absorption band for the absorption of major portion of solar spectrum leading to high absorption coefficient along with an excellent electron mobility.

1.4.1.2 Light Emitting Devices

The next most important application of the QDs was found to be in the fabrication of luminescence emitting devices like LEDs (Coe et al., 2002), fluorescent wearables (M. K. Choi et al., 2015), etc. An efficient technique to deposit the QDs film was researched and explored using several techniques like spin coating (Jialong Zhao et al., 2006), dip coating (Luther et al., 2008), spray coating (Kramer et al., 2015), drop casting (Pourret et al., 2009), electrophoretic deposition (Song et al., 2013). There has been a significant improvement in the flexible electronics while QD based devices serving as a platform for the same due to its unique optoelectronic properties. Further, the QDs can be printed on various substrates (Koh et al., 2011) using dry transfer printing (T. H. Kim et al., 2013), intaglio transfer printing (M. K. Choi et al., 2015), inkjet printing (Wood et al., 2009). The old printing techniques like contact printing (L. A. Kim et al., 2008), transfer printing (T. H. Kim et al., 2011), micro contact printing (Rizzo et al., 2008) suffered from inconsistencies in high- definition designs. Hence there was a need for the development of efficient routes for fabricating the QDs across

large areas. Dry transfer printing was one positive step towards that direction (M. K. Choi et al., 2015).

These solution-processed semiconductors (eg. QDs) offer an advantage of fabricating a low-cost optoelectronic device such as solar cells, LED's, etc., at a larger scales. And all the above-mentioned techniques provide an effective solution for the same.

1.4.2 Bioimaging/Cell imaging

The QDs have vast applications in nanobiotechnology, especially in the bio sensing and bio detection which resulted as a consequence of continuous research across the last couple of decades. Though the initial works were not quite directional towards the biological applications as considering the toxicity issues of the QDs and its inability to dissolve in the aqueous solutions. But time has yet proved that it can be well used in the bio applications by overcoming the above mentioned drawbacks which were holding it back for its potential biological usage. Later the QDs used were characterized in various bio applications like tumor labelling (X. Liu et al., 2017), cancer cells imaging (Suriamoorthy et al., 2010; Green et al., 2009) and drug delivery (Elizabeth et al., 2010), etc.

1.4.3 Chemical Sensors

Intensive research in the field of chemical sensors based on semiconductor QDs indicate their potential and breakthrough in performance in this field. The sensing using QDs can be carried out by different approaches, such as electrochemical, electrochemiluminescence, field-effect transistor (FET) based sensors, biosensors etc. Noticeable reports showing the detection of pesticides (J. Zhou et al., 2018); in fruits and vegetables (Nsibande & Forbes, 2016), detection of respiratory syncytial virus (Bentzen et al., 2005), fixing CO_2 (L. G. Wang et al., 2002), biosensors (Saran et al., 2011), determining and monitoring enzyme activity (S. Liu et al., 2014; Priyam et al., 2009), precise DNA quantification (Yi Zhang et al., 2012), detection of heavy metals (Zou et al., 2015), etc. demonstrate the versatility of QDs. For the target-based sensing,

a technique of bioconjugation can really be effective and brings much more hope, especially in the field of biosensing. The attachment of biospecific ligands to the QDs (bioconjugation), proves fruitful for the selective binding of proteins over it. This opens a range of application pathways of the biosensing and biodiagnosis. Reports are available for such bioconjugation based sensing (Chan & Nie, 1998; S. Wang et al., 2002).

The probes used for sensing the analytes can either be reversible or irreversible. The photophysical probes designed using the QDs are used over a wide spectrum from UV to IR. Hence, sensing of the analytes can take place in this complete range. Detection of crucial bio analytes like dopamine (S. Liu et al., 2013), glucose (X. Li et al., 2009), amantadine (Ai et al., 2012), microorganisms like *Helicobacter pylori* (Shanehsaz et al., 2013) etc. were also reported. Sensing of heavy metal ion or gas sensing is significant, in the perspective of security, thereby pledging acceptance in the sensing scenario. The utility of QDs, in the field of heavy metal ion or gas sensing is briefed in the coming section.

1.4.3.1 Heavy Metal Ions Sensing

The wonderful concept of sensing heavy metal ions using QDs was originated long back. Thereafter, the decades of research in the area paved the way for the preparation of numerous sensors using QDs, for the detection of several heavy metal analytes like mercury, arsenic, silver, copper and zinc (Yongfen Chen & Rosenzweig, 2002). Though the idea and the methodology used changed significantly over the years, the core concept remains the same to sense heavy metal ions in an efficient manner. Though, scientists across the globe found out sensors for majority of the heavy metal ions available, the race for the best is still on. The detection of these heavy metals is of crucial importance considering the dangers it posed to the environment. Over the decades, considerable number of QD based sensors were designed and developed and their potential is also explored to a noticeable extent. For example, Cheng et al. (2010) demonstrated Cu^{2+} ion detection based on the quenching of electrochemiluminescence of CdTe QDs. Recently, detection of lead ion (Pb^{2+}) was realized through ultrasensitive

photoelectrochemical (PEC) aptasensor based on MoS_2-CdS:Mn nanocomposites and CdTe quantum dots (QDs) (J. Shi et al., 2018). A linear range of 50 fM to 100 nM was reported with a detection limit of 16.7 fM, exhibiting its improved sensitivity.

1.4.3.2. Gas sensing

Gas sensing is again one of the critical applications of the quantum dots. The gas sensors designed using the QDs are reported for NO_2 (Forleo et al., 2010; Chizhov et al., 2014), acetone vapor (Nath et al., 2010). As the gas sensing is purely a surface phenomenon (Nath et al., 2010; L. Peng et al., 2008; Chakraborty et al., 2007; Rezlescu et al., 2006), QDs become an ideal candidate for the gas sensing applications due to its high surface to volume ratio.

Various approaches for the gas sensing were tested. One being the sensing of gases using polymer embedded nanocrystals. Nazzal et al, (2003) reported an easy permeability of the gas molecules across monolayer of ligands while photoexciting the electronic energy states of QDs. The PL properties of the nanocrystals responded reversibly and rapidly to its environment, upon photoirradiation. These polymers embedded photoactivated nanocrystals were found to be extremely stable under vacuum or inert atmosphere. The ligands monolayer is crucial as the colloidal semiconductor nanocrystals are usually coated with a compact (dense) monolayer of organic ligands creating a barrier for the diffusion of gas molecules between the environment and surface of the nanocrystals. The response here was observed to be specific to certain species, adding an extra layer of selectivity to the gas molecules. The possible reason for the photostimulated response was quoted to be due to photon-phonon coupling of the optical absorption and emission processes occurring in the nanocrystals.

Fluorescence based sensors are another category for the sensitive detection of analytes of interest. This method is specially featured with short analytical time, high sensitivity, low power cost, fast and accurate measurements, easy adaptability for in-situ detection etc. The sensing approach followed in this thesis is fluorescence based

using semiconductor QDs. Therefore, a brief literature review of fluorescence-based approaches, various sensing mechanism involved for the detection of different analytes, are detailed in the following section.

1.5 Fluorescence based Sensors

Compared to electrochemical and other sensors, fluorescence-based sensors are more favored due to its superior qualities such as, non-invasive nature, easy-to-handle methodology along with high sensitivity and selectivity. This kind of sensing is easy to notice, monitor and measure. It can be achieved through tagging a fluorophore to the specific target molecules. Further, the changes in the physical and the chemical properties of fluorophore could be monitored. A general approach over fluorescent-based sensing, and the different mechanisms involved will be discussed briefly in the following sections.

1.5.1 General approaches to Fluorescence based Sensors

Fluorescent-based sensing can be achieved through two major approaches; Intensity based sensing and Lifetime based sensing. In the intensity-based sensors, regular monitoring of the position or variation of the intensity of the excitation/ emission spectra of the fluorophore is performed whereas, the excited state lifetime of the fluorophore is checked in the presence of analyte of interest, for lifetime based sensors. A scheme of spectral observables for fluorescence sensing is shown in (Figure 1.2). We will be discussing these approaches in the coming sections.

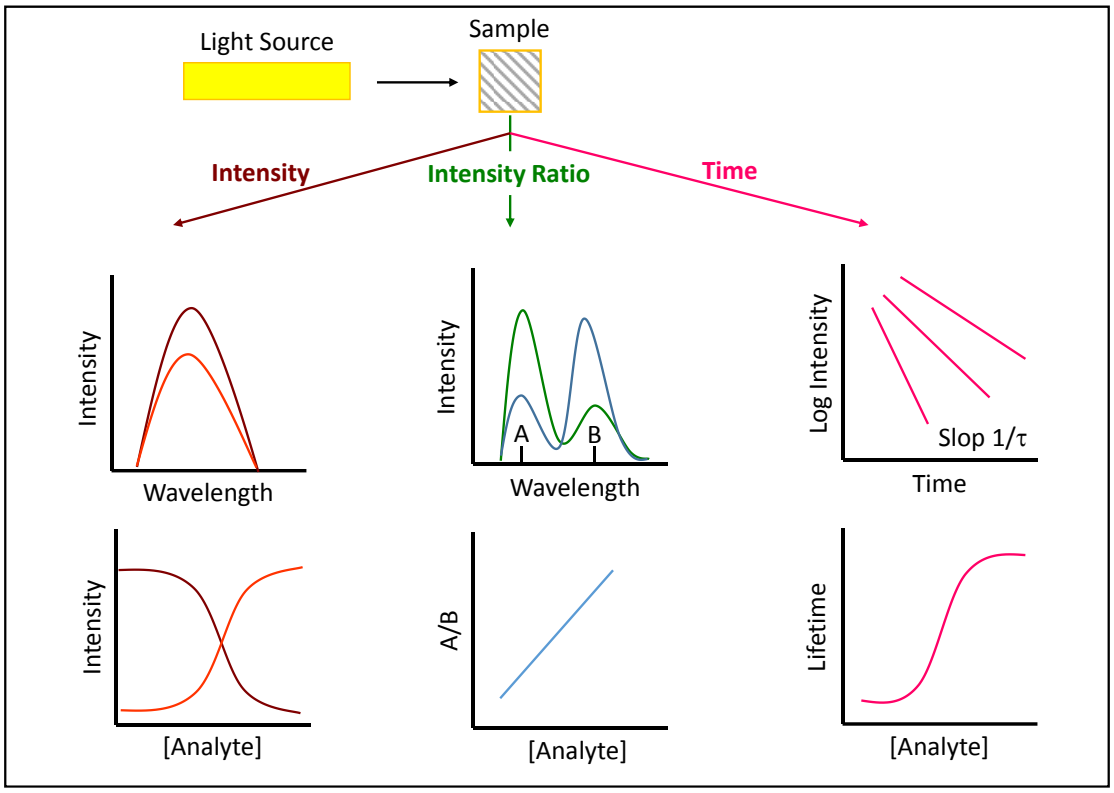

Figure 1.2. The sensing performed using intensities, intensity ratios (Intensity based sensors), and time-domain lifetimes (Lifetime based sensors)

1.5.1.1 Intensity Based Fluorescence Sensors

The change in intensity of the fluorophore such as quenching, enhancement or shifting of the position as a response to the presence of analytes, is continuously monitored and utilized for the selective detection of a specific analyte, in the intensity-based fluorescence sensors. A schematic of different types of intensity-based sensors are shown in Figure 1.3.

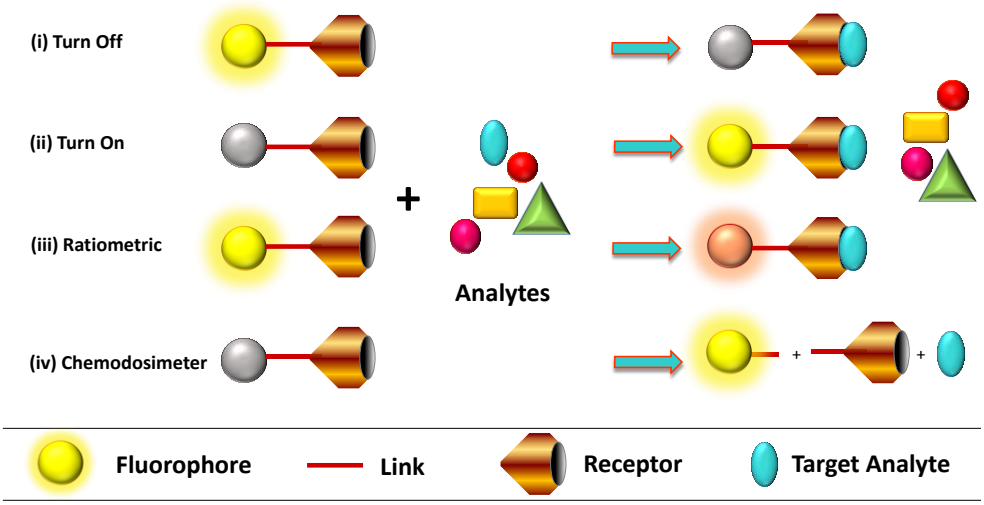

Figure 1.3. Scheme showing different types of intensity-based fluorescence sensors

1.5.1.1.1 Turn- off Fluorescence Sensors

Most of the reported works on the sensing is accompanied by the quenching process (Q. Ma & Su, 2011). What quenching necessarily means here is that, when the QDs are excited with an excitation wavelength, the QDs, which were initially giving a fluorescence, is now showing a reduced fluorescence or no fluorescence at all, if full quenching happened in the presence of analyte. In the normal scenario, when the QDs are excited, the electrons move from ground state to its excited state, which is a higher energy state. And, while coming back to its ground state, it releases the energy in the form of radiation which can be observed in the fluorescence spectrum. When quenching happens, the release of this emission energy is affected, and it releases a reduced amount of energy. This reduced amount of energy can be termed as quenching of energy or fluorescence quenching.

While designing the sensors, the important parameters to be considered include the brightness, photostability and wavelength range of the fluorescent probe. Myriad reports are available focusing on the turn-off detection of biologically relevant molecules, pesticides, or explosives using fluorescent based sensors by manipulating the ligand functionality of the fluorophore and binding motif platform of flourophores and the target molecule/ion. For example, fast and simple detection of vancomycin, a

glycopeptide antibiotic has been realized through turn off detection strategy using glutathione protected CdTe QDs (W. Liang et al., (2015). The mechanism of quenching is found to be dynamic with an electron transfer process with a detection limit of 0.4605 ng mL^{-1} within a dynamic range of 1.534 ng mL^{-1}–20 mg mL^{-1}. Super selective and ultrasensitive detection of picric acid was realized using nanocomposite devised from poly(vinyl alcohol) grafted polyaniline with MSA- Capped CdTe and CdTe/ZnS core/shell QDs (Dutta et al., 2015), with detection limit as low as 0.65 nM. The mechanism of quenching is proposed to be a combination of inner filter effect and ground state electrostatic interaction between the picric acid with the polymers present. Semiconductor based QDs have been continuously explored for heavy metal ion detection as well. A typical example of turn-off detection for the selective and sensitive detection of Cu^{2+} ions was proposed by Yongfen Chen & Rosenzweig (2002). Utility of Thioglycerol or L-cysteine capped CdS QDs were proved for the determination of $Cu^{2+}$and Zn^{2+}ions with detection limits of 0.1 µM and 0.8 µM respectively. CTAB-modified CdSe/ZnS QDs in the presence of thiosulfate was also found to be effective for the ultrahigh sensitive detection of Cu^{2+} ions, with a detection limit of 0.15 nM (Jin & Han, 2014). The mechanism of detection includes cation exchange, fluorescence resonance energy transfer etc.

1.5.1.1.2 Turn-on Fluorescence Sensors

The fluorescence enhancement (Turn-on) phenomenon is difficult to observe as compared to the fluorescence quenching (Turn-off) phenomenon because of the complexities in its development, and so reported less in the literature compared to the turn off sensors. This kind of effect in the QDs could be observed where the activation of the non-radiative electron/hole recombination pathway happens in the QD-analyte system. In most of the reported works on fluorescence enhancement principle, usually, the QDs are bonded with molecule, which quenches its fluorescence. To this, an analyte of interest is introduced which basically recovers the fluorescence of the QDs (Q. Zhao et al., 2013; Shang et al., 2009; Tan et al., 2015).

The turn-on sensors offer more improved selectivity over turn-off sensors. The turn-on sensors reported using fluorescent semiconductor quantum dots are enriched with good brightness and high quantum yield. For example, highly selective turn on sensing of trace amount of cadmium ions in water phase was proposed by S. N. Wang et al., (2018) using EDTA- etched CdTe@CdS QDs, with a detection limit of 0.032 µM, within a linear range of 0.05 to 9 µM. In this method, the surface of CdTe@CdS QDs are initially, etched by EDTA, which produces Cd^{2+}recognition sites, resulting in the quenching of fluorescent emission. Introduction of Cd^{2+}can restore the emission after identification of these sites. Another turn-on sensor was proposed for the determination of trace amount of cyanide, a lethal poison using glutathione capped CdTe QDs, with the aid of silver nanoparticles (Ensafi et al., 2015). The detection limit of the sensor is 0.004 µg/mL and dynamic range is 0.01-2.5 µg/mL. A novel turn on sensor for Cu^{2+} ions was developed by L. Ding et al. (2018) using graphene oxide (GO)-dsDNA-CdTe QDs. In the presence of GO complexed with DNA, the fluorescence emission of CdTe QDs were initially quenched due to energy transfer. In the presence of Cu^{2+}, irreversible breaking of DNAs at the cleavage sites can happen due to the catalytic reaction of the analyte, which ultimately lead to the formation of G-quadruplex formation. The removal of CdTe QDs from the surface of two-dimensional GO further results in the recovery of fluorescence emission, due to the shutting of energy transfer. Label-free detection of melamine employing CdTe/CdS QDs, and gold nanoparticles (AuNPs) is another example of turn-on detection using semiconductor QDs (Jingjin Zhao et al., 2014). In this method, the fluorescence intensity of CdTe/CdS is initially quenched in the presence of AuNP due to energy transfer from CdTe/CdS to AuNPs. In the presence of melamine, the multiple combination between melamine and AuNPs can result in the aggregation of AuNPs, which ultimately can restore the fluorescence intensity. The detection limit of the sensor is found to be $3x10^{-8}$ M, with a linear range of $5x10^{-8}$ to $1x10^{-6}$ M.

1.5.1.1.3 Ratiometric Fluorescence Sensors

Factors such as instrumental efficiency, environmental conditions, and the probe concentration can influence results obtained from single wavelength modulation type sensors. But the comparison of fluorescent intensity ratios at two different wavelengths before and after analyte recognition can minimize this measurement errors, the principle used in ratiometric detection of an analyte (Sahoo et al., 2012). In ratiometric fluorescent sensors, dual emission fluorescent materials are being used. In the presence of target molecules/ions these signals will respond differently. In this way, an internal self-calibration is possible for ratiometric sensors. For example, bi-functional ratiometric sensor for the detection of both L-Histidine and Cu (II) with high Stern Volmer constant (Ksv) values ($6.0507 * 10^8\ M^{-1}$ and $2.7417 * 10^7\ M^{-1}$respectively), which directly denotes the proportion of quenching and low detection limits of 0.56 µM for L-Histidine and 0.25 nM for Cu (II) were realized by dual emission hybrid material CdTe@ZIF-365 (X. Z. Wang et al., 2020). Upon addition of L-Histidine, the emission band of CdTe@ZIF-365 located at 304 nm found to be gradually increasing, whereas band at 641 nm found to be getting decreased and the ratio of fluorescent intensities after the addition of L-Histidine (I_{304}/I_{641}) is found to be 3.149, with a detection range of 0-9.5 µM. Whereas in the presence of Cu (II), fluorescent band at 304 nm remains constant, and 641 nm found to be decreased gradually, with intensity ratio of I_{304}/I_{641} 7.64 and detection range of 0-0.0075 µM. Another dual emissive ratiometric probe made of molecularly imprinted polymer-coated QDs modified with mesoporous structured epitope-imprinted silica materials ($QDs@SiO_2@EMSiO_2$) were fabricated for the sensitive detection of tyrosine phosphopeptide- pTyr (Saeedzadeh Amiri & Milani Hosseini, 2019). At an excitation of 400 nm, the probe shows two emissions at 520 nm and 625 nm, in which, pTyr can selectively quench emission at 625 nm. The detection limit of the probe is found to be a low value of 34 nM and a detection range of 0.07-230 µM.

1.5.1.2 Fluorescence Lifetime Based Sensors

Due to economic and time constraints, the fluorescence sensors working on the modulation of lifetime of the fluorophores are comparably less in number. However, the lifetime-based sensors are highly advantageous. Since the fluorescence lifetime is independent of the concentration of the fluorophore, any local changes in the concentration of the fluorophore due to photobleaching wouldn't influence the sensitivity of the sensor. This can be a highly useful strategy for sensing, especially for the cell imaging applications using fluorescence microscope, as the local concentration of the fluorescent probe in each part of the cell may be unknown. Further, compared to the intensity-based sensors, lifetime based sensors are well isolated from any kind of wiggle arising due to the instrumental disturbance (McCranor et al., 2014; Tantama et al., 2011).

1.5.2 Mechanism of Fluorescence Sensing

The sensing of the target analyte can be achieved using various sensing phenomena. The various detection signals obtained for sensing could be anything from the change in wavelength or fluorescence intensity or the lifetime of the fluorescing material, etc. These changes can be tuned, analyzed and could be used as a probe for the sensing of that specific analyte. These changes are mainly driven by electron transfer, energy transfer or the formation of non-fluorescent moieties. Various mechanisms involved are briefly discussed below.

1.5.2.1 Static Quenching Vs Dynamic Quenching

The fluorescence quenching can be governed by different mechanisms, the most common being, static and dynamic quenching. Both the static and dynamic quenching require molecular contact between the fluorophore and quencher (Lakowicz, 2006).

Static quenching comes into effect due to the binding of fluorophore with quencher resulting into a non-fluorescent complex. Hence, static quenching requires

the presence of strong molecular interactions like electrostatic or π-π interactions, resulting in the ground state molecular complex formation.

Dynamic quenching is a consequence of collisional encounters between the fluorophore and quencher; hence it's called collisional quenching too. Here, diffusion of quencher to the photo-excited fluorophore during its lifetime is a crucial condition. Upon this association, the fluorophore returns to the ground state, without any photonic emission. This kind of quenching does not result in any kind of photochemical reaction, which, portrays the interaction between the quencher and the fluorophore happened without causing any permanent change in the molecules. Therefore, dynamic quenching relies on the extent of diffusion of quencher, and the lifetime of the fluorophore. Dynamic quenching can be described by the well-known Stern-Volmer equation:

$$F_0/F = 1 + K_D[Q] \quad \textbf{\textit{or}} \quad 1 + k_q \tau_0[Q]$$

Where, F_0 and F are the fluorescence intensities in the absence and presence of quencher, respectively; K_D is the Stern-Volmer quenching constant, k_q is the bimolecular quenching constant; τ_0 is the lifetime of the fluorophore in the absence of quencher and Q is the quencher concentration.

To distinguish between the static and collisional quenching, certain pathways exist. One being the analysis of the absorption spectra of the fluorophore in the presence of the quencher while other being the analysis of temperature-dependent steady-state fluorescence spectra. In the case of static quenching, the ground-state complex formation can lead to drastic changes in the absorption spectral features of the fluorophore. Collisional quenching, on the other hand, being an excited state process, does not result in any changes in the absorption spectra of the fluorophore, in the presence of an analyte. As the collisional quenching is a diffusion-controlled process, upon increment in temperature, the quencher can diffuse quickly facilitating high extent of quenching. But, at elevated temperatures, the ground state complex between fluorophore and quencher, will be destroyed and there will be hike in emission,

consequently. Time-resolved fluorescence measurement proves to be an excellent method to distinguish between the two.

Static quenching is immune to carry out any changes in the lifetime as it forms non-fluorescent ground state complex. On the other hand, in the collisional quenching, the lifetime of the fluorophore is supposed to decrease. This is due to the evolution of a new non-radiative component which can be driven by the equation,

$$\tau = 1/(\Gamma + k_{nr} + k_q)$$

where τ is the lifetime, Γ is the emissive rate, k_{nr} is the rate constant for non-radiative process and k_q is the rate constant due to quenching.

1.5.2.2 Energy transfer and Electron Transfer

1.5.2.2.1 Förster resonance energy transfer (FRET)

There are two types of energy transfers which commonly exists, Förster resonance energy transfer (FRET) and electron transfer. During FRET, the transfer of energy happens from a donor particle to an acceptor particle under the condition that the donor and the acceptor should lie in close proximity to each other. Also, the emission spectrum of the donor particle should overlap with the absorption spectrum of the acceptor particle. If such conditions exist, it gives a clear cut indication for the existence of FRET. Schematically, FRET can be represented as shown in Figure 1.4

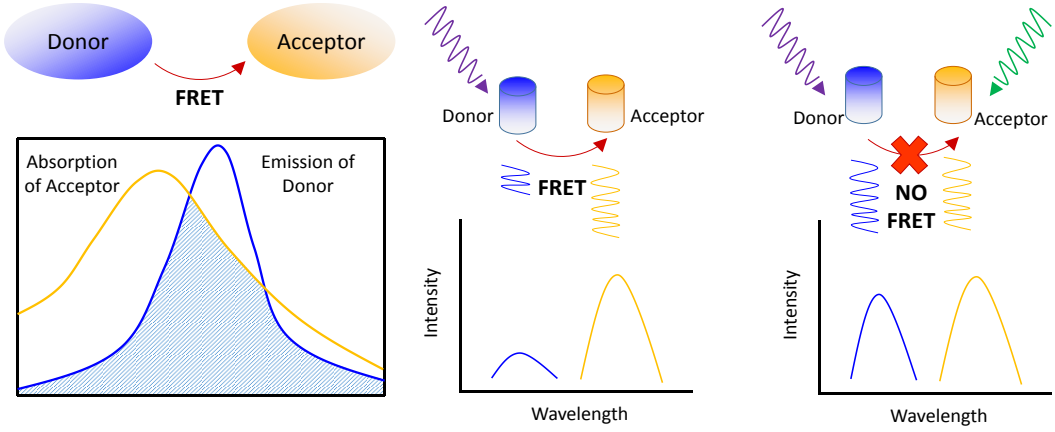

Figure 1.4. Schematic representation of FRET

The major trigger for the FRET-based sensing strategies is the modulation of FRET efficiency, either by adjusting the distance or by changing the spectral overlap between the donor and acceptor (Dennis et al., 2012; Moquin et al., 2013). Thorough research is happening in the field of semiconductor based QDs for the design and fabrication of FRET assays. For example, a novel assembled nanobiosensor QDs-concanavalin A (ConA)-conjugated CdTe QDs and β-Cyclodextrins (β-CDs) -modified AuNPs was designed for the direct determination of glucose in serum with high sensitivity and selectivity (Tang et al., 2008). This specific combination of ConA with β-CDs allows these two moieties to be in proximity for a hyper-efficient FRET. Upon addition of glucose into the sensing system, glucose will bind with ConA. This displaces the AuNPs-β-CDs segment resulting in the fluorescence recovery of the quenched emission of QDs. The detection limit of this sensor is found to be 50 nM, with a Stern–Volmer quenching constant K_{SV} =5.8 x10^{9} m^{-1}.

Y. Wang et al. (2017) has presented methodology for the detection of dopamine (DA) using CdTe QDs/NaYF4:Yb,Tm up-conversion nanoparticles (UCNPs) FRET systems. In this report, they have fabricated near-infrared (NIR) excitation of CdTe QDs (around 980 nm) with new broad emissions at 550, 590 and 630 nm, based on FRET from UCNP; NaYF4:Yb,Tm. Through in-situ growth of CdTe QDs (energy donors) on the surface of UCNPs (acceptors), FRET dyad was constructed. It has been observed that, the FRET-sensitized QD emission (630 nm) was sensitive to the presence of DA. The oxidized product of DA; dopamine quinone absorbed on the surface of QDs, which lead to the separation of QDs from UCNPs. As a result, the FRET process was stopped leading to the quenching of the FRET-sensitized QD emission (630 nm). The sensor is applicable for the detection of DA in the range from 10 to 300 nM, with a detection limit of 8 nM (S/N=3). Another FRET based sensing was proposed by Ramírez-Herrera et al. (2017), for the sensitive ratiometric detection of arginine, using CdTe quantum dots and Cresyl violet. The linear range of the sensor was from 1 to 30 μM arginine concentration, and the detection limit is found to be 0.51 μM.

The FRET-pair using aptamer-based sensing is also common. Aptamers are artificially synthesized single-stranded DNA or RNA sequences (Iliuk et al., 2011). The fluorescently labeled aptamers initially bind to a quenching material, where the emission from the fluorophore will be quenched by FRET. Upon interaction with a suitable target, these aptamers will be released, and the possibility of FRET is nullified, along with the recovery of the fluorescent emission. For example, Sabet et al. (2017), employed aptamer based FRET mechanism, using CdTe QDs and AuNPs as donor and acceptor respectively for the detection of a food pollutants Aflatoxin B1 (AFB1). Aptamer-conjugated CdTe QDs were absorbed on to the surface of AuNPs due to electrostatic interaction between exposed bases of aptamers and AuNPs. Due to the suitable overlap between fluorescence emission of CdTe QDs and the absorption spectrum of AuNPs, the fluorescence of QDs were quenched substantially. In the presence of the target aflatoxin B1, QD-aptamer- aflatoxin B1 complex will be formed, which lead to single stranded DNAs (ssDNAs) to get distance from AuNPs, resulting in the recovery of fluorescence emission from CdTe QDs. Under optimized conditions the limit of detection of this sensor was found to be a low value of 3.4 nM with linear range of 10 – 400 nM.

1.5.2.2.2 Electron transfer

Photoinduced electron transfer (PET) is another type of quenching mechanism, where a complex is formed between the electron donor (Donor) and the electron acceptor (Acceptor) $(Donor^{+}\bullet\ Acceptor^{-})^{*}$ upon excitation, as seen in Figure 1.5. This charge transfer complex can return to the ground state after excitation in non-radiative manner. The electron transfer can be termed as a phenomenon where the transfer of electrons happens from the QDs to the analytes in the excited state. The best possible way by which such transfers can be decoded is by measuring the lifetime of the QDs through the analysis of decay curves. For doing so, the nanosecond LED can be used to excite the sample. The nanosecond LED should have the wavelength comparable to the excitation wavelength of the QDs. The electron transfer can result in the possible increase or decrease of the decay time of the QDs.

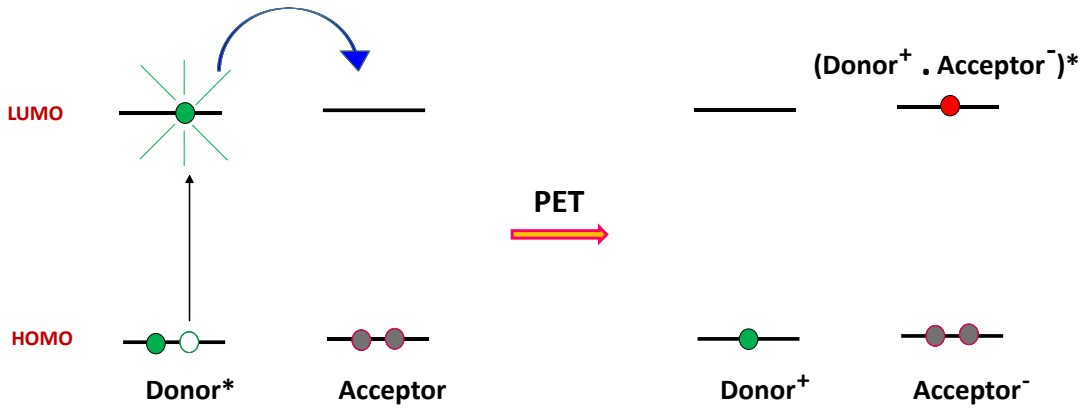

Figure 1.5. Molecular orbital schematic for photoinduced electron transfer

Considerable reports are available on the effective metal ion sensing utilizing the quenching of fluorescence properties of semiconductor based QDs, via electron transfer mechanisms. For example, a portable devise for the detection of Ag^+ was fabricated using CdTe QDs as fluorescence probe via an electron transfer process (Bin Chen et al., 2019). The fluorescence lifetime of QDs shows an increasing tendency with Ag^+ addition, which dictates dynamic nature of the quenching. The mechanism of quenching was also proposed with the help of rigorous experimental study. According to the study, traps on surface of QDs are effectively passivated by the initial absorbed Ag^+. After this saturation of initial traps, the excess Ag^+ facilitates electron transfer process, resulting in fluorescence quenching. The linear detection range using the device was from 5 nM to 200 nM, with a detection limit of 5 nM. Detection of copper ion is proposed by Tang et al., using highly luminescent water-soluble CdTe nanowires (Tang et al., 2005). According to the report, the luminescence intensity of CdTe NWs decreased by 50% along with a red shift of ~6 nm in solutions containing 2 µM of copper ion. Compared to the electrode potential of all the metal ions used in this study, the electrode potential of Cu^{2+}/Cu^+ is most appropriate for the effective transfer of electron from the NWs to the Cu^{2+}ions. The limit of detection of the sensor is 0.078 µM with a dynamic range of f 0 ~ 4 µM.

The applicability of semiconductor QDs for the detection of biologically relevant molecules are also reported. For example, a ratiometric turn on fluorescence

biosensor was developed by Liang et al. (2017), for detection of double strand DNA (dsDNA). Water-soluble fluorescent carbon dots (CDs) having an emission at 435 nm along with 3-mercapropionic acid-coated CdTe QDs with emission at 599 nm constitute the sensor. Emission of CdTe QDs was quenched by mitoxantrone via electron transfer and was restored in the presence of dsDNA. The fluorescence intensity of CDs was constant, which paves a way for the ratiometric means of dsDNA detection. The dynamic range of the sensor is 0 to 50 nM, and the detection limit is 1.0 nM. Another sensitive biosensor based on turn off–on strategy for the dual detection of spermine and heparin in human serum was also proposed using CdTe QDs coated with amphiphilic conjugated polythiophenes (Tawfik et al., 2018). Initially, the emission of QDs is found to be quenched by heparin due to electron transfer mechanism through electrostatic and hydrogen bonding interactions. By introducing spermine, heparin has been removed from the surface QDs due to the strong electrostatic interactions between spermine and heparin. This resulted in the significant fluorescence recovery of the sensors. Under optimum conditions, the sensors displayed excellent detection limits for heparin (1.59 nmol L^{-1}) and spermine (0.88 nmol L^{-1}) with linear ranges of 1–11 μmolL^{-1} and 1–10 μmolL^{-1}, respectively. Turn off detection of Cytochrome c (Cyt c) was also realized using TGA capped CdTe QDs within a range of 0.5−2.5 μM and a detection limit of 0.5 μM (Amin et al., 2017). Strong electrostatic interaction between the oxidized Cyt c and TGA-capped QDs favor photoinduced electron transfer from the excited QDs to the oxidized Cyt c which causes the quenching of TGA-capped QDs emission.

1.5.2.3 Inner Filter Effect

Inner filter effect (IFE) is another common quenching mechanism, which arises due to the overlap of absorption spectrum of quencher with the excitation or emission spectra of a fluorescing material (S. Lu et al., 2016). As the portion of the excitation or the emitted photons are being absorbed, a decrease in emission of fluorescing material could be easily noted. Therefore, quenching of fluorescence by IFE does not claim any molecular interactions between fluorescing material and quencher. A schematic of IFE can be represented as shown in Figure 1.6.

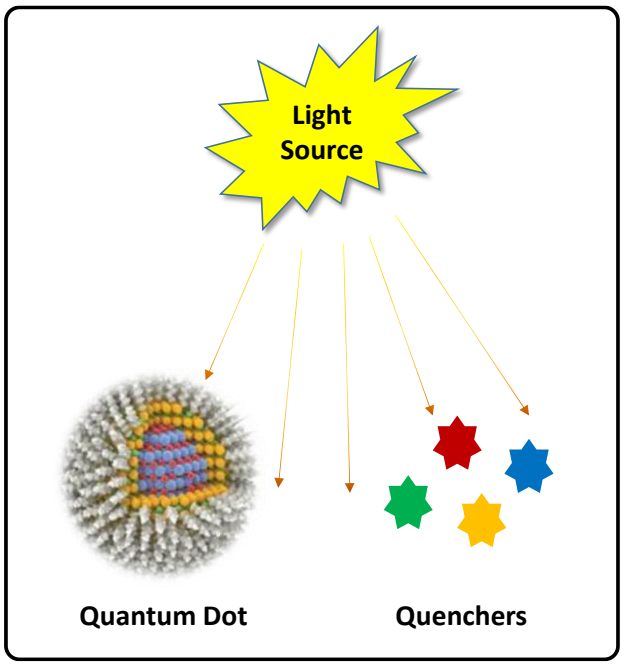

Figure 1.6. Scheme representing IFE.

As per reports, IFE can act as a primary sensing mechanism. It can even supplement other mechanisms. For example, alkaline phosphatase detection has been realized based on IFE of p-nitrophenol (pNP) on the fluorescence of CdTe/CdS QDs (Mao et al., 2019). pNP is a hydrolysate of p-nitrophenol phosphate disodium salt under the catalysis of ALP. Since the absorption spectra of pNP overlaps with the excitation spectra of the CdTe/CdS QDs the fluorescence of QDs got quenched effectively, due to IFE. The dynamic range of the sensor is 2.2 to 220 U/L with the limit of detection as low as 0.34 U/L. Another biosensor based on IFE was reported by H. Liu et al. (2017) for the sensitive detection of arginine using highly fluorescent thioglycolic acid-capped CdTe QDs with citrate-stabilized gold nanoparticles (AuNPs). The fluorescence of CdTe QDs was significantly quenched in the initial stage, by AuNPs via the IFE. Addition of arginine triggered the aggregation of AuNPs, which gradually recover fluorescence of CdTe QDS, achieving a "turn on" sensing strategy for arginine. A good linear relationship ranging from 16 to 121 μg L^{-1} with a limit of detection of 5.6 μg L^{-1}. Another turn-off- on sensor using AuNP and CdTe QDs following IFE strategy was proposed by Xia et al. (2016), for the selective detection of beta-amyloid oligomers

(AβOs). Here, PrP (95–110), an AβOs-specific binding peptide from cellular prion protein, induce the aggregation of AuNPs suspension; thus, the IFE of AuNPs on the fluorescence of CdTe QDs was weakened and the fluorescence intensity was recovered. The detection limit of the sensor is found to be 0.2 nM, with a dynamic range of 1–60 nM. Detection of Vitamin B12 using thioglycolic acid capped CdTe QDs as turn-off sensor was proposed by Shamsipur et al. (2019) based on the considerable spectral overlapping between absorption spectrum of B12 and emission spectrum of the QDs leading to IFE. Under the optimum conditions, the sensor showed a relative linear relationship against B12 concentration in the ranges of 0.02–0.4 and 1.5–70.0 μM with a detection limit of 2.0×10^{-8} M.

1.6 Objective and Scope of the Work

For fluorescent based sensors, the most crucial parameter is the choice of fluorophore to be used. Recent years have witnessed an upsurge of scientific interest towards the discoveries, synthesis and characterization of various fluorescence materials such as noble metal clusters, carbon-based nanoparticles, semiconductor quantum dots, etc. The advantage of these fluorophores over conventional fluorescent dyes includes low photo- bleaching, high resistance to photo or chemical degradation, large and tunable wavelength window etc.

Among the various semiconductor quantum dots available, we tried to study and focus our attention to the widely studied material CdTe. CdTe QDs are highly studied because of the primary advantage of large excitonic Bohr radius of 7.3 nm along with a narrow bulk band gap of 1.475 eV. The yield of CdTe QDs, being an attractive parameter, which can be extended even beyond 90%, proves as a highly promising candidate for the fluorescence-based sensing studies. In addition to it, CdTe QDs are blessed with typical characteristics such as size-dependent fluorescence emission peaks, narrow and symmetric emission spectra, broad and continuous absorption spectra etc. Considering these excellent properties, we attempted to address some of the challenges and to explore the utility of these wonder materials.

It is noteworthy that, CdTe QDs possess high toxicity due to the heavy metals. Though, considering the in-vitro applications of the same, the CdTe sensor opens new possibilities for its usage. Hence, toxicity is not a concern for using them as sensors, even for the detection of biologically relevant moieties. The importance of choice of ligands are of paramount importance in this scenario. We cannot expect the QDs synthesis without the appropriate ligand to wrap it up. The ligand basically protects the external surface of the QDs from any kind of erosion and provides stability to it, which can effectively prevent the leaching of these heavy metals. Moreover, the possibility of secondary tethering of suitable ligands or receptor units onto the surface of these QDs, which can govern different parameters such as selectivity, sensitivity, response time to the sensor without causing appreciable fluorescence loss, is an added advantage to make use of it as fluorescence sensor.

In the present thesis, we tried to synthesize CdTe QDs using various branched mercapto ligands, having a methyl group as a side chain. So, these side chains bring significant changes in the QDs, such as improvement in the sensitivity, high photoactivity and so on. These advantages help us to achieve decent selectivity and sensitivity when we used these QDs for the sensing various heavy metal ions such as Hg^{2+} and Cu^{2+}. The position of these side chain is also crucial to further narrow down the properties of the QDs.

In this regard, we identify the specific objectives of present research as follows

- To explore an easy, rapid and eco-friendly synthetic routes for CdTe QDs with variety of surface functional ligands
- Examine the utility of branched ligands for obtaining extra stability to the QDs
- Establish fluorescence based chemical sensors based on CdTe QDs to screen highly toxic metal ions, or biologically relevant molecules.
- Tuning of surface functionalities of the QDs to ensure different selectivity towards different metal ions keeping QDs core same.

The work presented in this report is useful in terms of synthesis of highly fluorescent CdTe QDs employing facile synthetic methods, understanding the role of branched ligands on the fundamental properties of CdTe QDs, unravelling the mechanism of interaction of various analytes with QDs, studies pertaining to the response of QDs towards light etc. We envisage that, the materials and their enhanced properties may open various technological possibilities in near future.

1.7 Organization of the Thesis

This thesis discusses the usage of some novel organic ligands which were used as a stabilizer during the synthesis of CdTe QDs. The synthesized QDs have shown the promising nature for sensing various metal ions with good sensitivity and selectivity.

Chapter 1 considers an elaborate literature review on general properties, synthesis and applications of semiconductor based QDs. General approaches to fluorescence sensing and various types of mechanisms involved are discussed in detail, with a few representative examples.

Chapter 2 addresses materials and methods used for the synthesis and characterization techniques used.

In chapter 3, we report the synthesis of CdTe QDs using a branched ligand, 3-mercaptoisobutyric Acid (3MIBA), consisting of a methyl group positioned at the 2^{nd} carbon atom from the thiol group side. Here, the CdTe QDs are used for the sensing of the mercury ions which is an essential metal ion to detect, considering the nature of its toxicity. The detailed sensing mechanism is also discussed in the chapter 3 of this thesis.

In chapter 4, the similar kind of work was carried out but with a totally novel ligand viz. Ethyl 2-Mercaptopropionate (E2MP). This ligand is also branched where a side methyl group is positioned at the 1^{st} carbon atom from the thiol group in the ligand structure. This system of CdTe QDs was observed to sense the copper ions which is again one of the significant metal ions to detect. The synthesis and the detailed sensing mechanism are discussed in the chapter 4 of this thesis.

While in chapter 5, we synthesized CdTe QDs using another novel ligand 3-methoxybutyl-3-mercaptopropionate (3MB3MP). Continuing the tradition of using the branched ligand, the ligand selected here, too, consists of a side methyl branch where the branched side methyl group is positioned at the 6^{th} carbon atom from the thiol group in the ligand structure. The ligand is larger in length compared to the previously used ligands viz. 3MIBA and E2MP. Here, the QDs are used for the sensing of hydrogen peroxide (H_2O_2) using photo enhancement strategy. The synthesis and the sensing mechanism for the same is discussed in the chapter 5 of this thesis.

The chapter 6 is mainly about the concluding remarks from the research work which is carried out in this thesis. There are several conclusions which are drawn from this thesis and are listed separately in this chapter.

CHAPTER 2

MATERIALS AND METHODS

This chapter gives a detailed description of the materials used, synthetic strategy followed for the synthesis of the CdTe QDs capped with different branched ligands and various characterization instruments used for studying the morphology, composition, and optical characterization of the materials.

2.1 Reagents and Materials

Cadmium chloride hydrate ($CdCl_2.H_2O$, 99.99%) and ethyl 2-mercaptopropionate (E2MP) (98%) were purchased from Alfa Aesar. Tellurium dioxide (TeO_2, 99.99%) powder was purchased from Sigma Aldrich. Sodium borohydride ($NaBH_4$, 97%) and 3- mercaptoisobutyric acid (3-MIBA) (97%) lead nitrate ($PbNO_3$) were purchased from Otto Chemicals pvt. Ltd. and TCI chemicals respectively. Cobalt sulphate ($CoSO_4$), tin chloride ($SnCl_2$), silver nitrate ($AgNO_3$), ferrous sulphate ($FeSO_4$), nickel sulphate (NiSO4), calcium carbonate ($CaCO_3$), aluminum nitrate $Al(NO_3)_3$, copper sulphate ($CuSO_4$), sodium carbonate (Na_2CO_3), potassium chloride (KCl), ferric chloride ($FeCl_3$), magnesium sulphate ($MgSO_4$), manganese nitrate $Mn(NO_3)_2$, barium chloride ($BaCl_2$), mercuric chloride ($HgCl_2$), hydrogen peroxide (H_2O_2), zinc Sulphate ($ZnSO_4$) sodium hydroxide (NaOH) were purchased from Merck, India.

Doubly distilled water was used throughout the experiments. All chemicals were used as received without any further purification.

2.2 Structures of the Ligands Used

The following branched ligands with side methyl group were used in the studies described in the thesis.

1. 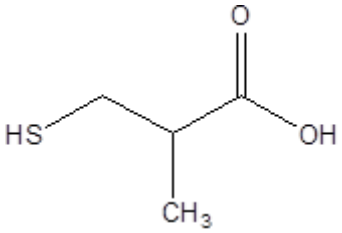

3-Mercaptoisobutyric acid (3-MIBA)

2. 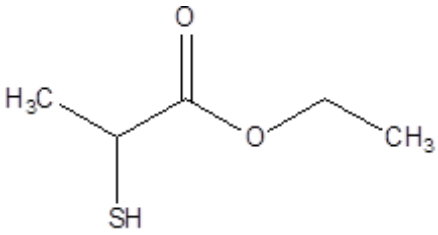

Ethyl- 2-mercaptopropionate (E2MP)

3. 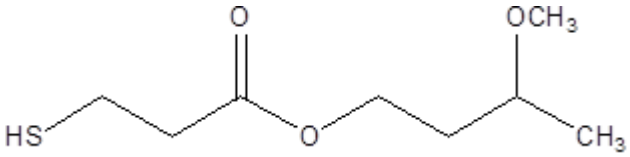

3-Methoxybutyl 3-Mercaptopropionate (3MB3MP)

Figure 2.1. Structures of different ligands used for the synthesis of CdTe QDs

2.3 Synthesis Methods

Various CdTe QDs used in this thesis has synthesized using colloidal method as shown in the scheme 2.1.

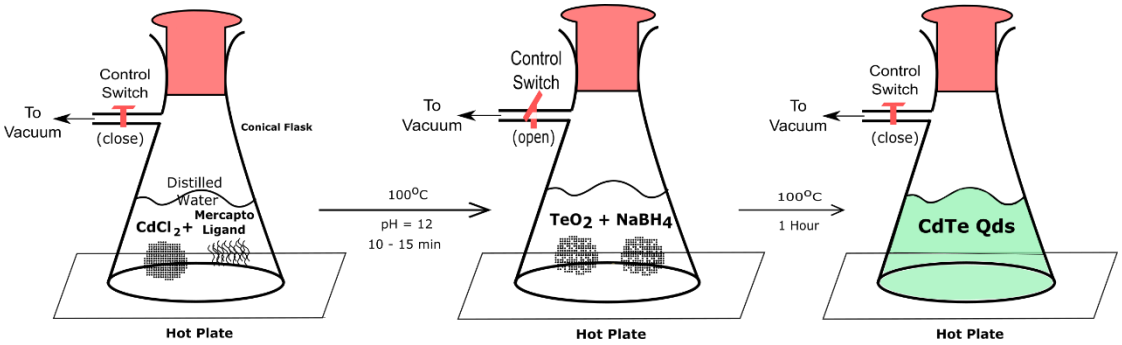

Figure 2.2. Scheme showing the colloidal synthesis of Cde QDs using various ligands

2.3.1 Synthesis of CdTe@3-MIBA

The quantum dots were prepared by the colloidal synthesis route. Briefly, 25 mM of 3-MIBA was added to 10 mM cadmium chloride monohydrate in 50 ml distilled water and was stirred on a hot plate. The pH of the solution was changed to 12 by adding 1 M NaOH solution. To this, 2 mM TeO_2 and 4 mM $NaBH_4$ were added sequentially followed by the vacuum. The reaction was carried out at 100 °C for one hour. The resultant solution was removed from the hot plate and cooled using an ice bath. The solution was centrifuged to remove the unreacted chemicals using ethanol followed by a dialysis for 12 h for the purification of the sample. The sample collected was then redispersed in distilled water and used for the analysis by using various characterization tools.

2.3.2 Synthesis of CdTe@E2MP

The QDs were prepared by colloidal synthesis route in a vacuum Erlenmeyer flask. Briefly, 10 mM cadmium chloride monohydrate was taken in a flask and mixed with 100 ml distilled water. To this, 25 mM of E2MP was added. The flask was kept on a hot plate at 100°C under constant stirring. The pH of the solution was adjusted to 12 with the addition of 1 M NaOH solution. To this, 2 mM TeO_2 and 4 mM $NaBH_4$ were added subsequently followed by vacuum. The reaction was carried out for about an hour following which the solution was removed from the hot plate and provided with sudden cooling using an ice bath to arrest further growth of QDs to maintain the homogeneity in the sample. The synthesized sample was washed using ethanol and centrifuged at 8000 rpm for the removal of unreacted chemicals. To purify the sample further, it was subjected to dialysis for 12 h using a molecular weight cut off sizing tube of 0.5 kDa. The sample collected was re-dispersed in distilled water followed by storage at 4 °C.

2.3.3 Synthesis of CdTe@3MB3MP

The synthesis of CdTe QDs using 3-methoxybutyl-3-mercaptopropionate as capping agent was realized by the colloidal synthesis route in a vacuum Erlenmeyer flask. In a typical synthesis procedure, 10 mM cadmium chloride monohydrate and 100 mL of distilled water were taken in the flask, into which, 25 mM of 3-methoxybutyl-3-mercaptopropionate was added. The flask was kept on a hot plate at 100°C with constant stirring. With the addition of 1 M NaOH solution, the pH of the solution was adjusted to 12. Then, 2 mM TeO_2 and 4 mM $NaBH_4$ were added subsequently into this solution followed by vacuum. The reaction was kept at 100°C for about an hour. Then, the solution was removed from the hot plate and suddenly cooled using an ice bath to arrest the further growth of QDs and to maintain the homogeneity of the solution. The purification of the solution was carried out by washing the sample using ethanol and centrifuged at 10000 rpm. To purify the sample further, it was subjected to dialysis for 12 h using a molecular weight cut off sizing tube of 0.5 kDa. The sample collected was re-dispersed in distilled water followed by storage at 4 °C.

2.4 Characterization

UV-visible spectra were recorded using a Carry 100 UV-visible spectrometer (USA). All steady state fluorescence measurements (excitation and emission) were carried out using FluoroMax-4C Spectrofluorometer (Horiba Instruments, USA). Both excitation and emission slit widths were fixed at 5 nm with an integration time of 0.1 ns. Time resolved fluorescence measurements were performed using time-correlated single-photon counting (TCSPC). The obtained lifetime profiles were fitted using DAS software by maintaining χ^2 value around 1 for obtaining the best fit and the corresponding decay parameters were noted. The average lifetime values were calculated using the equation

$$< T >= \frac{\sum_i \alpha i T i^2}{\sum_i \alpha i T i}$$

Where, <τ> is the average lifetime, and αi is the contribution from the component, τi. Fourier transform infrared (FTIR) analysis was performed using Spectrum 100 from Perkin Elmer FTIR spectrometer (USA) in transmission mode using KBr pellet. The transmission electron microscopy (TEM) analysis was carried out using JEM 2100, LaB_6 from Jeol (Japan). The x-ray crystallography (XRD) was carried out using Ultima IV from Rigaku (Japan) and Bruker AXS D8 Advance (USA). Zeta potential measurements were performed using Zetasizer Nano ZS series, Malvern Instruments, Malvern, UK. Surface chemistry of CdTe@E2MP QDs were tested by X-ray photoelectron spectroscopy (XPS) using PHI 5000 Versa Probe II (ULVAC-PHI Inc., USA) with micro focused (15 KV) monochromatic Al-Kα X-Ray source (hν = 1486.6 eV). Both survey spectra and narrow scan (high-resolution spectra) were recorded. Electrochemical measurements were carried using Metrohm Autolab Potentiostat/Galvanostat (Netherlands).

Photostability experiments were carried out by irradiating aqueous solution of various QDs under 360 nm UV lamp (16 W power) and fluorescence spectra of photo-irradiated sample were recorded at specified time intervals.

2.5. Calculation of quantum yield

Quantum yield of the QDs is calculated by using quinine sulfate as a standard (literature quantum yield of the quinine sulphate, φ_o= 0.54 at 350 nm) according to:

$$\varphi_c = (\varphi_o \times I_C \times A_o \times \eta_c^2)/(I_o \times A_c \times \eta_o^2)$$

where,

φ_o and φ_c are the photoluminescence quantum yield of the standard (Quinine sulfate) and sample (QDs), respectively.

I_o and I_C are the integrated emission intensity of the standard and sample, respectively.

A_o and A_c are the absorbance of the standard and sample, respectively

η_o and η_c are the refractive index of the reference and sample solutions, respectively

2.6. Real sample preparation

For real sample detection, spiked samples were prepared by adding known concentrations of various analytes (Hg^{2+}, Cu^{2+}, H_2O_2) into samples such as tap water, pond water, rainwater. Urine sample was diluted with water prior to spiking. Aliquots of these solutions were taken into a cuvette containing 2.5 mL of CdTe QD solution and mixed thoroughly. The PL emission spectra was collected at respective excitation wavelength, each time.

For a test strip assay, 10 µL of respective CdTe QD solutions were drop-casted on a thin layer chromatography (TLC) plate and kept for drying naturally. Various analyte solutions of different concentrations were then added drop-by-drop over these spots on the TLC plate. The response was discerned after an incubation period of 5 min, using a UV light source (365 nm, 16 W). All experiments were performed at room temperature.

2.7. Cyclic voltammetry study

The CdTe QDs were dispersed in 1:1 ratio solution of 5 mL of water-isopropanol. Into this, 10 µL of Nafion binder was added. The net concentration of the QDs were maintained at 1 $mg.mL^{-1}$, in all the experiments. 7 µL of this solution were drop casted on a highly polished glassy carbon electrode and kept for drying naturally. Cyclic voltammetry (CV) was recorded with the help of Metrohm Autolab Potentiostat/Galvanostat using three-electrode system. QD deposited glassy carbon electrode is the working electrode, whereas Ag-AgCl and Pt wire respectively are reference and counter electrode. For bandgap measurement studies, all potentials were calibrated to the reference potential of normal hydrogen electrode (NHE) or vacuum level, using ferrocene/ferrocenium couple in acetonitrile as an internal standard, and sodium perchlorate as supporting electrolyte. For analyzing the redox nature of QDs, CV measurements were taken in a buffer solution of pH 9.2 as electrolyte. All the voltammetric measurements were carried out, at room temperature in laboratory conditions.

CHAPTER 3

BRANCHED MERCAPTO ACID CAPPED CdTe QUANTUM DOTS AS FLUORESCENCE PROBE FOR Hg^{2+} DETECTION

In this chapter, we demonstrate the applicability of CdTe quantum dots prepared by colloidal synthesis route using the branched mercapto acid; 3-mercaptoisobutyric acid (3-MIBA) as fluorescence probe to detect Hg^{2+}. The performance was linear in the range of 1.5–100 nM with a limit of detection of 1.5 ± 0.5 nM. The results demonstrated that fluorescence quenching of CdTe@3-MIBA by mercury follows different routes: (i) excitonic electron transfer from the CdTe@3-MIBA to Hg^{2+} thus preventing emission (ii) strong affinity of Hg towards S causes depassivation of capping agents thus resulting in aggregation of quantum dots.

3.1 Introduction

Mercury, a global pollutant, is released from number of natural processes and various anthropogenic sources. The bio-accumulative and persistent character of Hg^{2+} and its permeability through membrane cause undesirable effects including health problems in brain and kidney, central nervous system of the fetus, hearing and vision loss, etc. (Manavi & Mazumder, 2018; Clarkson et al., 2003). The growing environmental and health concerns necessitates the development of a simple, reliable, sensitive and selective detector for mercury. Conventional Hg^{2+} detection methods including inductively coupled plasma mass spectroscopy, atomic absorption spectroscopy, and atomic emission spectroscopy are time consuming and require expensive instrument and highly precise and tedious sample preparation. Recently, fluorescence nanosensors have received immense interest due to its rapid response, simplicity, high sensitivity and selectivity towards the detection of Hg^{2+}. The detection limit and dynamic range of a fluorescence sensor is to a great extent determined by the physicochemical properties of the chromophore.

Quantum dots, zero dimensional fluorescent materials, hold several advantages over the organic dye chromophores. Organic dyes suffer from the limitations such as low water solubility, strong hydration, low intensities, photo-bleaching, narrow excitation and broad emission spectra. This has driven an extensive research in the quantum dots-based fluorescence probe in the last decade (Resch-Genger et al., 2008; Borse et al., 2016). During the past few years, semiconductor quantum dot (QD) based fluorescence sensors for detection of Hg^{2+} have been receiving more attention due to their high selectivity and sensitivity (Xi et al., 2016; Tabaraki & Sadeghinejad, 2018; Hua et al., 2017; L. Q. Lu et al., 2017). Cadmium Telluride (CdTe) quantum dots are gaining an increasing attention owing to its inherent properties such as high quantum yield, excellent photo stability, narrow emission wavelengths and size dependent fluorescence frequency, large excitonic Bohr radius (7.3 nm), narrow bulk band gap (1.475 eV), etc. (Duan et al., 2009; Jian Zhu et al., 2017). Moreover, these QDs can be synthesized directly in aqueous phase which offers an added advantage along with reproducible results. Therefore, CdTe QDs were opted. The growth of core-shell supramolecular assembly of nano-sized CdTe core with surface ligand shell, is strongly governed by the surface ligands. The capping ligands influence the response of the CdTe fluorescence probe to various metal ions. Remarkable enhancement in the selectivity and sensitivity of CdTe fluorescence probes has been reported with various capping agents (Chao et al., 2013; T. Yang et al., 2013; X. Ding et al., 2015). Mercapto salts paved their way on becoming one of the most used capping ligands due to the strong affinity of the sulphur groups present in capping ligand towards the quantum dots. Also, miscibility in the aqueous medium is critical for bio applications. Hence, ligands having carboxylic groups attached to them are preferred for the synthesis of QDs, as it can attest the solubility in water. Though the most used ligands, namely, thioglycolic acid (TGA) and mercaptopropionic acid (MPA) for the aqueous synthesis of CdTe, are linear mercapto acids, recent reports evidence the better fluorescence with branched mercapto acids (Fang et al., 2012b; K. Ma et al., 2013a). The position and amount of methyl groups, influencing the properties such as growth rate, size distribution and solution stability, govern the fluorescence of QDs with branched

mercapto acids. QDs surrounded by thiol ligands with one methyl group are reported to show better properties in terms of narrow size distribution, enhanced fluorescence intensity and high quantum yield (Fang et al., 2012a) and long-term stability in solution phase (K. Ma et al., 2013b), and better sensing properties (Choudhary & Nageswaran, 2019) compared to MPA derivatives with two methyl side groups (K. Ma et al., 2013a).

In the present chapter, we used CdTe quantum dots prepared by using the branched mercapto acid with one methyl side group i.e., 3-mercaptoisobutyric acid (3-MIBA) as a stabilizing agent. 3-MIBA capping ligand confines the growth of the quantum dots and limiting its size to maintain the quantum effects. A complete characterization of CdTe quantum dots and CdTe-Hg^{2+} is carried out to confirm the formation of quantum dots and to understand the fluorescence-based detection of Hg^{2+} ions using CdTe quantum dots, which performs as both signaling and analyte specific material. Signaling is through the fluorescence quenching during the interaction of quantum dots with the metal ions. Hence the sensor acts as a turn off sensor. The synthesized CdTe quantum dots are used as a probe for the sensing of mercury in the aqueous solutions.

3.2 Results and Discussions

3.2.1 Characterization of CdTe@3-MIBA

Size-dependent optical properties of QDs necessitate the determination of size and shape of the QDs by TEM. TEM images of as synthesized CdTe@3-MIBA QDs for the reaction times of 1 h, are presented in Figure 3.1. The image reveals the spherical structure and uniform distribution of quantum dots, with an average size of 2.29 nm. Though the aureole present in the selected area electron diffraction (SAED) pattern of QDs doesn't suggest the crystalline nature of the synthesized quantum dots, since it is difficult to probe the individual quantum dot, in order to investigate its crystalline nature, we need to perform other reliable technique such as XRD, Raman etc.

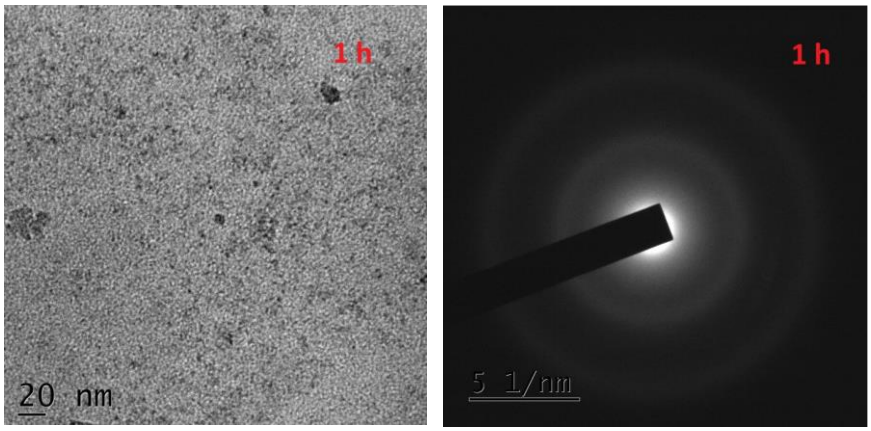

Figure 3.1. TEM images of CdTe@3-MIBA QDs with SAED pattern.

Figure 3.2a presents the IR spectra of CdTe@3-MIBA QD and 3-MIBA, which was employed to elucidate the binding of capping agent. The FTIR spectrum of CdTe@3-MIBA exhibits a broad band around 3320 cm^{-1} attributable to OH stretch. The peaks observed at 2938 and 2882 cm^{-1}, and 1701 cm^{-1} in 3-MIBA spectrum are attributed to -CH and C=O stretching from the carboxyl group respectively. Characteristic thiol peaks of 3-MIBA were observed at 2567 cm^{-1} and 2645 cm^{-1} which disappear in CdTe@3-MIBA QDs confirming the binding of the capping agent with the QD. 3-MIBA co-ordinates with CdTe through breakage of SH bond and formation of new coordinate bond between thiols and the dangling bonds of Cd and Te on the surface of CdTe QDs due to the strong affinity of metal ions towards thiolate ions. The C-O-H peak at CdTe@3-MIBA QDs was observed at 1400 cm^{-1}. The characteristic peak of C=O from the 3-MIBA is shifted to a lower wave number of 1551 cm^{-1} from 1701 cm^{-1} suggesting a distortion due to high density of the QDs capped with 3-MIBA ligand in the system along with its conformational changes (Gipson et al., 2015; Coates, 2006). This might be the reason for the huge shift in the characteristic peak of C=O during the formation of the quantum dots. Similarly, the peaks corresponding to CH stretching observed at 2938 and 2882 cm^{-1} are shifted to a slightly lower wave numbers of 2916 and 2851 cm^{-1} respectively.

Raman spectral analysis was used for the further analysis of QDs structural as well as crystalline information. Figure 3.2b shows the Raman spectra of the sample,

recorded using an excitation source of 514 nm laser. The Raman peak at 162 cm^{-1} correspond to the longitudinal optical (LO) and its second order mode (2LO) at 331 cm^{-1}. Raman spectral analysis can provide a glimpse of the crystallinity of the QDs synthesized. The intense 2LO Raman peak shows the crystalline nature of the QDs. Peaks at 125 and 142 cm^{-1} correspond to the A1 and E1 mode of Te and the fundamental transverse optical mode of CdTe, which further demonstrate the successful formation of CdTe QDs.

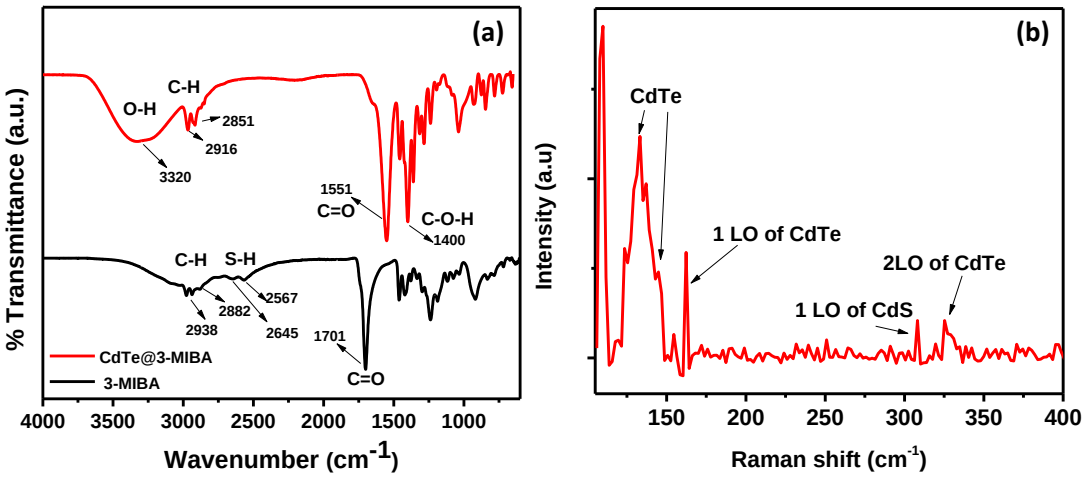

Figure 3.2. a) FTIR spectra of 3-MIBA ligand and CdTe@3-MIBA QDs b) Raman spectra of CdTe@3-MIBA QDs.

The typical XRD pattern of CdTe QDs is depicted in Figure 3.3, which further confirms the crystalline nature of the CdTe@3-MIBA QDs. The spectrum exhibits three major diffraction peaks at 2θ= 24°, 38.8° and 44.4° attributable to the planes (111), (220) and (311) respectively, which matches with the JCPDS card number 15–0770; thus, confirming the formation of the CdTe quantum dots. The interplanar spacing and full width half maximum of the XRD peaks of the planes (111), (220) and (311) were calculated as 3.7, 2.3 and 2 Å, and 0.42, 0.66 and 0.77 rad respectively using Bragg's law and Scherrer's equation. The peaks with irregularity in baseline are observed to be broad due to the presence of poly-crystalline nature of the synthesized quantum dots.

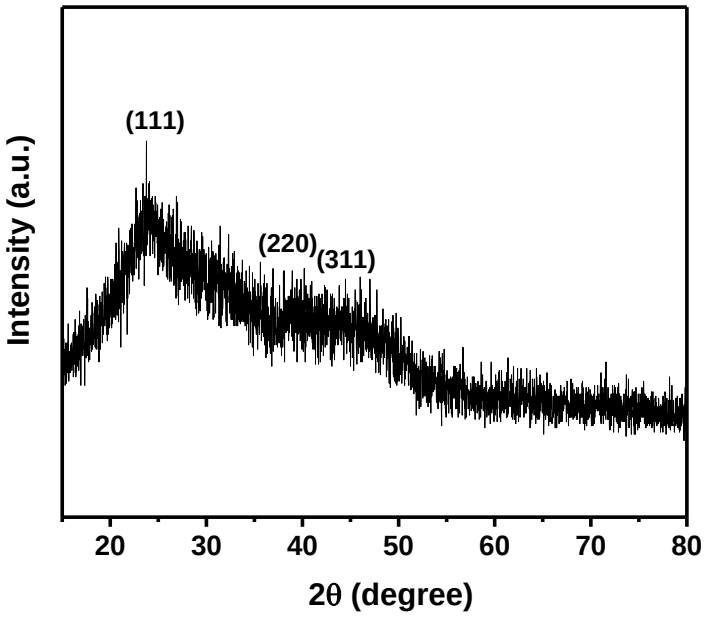

2 theta peaks	Interplanar Spacing (*d*) (A°)	Crystal Planes	FWHM (radians)
24°	3.7	(111)	0.42
38.8°	2.3	(220)	0.66
44.4°	2	(311)	0.77

Figure 3.3. XRD pattern of CdTe@3-MIBA.

XPS analysis were carried out to determine the elemental composition and to identify the chemical states of the elements present in the CdTe@3-MIBA QDs. Figure 3.4a shows the survey scan spectrum of CdTe QDs, with peaks corresponding to Cd and Te, along with the peaks for C, S, O etc., elements present in the ligand. In the HRXPS spectra, the binding energy of $Cd3d_{3/2}$ and $Cd3d_{5/2}$ are found to be at 411.45 and 404.75 eV respectively, and the peak corresponding to $3d_{3/2}$ and $3d_{5/2}$ of Te are located at 582.35 and 571.95 eV. This is in agreement with the values reported for Cd linked to Te in CdTe material (Shen et al., 2013). The existence of these peaks confirms the formation of CdTe QDs. The absence of any other peaks in the higher binding energy region of Cd or Te rules out the possibility of oxidation of the QDs. The HRXPS spectra of S shows peaks at 161.65 and 162.85 eV corresponding to $S2p_{3/2}$ and $S2p_{1/2}$ of organic stabilizer, bonded to the surface of QDs (marked as S-R in Figure 3.4d

legend). The HRXPS spectra of C and O indicate the peaks corresponding to the groups present in the ligands. The peaks corresponding to 1s of O and C are deconvoluted into three each, corresponding to O-H, O-C and O=C for O and that of C into C=O, C-O and C-C of the ligand, 3- mercaptoisobutyric acid.

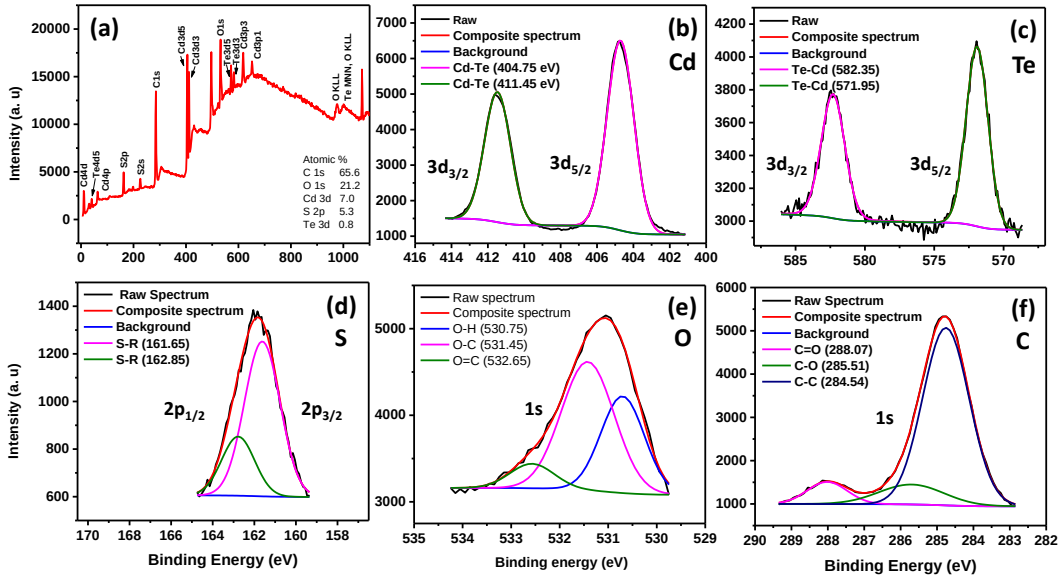

Figure 3.4. a) Survey scan spectra of CdTe@3-MIBA. b - f) HRXPS spectra of Cd, Te, S, O and C respectively

UV–visible absorption and photoluminescence spectra were recorded to characterize the optical properties of CdTe@3-MIBA QDs. One can observe the CdTe QDs exhibiting a characteristic absorption peak at 320 nm as shown in Figure 3.5 and a wide absorption band at 490 nm (see inset of Figure 3.5). The characteristic peak of 3-MIBA observed at 290 nm was observed at 275 nm in the case of CdTe@3-MIBA QDs. This result suggests the possible attachments or interaction of thiol ligands from capping agent with the QDs. The emission spectra of CdTe@3-MIBA QDs were recorded at different excitation wavelengths (λ_{ex}). The maximum emission was observed at 520 nm at an excitation of 340 nm. This high emission was reflected in its quantum yield (QY) value as well. QY of the CdTe@3-MIBA QDs was calculated using quinine sulphate as standard and obtained a comparable value of 22.83 %. One of the interesting optical properties of CdTe@3-MIBA QDs is its excitation

independent emission, with high green emission under UV radiation (Figure 3.6). This result evidences the uniform distribution of the quantum dots in the solution.

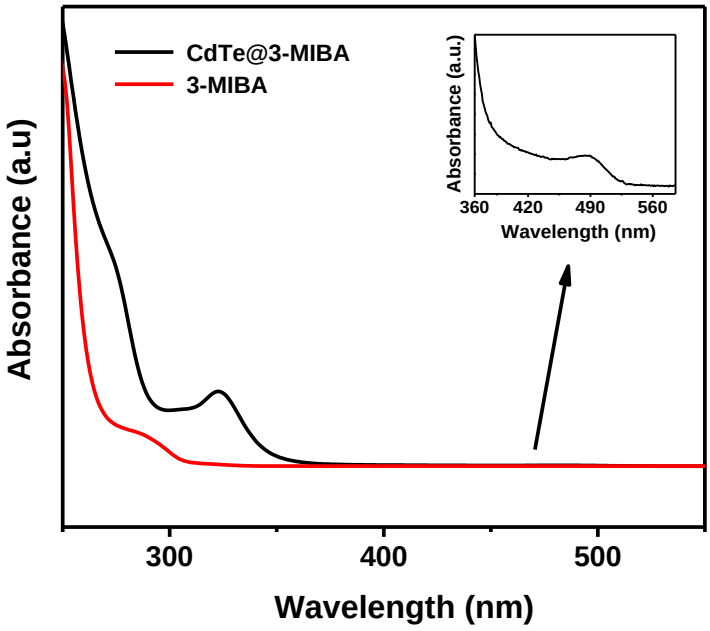

Figure 3.5. Absorption spectra of 3-MIBA capping ligand and CdTe@3-MIBA QDs.

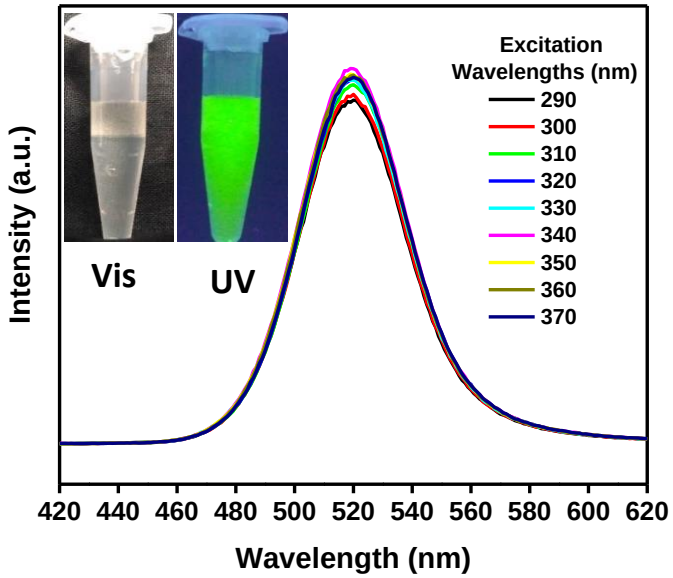

Figure 3.6. PL Spectra exhibiting an excitation independent nature of the CdTe QDs, with emission maximum at 520 nm for an excitation of 340 nm. Inset shows the photograph of CdTe@3-MIBA QDs under visible and UV radiation.

Fluorophores of having high temporal and photostability is demanded in the realm of fluorescence imaging and sensing applications. Therefore, we checked the temporal as well as photostability of CdTe@3-MIBA QDs. As can be seen in Figure 3.7, even after seven months of preparation, 90% of the fluorescent intensity is remaining, which proves the excellent stability of the QDs synthesized using the branched ligand, 3-mercaptoisobutyric acid. For photostability studies, CdTe@3-MIBA QDs were irradiated with UV light (365 nm, power: 16 W) continuously and PL intensity was subsequently recorded at different time intervals. Even after irradiation of QDs for 60 min, 50% of the initial intensity was maintained, which reflects its photo-stable nature.

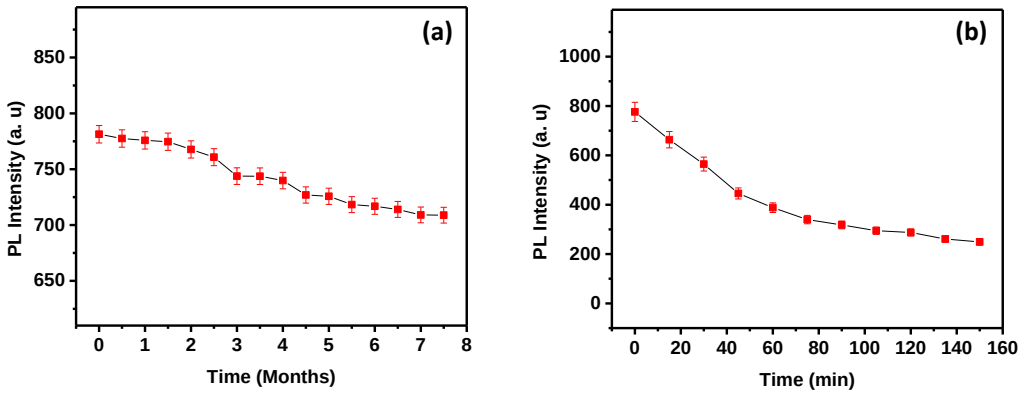

Figure 3.7. (a) Temporal and (b) photostability of CdTe@3-MIBA QDs

A glimpse at the electronic structure of the QDs were obtained from UV-Vis absorption studies as well as cyclic voltammetric (CV) analysis. The band gap energy of QDs is the energy required to excite an electron from the valence band (VB) to its conduction band (CB). The determination of the band gap energy is imperative in predicting its photophysical as well as photochemical properties. The bandgap energy of the QDs were calculated from Tauc plot extrapolation. The Tauc method used the following equation in order to find the band gap

$$(\alpha \cdot h\nu)^{1/\gamma} = B(h\nu - E_g)$$

Where h is the Planck constant, α is the energy-dependent absorption coefficient ν is the photon's frequency, E_g is band gap energy, and B is a constant. The γ factor can have two values (1/2 or 2) depending on the whether the transition is direct or indirect, respectively.

A Tauc plot of $(\alpha \cdot h\nu)^2$ vs hν was plotted and the bandgap was calculated using extrapolation (Figure 3.8a). The E_g of CdTe@3-MIBA is found to be 2.56 eV. It has been reported that, due to the confinement of the electrons and holes, with decreasing the size of the QDs, the band gap energy increases. Therefore, the moderately higher bandgap value of CdTe@3-MIBA QDs is owing to the small size of QDs (~ 2.3 nm) (S. et al., 2018). The valence band of the QDs can be calculated using cyclic voltammetric studies (Figure 3.8b). For this purpose, we have used ferrocene/ferrocenium couple as internal standard. Briefly, the QDs were deposited on glassy carbon electrode, dried naturally and used as working electrode. The cyclic voltammogram was obtained using acetonitrile electrolyte containing ferrocene/ferrocenium couple as internal standard and sodium perchlorate as supporting electrolyte, using a three-electrode set up. The VB level of QDs can be calculated using the equation

$$E_{Homo} = -(E_{OX} + 4.8 - E_{1/2})$$

Where, E_{OX} is the onset oxidation potential (E_{OX}) obtained using QD as working electrode and $E_{1/2}$ is the half wave potential of ferrocene/ferrocenium couple ($E_{1/2}$) obtained using bare glassy carbon electrode as working electrode,

The energy of VB is calculated to be -4.68 eV and CB was calculated using VB energy value and bandgap energy (E_g). An energy level diagram has been constructed from the obtained information as depicted in Figure 3.8a inset.

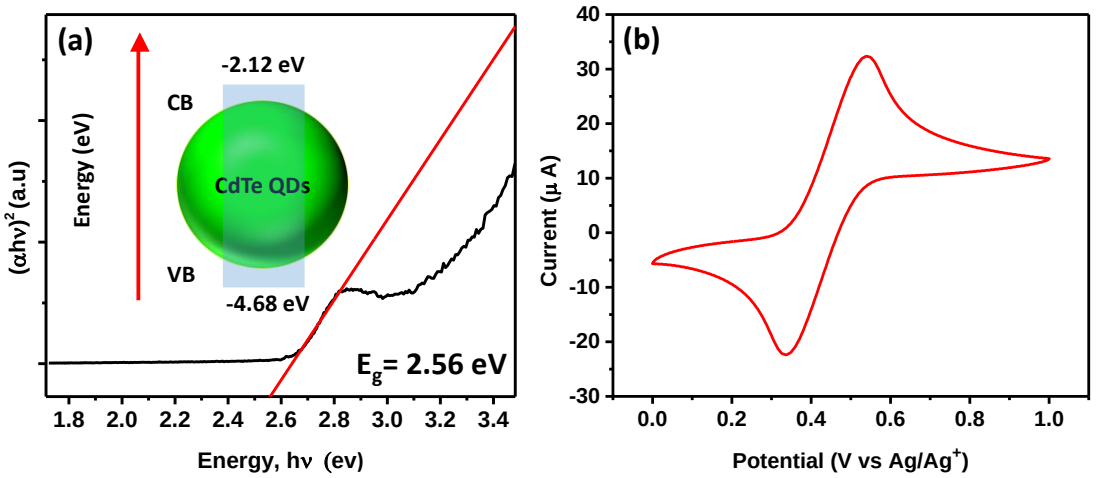

Figure 3.8. a) Tauc plot of CdTe@3-MIBA QDs. Inset shows electronic band structure diagram of CdTe@3-MIBA QDs b) The cyclic voltammogram of acetonitrile solution of ferrocene/ferrocenium couple as internal standard and CdTe@3-MIBA QDs deposited glassy carbon electrode as working electrode.

3.2.2 Fluorescence quenching of CdTe@3-MIBA QDs by Hg^{2+}

The fluorescence quenching process induced by quencher molecule enables the use of quantum dots as a probe to detect various analytes. Fluorescent sensor for Hg^{2+} is based on the fluorescence quenching of CdTe@3-MIBA QD probe by Hg^{2+}. Decrease in the fluorescence intensity of the probe induced by the quencher molecule usually changes with the concentration of the quencher molecule. Therefore, a detailed study was performed on the fluorescence quenching of CdTe@3-MIBA QDs by Hg^{2+} ions by varying the concentration of Hg^{2+} to determine the linear range and limit of detection (LOD) of the sensor.

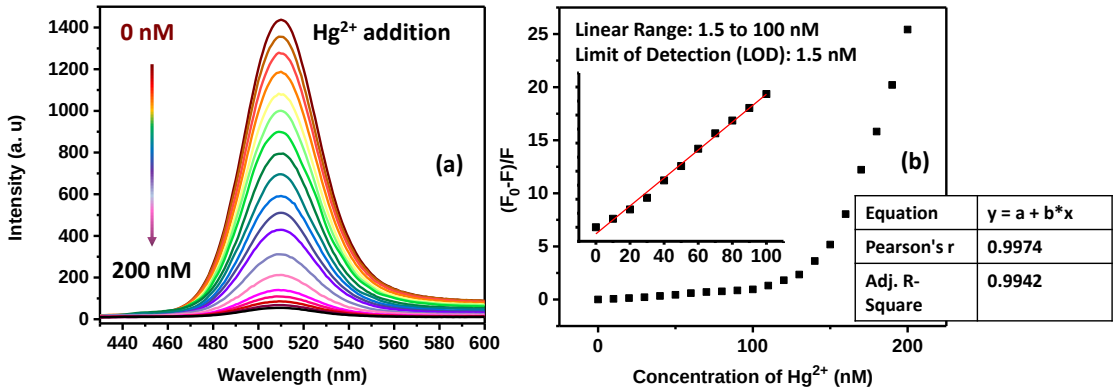

Figure 3.9. (a) Fluorescence emission spectra of CdTe@3-MIBA QDs with increasing concentration of Hg^{2+} ions, (b) $(F_0 – F)/F$ vs concentration of Hg^{2+}.

Figure 3.9(a) exhibits the fluorescence emission spectra of CdTe@3-MIBA QDs with λ_{ex}=340 nm after adding Hg^{2+} with different concentrations. Symmetric emission peak observed at 520 nm exhibits the decay in the peak intensity of CdTe@3-MIBA QDs with addition of Hg^{2+} ions of varying concentration. The concentration of the Hg^{2+} against the relative quenching intensity [$(F_0-F)/F$] was plotted and presented in Figure 3.9(b). It is observed that CdTe@3-MIBA QD probe exhibit a linear quenching intensity within a concentration range of 1.5 nM to 100 nM. The fluorescence quenching in this concentration range can be well described by the following Stern-Volmer equation

$$F_0/F = 1 + K_{SV}[Q]$$

where, F_0 and F are the respective actual and quenched fluorescence intensities of CdTe@3-MIBA QDs in the absence and presence of the quencher, K_{SV} is the Stern-Volmer constant, whereas [Q] is the concentration of the quencher, ie. Hg^{2+} concentration. The relative fluorescence intensity deviates from linearity toward the y-axis with the successive addition of Hg^{2+} from 100 to 200 nM. This indicates that more than one type of quenching processes (static/dynamic quenching) are involved here (Singh et al., 2019) . Comparison of the current work with the available CdTe based QDs with different capping ligands presented in Table 3.1 sheds a light on its significance.

Table 3.1. Comparison of performance of Hg^{2+} sensor using CdTe QDs with various capping ligands.

CdTe QDs capped by different ligands	Linear range	LOD	Reference
BSA-coated CdTe QDs based fluorescence probe	0.001μM - 1μM	1nM	(Jian Zhu et al., 2017)
BSA coated CdTe QDs	10nM - 1uM	4.5nM	(F. Yang et al., 2011)
MPA-capped CdTe QDs	0 nM - 128 nM	0.5 nM	(Bo Chen et al., 2004)
dBSA-coated CdTe QDs	12nM-1.5uM	4nM	(Yun-sheng Xia & Zhu, 2008)
MSA capped CdTe QDs	0.005μM - 0.5uM	-	(Q. Ma et al., 2011)
MPA-capped CdTe QDs	8nM - 3000nM	4.2nM	(Y. Q. Wang et al., 2012)
MPA-capped CdTe QDs	2nM - 14nM	1.55nM	(T. Li et al., 2011)
Cysteamine (CA)-capped CdTe QDs	6nM - 450nM	4.0nM	(X. Ding et al., 2015)
TGA-capped CdTe NCs	3.33 – 667nM	3.33nM	(Chao et al., 2013)
N-acetyl-L-cysteine-(NAC-) capped CdTe QDs	20nM - 430nM	8nM	(T. Yang et al., 2013)
DMSA capped CdTe QDs immobilized on FTO electrode surface	1nM - 1mM	0.3nM	(Wen et al., 2015)

MPA-capped CdTe QDs	8nM - 2uM	2.7nM	(Duan et al., 2009)
MSA-capped CdTe QDs	0.6μM - 20μM (GSH) 2μM - 20μM (Cys)	0.1μM (GSH) 0.6μM (Cys)	(Han et al., 2009)
3-MIBA capped CdTe QDs	1.5 nM – 100 nM	1.5nM	This work

3.2.3 Mechanism of Fluorescence Quenching

Fluorescence quenching of quantum dots on addition of quencher molecules are caused by either static quenching or dynamic quenching. Quenching rate constant (k_q) obtained from the relation $k_q=K_{SV}/\tau$, using Stern-Volmer constant and lifetime of QDs can suggest the type of quenching mechanism. Dynamic quenching process plays a major role when the quenching rate constant is in the order of diffusion limited rate constant ($10^{10} M^{-1} s^{-1}$) obtained from Smoluchowski equation (Santhosh et al., 2011).

$$k_{diff} = 8RT/3\eta$$

Where, k_{diff} is the diffusion rate constant, η is the viscosity of the solvent, R is the collision radius and T is temperature. The obtained k_q value (3.48×10^{14} M^{-1} s^{-1}) suggests that the static quenching plays a major role in the fluorescence quenching of CdTe by Hg^{2+}. To investigate the quenching phenomena further, absorption spectra of CdTe@3-MIBA were recorded in absence and presence of Hg^{2+}. As the absorption spectra of CdTe@3-MIBA did not show any appreciable shift in the absorption band with the addition of Hg^{2+} (Figure 3.10), it clearly excludes the possibility of the formation of ground state complex between CdTe@3-MIBA and Hg^{2+}.

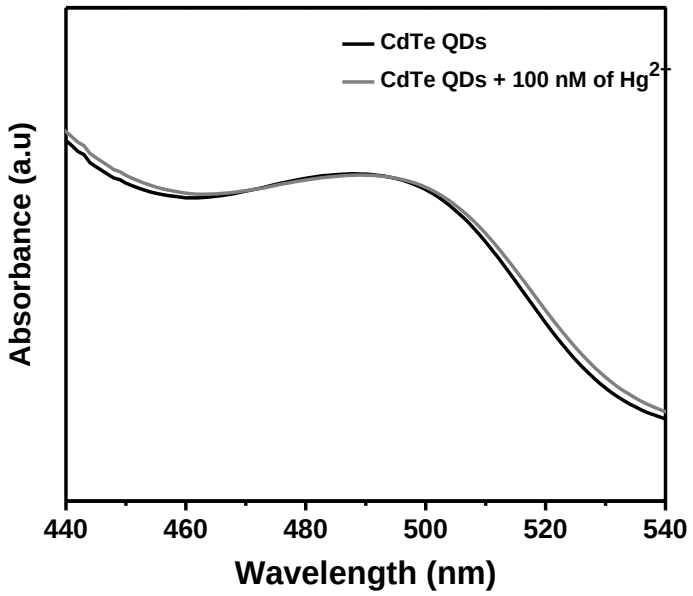

Figure 3.10. Absorbance spectra of CdTe@3-MIBA QDs before and after the addition of Hg^{2+} ions.

The stability of any colloidal solutions is governed by its surface charges. The higher the charges, the lower will be the possibility for the colloidal particles to come together and coalesce. Therefore, the zeta potential studies were performed to reveal the stability of CdTe@3-MIBA in the presence of Hg^{2+} ions and to understand the mechanism of interaction between QDs and Hg^{2+} ions. It has been observed that upon addition of Hg^{2+}, the zeta potential value of CdTe@3-MIBA found to be decreased substantially as shown in Table 3.2, and we hypothesize that due to the interaction with Hg^{2+} ions, which removes the ligands due to the affinity of the Hg towards sulphur in 3-MIBA capped CdTe, the surface charges of QDs change. As a result of the removal of the capping ligands by Hg^{2+} ions, the stability of the QDs is lost and thus leads to the aggregation of the QDs and their settling as depicted in TEM image (Figure 3.11c). This aggregation causes an increment in the overall size of the quantum dots. However, TEM images at lower concentrations (Figure 3.11 b) shows no substantial changes in

the morphology of QDs within the linear range. A TEM micrograph of CdTe@3-MIBA QDs (Figure 3.11 a) before addition of Hg^{2+} is also shown for comparison.

Table 3.2. Zeta potential values for CdTe@3-MIBA QDs with increasing Hg^{2+} ions.

Sample	Zeta Value (mV)
CdTe QDs	-27
CdTe QDs + 20 nM Hg	-26
CdTe QDs + 40 nM Hg	-25
CdTe QDs + 80 nM Hg	-22
CdTe QDs + 160 nM Hg	-21
CdTe QDs + 320 nM Hg	-18

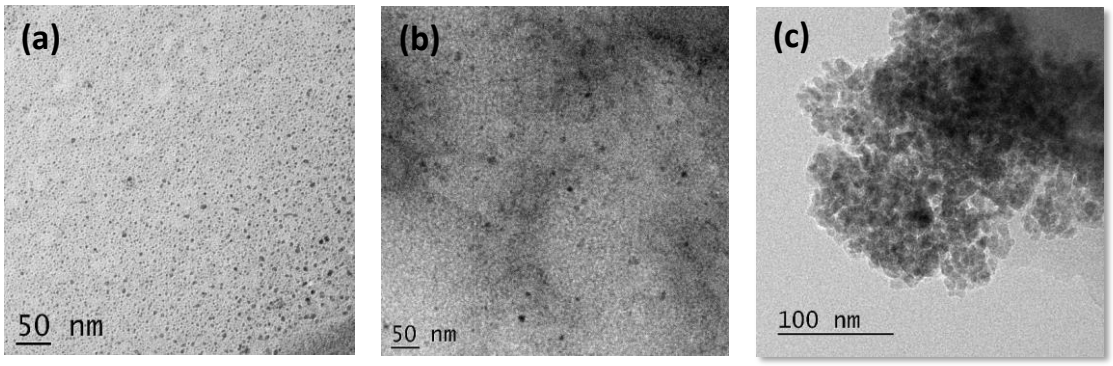

Figure 3.11. TEM image of CdTe@3-MIBA (a) with Hg^{2+} ions in two different concentrations (b) 50 nM of Hg^{2+} showing intact QDs and (c) 500 nM Hg^{2+} showing an aggregated structure.

To unfold the presence of any excited state phenomenon, we conducted detailed photo-physical studies as well. The fluorescence lifetime of quantum dots can get affected by energy transfer as well as electron transfer. The absence of spectral overlap of absorption spectra of the quencher (Hg^{2+} ions) and the emission profile of the fluorophore (CdTe@3-MIBA), readily circumvent the possibility for Forster resonance energy transfer, leaving a clear signal for the existence of the electron transfer (Figure 3.12).

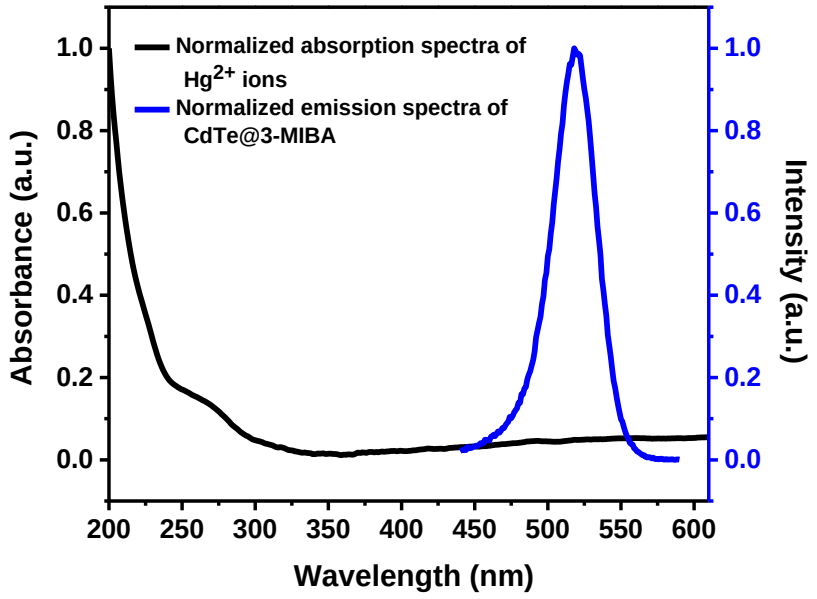

Figure 3.12. Spectral overlap of emission of CdTe@3-MIBA and absorption of Hg^{2+}.

To ascertain the possibility of quenching by electron transfer, time resolved emission spectra of CdTe@3-MIBA at different concentration of Hg^{2+} were collected, using a 344 nm pulsed diode laser with a pulse duration of ~1 ns. If there is an excited state electron transfer between CdTe@3-MIBA and Hg^{2+}, the lifetime of the former would decrease with quencher concentration owing to the emergence of new non-radiative routes. Here, after the addition of the mercury, when the sample is exposed to the UV light, the absorbed energy by the quantum dots was dissipated in the form of the non- radiative recombination of the holes and electrons. With an increasing concentration of mercury, the number of non- radiative recombination of the holes and electrons increases. Initially the lifetime is taken with the mercury free QDs sample followed by the sequential addition of mercury with increasing concentration and the lifetime is recorded against a common prompt. The response obtained from the fluorescence decay of CdTe@3-MIBA QDs in the presence of varying concentration of Hg^{2+} depicted in Figure 3.13 was fitted with a biexponential decay

$$I(t) = A_1 \exp^{(-t/\tau 1)} + A_2 \exp^{(-t/\tau 2)}$$

where I(t) is the fluorescence intensity at time t, τ_1 and τ_2 are lifetime components, A_1 and A_2 are the corresponding amplitude.

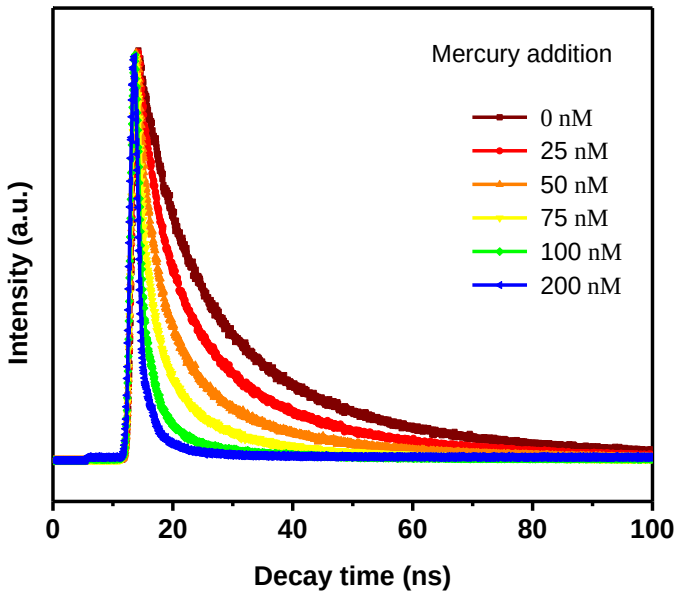

Figure 3.13. Fluorescence decay of CdTe@3-MIBA QDs after addition of different concentrations of Hg^{2+}.

Table 3.3. Time-resolved fluorescence decay of CdTe@3-MIBA QDs with different concentration of Hg^{2+} ions. (τ_1 and τ_2 are lifetime components, A_1 and A_2 are corresponding amplitude, and τ is the average lifetime).

System	τ_1[ns]	A_1 [%]	τ_2[ns]	A_2 [%]	<τ> [ns]	χ^2
QDs + 0 nM Hg^{2+}	6.66	20.34	23.04	79.66	21.91	1.08
QDs + 25 nM Hg^{2+}	4.70	27.30	19.13	72.70	17.91	1.09
QDs + 50 nM Hg^{2+}	4.00	28.29	17.34	71.71	16.23	1.18
QDs + 75 nM Hg^{2+}	3.22	34.51	15.24	65.49	14.04	1.21
QDs + 100 nM Hg^{2+}	2.51	45.17	12.65	54.83	11.23	1.19
QDs + 200 nM Hg^{2+}	1.90	57.57	9.80	42.43	8.15	1.18

The lifetime results presented in Table 3.3 fitted with biexponential behaviour exhibiting short lived and long-lived components. The lifetime components clearly indicate that the fluorescence lifetime of CdTe@3-MIBA QDs decreases with the increasing concentration of mercury. Decrease in the lifetime of CdTe@3-MIBA QDs

with increasing concentration of Hg^{2+} is attributed to the electron transfer from the donor (CdTe@3-MIBA QDs) to the acceptor (Hg^{2+}) as shown in Scheme 3.1.

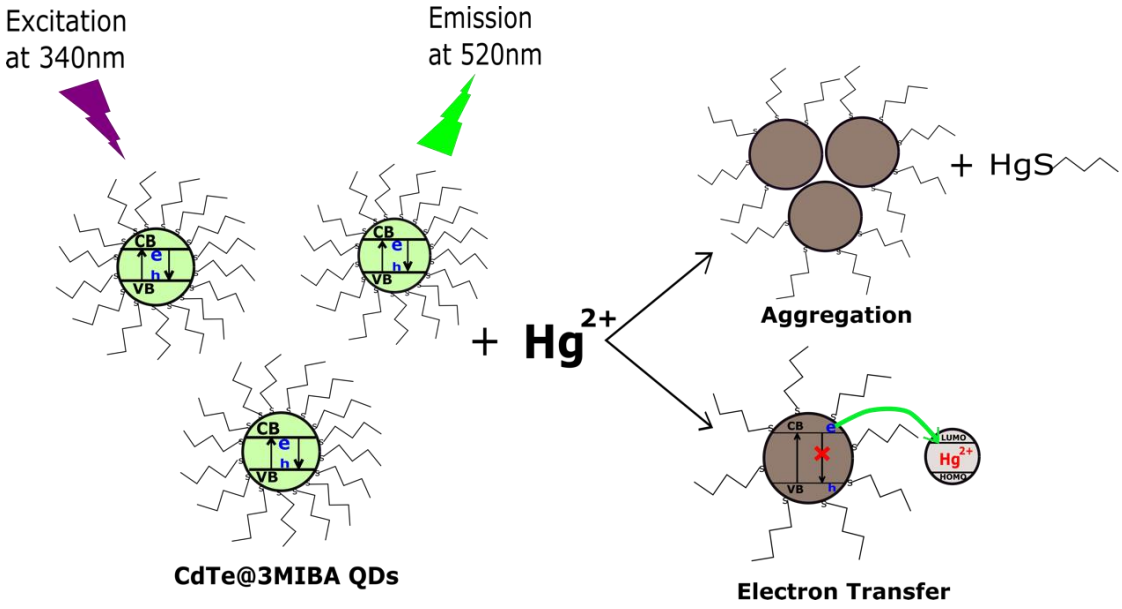

Scheme 3.1. Quenching mechanism of CdTe@3-MIBA QDs by Hg^{2+}.

Further, XPS analysis offer proof of electron transfer between CdTe@3-MIBA QDs and Hg^{2+}. As is evident from Figure 3.14, the HRXPS peaks of Cd and S show no significant changes compared to the peaks of Cd and S corresponding to CdTe@3-MIBA QDs. While the HRXPS spectra of Te after interaction with Hg^{2+} shows an extra peak corresponding to its oxidation, along with the peak for Cd-Te. In addition, the HRXPS peaks of Hg is split in to four peaks corresponding to Hg $4f_{7/5}$ and Hg $4f_{5/2}$ peaks of +2 and zero oxidation peaks, respectively at 108.8, 111.7 and 102.3, 106.6 eV. By considering the reduction potentials, Hg^{2+} is more likely to get reduced (+0.85 V) and Te^{2-} is more likely to get oxidized (E_{red} = -1.14 V) compared to S^{2-} (+0.14 V) and Cd^{2+} (-0.40 V). These observations unambiguously prove the involvement of electron transfer between the fluorophore and the quencher. Also, we have performed cyclic voltammetric analysis of CdTe@3-MIBA QDs, using a three-electrode setup, with Ag/AgCl as reference electrode, Pt wire as counter electrode and QDs deposited on glassy carbon as working electrode. A buffer of 9.2 pH was used as electrolyte. A clear oxidation and reduction peaks were obtained for QDs at -0.7515 and -0.9638 V

respectively, with the difference between the anodic and cathodic peak potentials; called peak-to-peak separation (ΔEp) of 0.2123 V. We know that, when there is less barrier for electron transfer, the reaction will be easier and faster and thus less negative (positive) potentials are required to observe reduction (oxidation) reactions, giving rise to smaller ΔEp. In the presence of Hg^{2+} ions in the buffer solution, when we performed the electrochemical study, the oxidation and reduction are found to be respectively at -0.7539 and -0.9248 V, with a ΔEp of 0.1709 V. This further demonstrates the involvement of electron transfer between CdTe@3-MIBA QDs and Hg^{2+}. The results are illustrated in Figure 3.15.

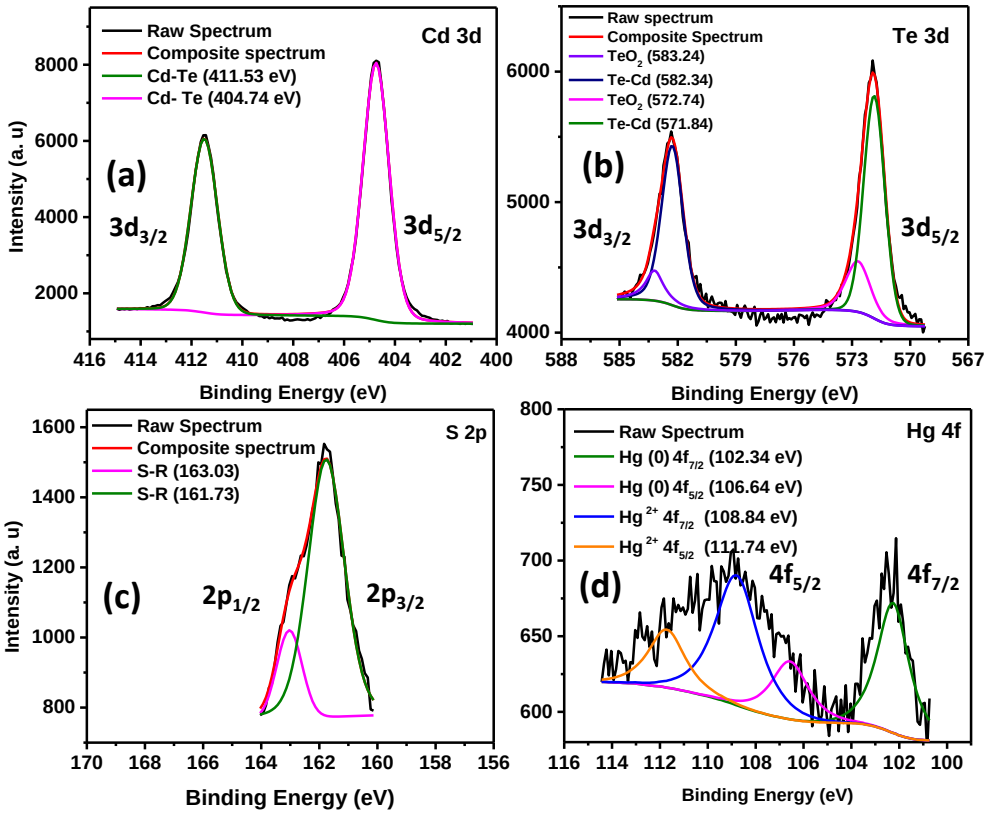

Figure 3.14. Deconvoluted XPS peak of Cd (a), Te (b), S (c) and Hg (d) of CdTe@3-MIBA QDs after interaction with Hg^{2+}

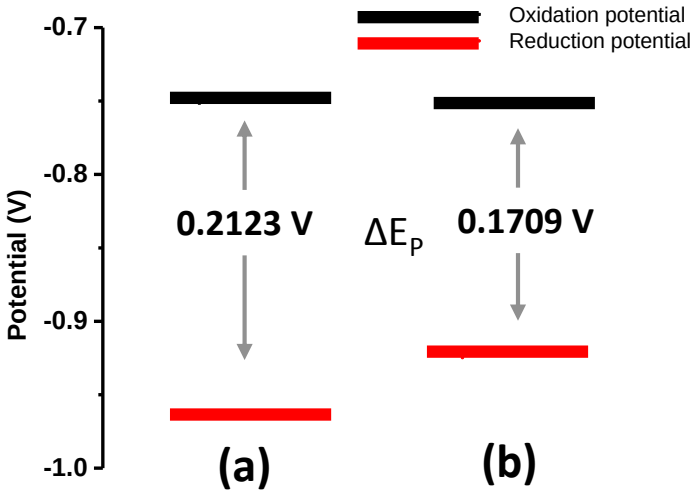

Figure 3.15. Alignment of the oxidation and reduction potential of CdTe@3- MIBA QDs alone (a) and in the presence of Hg^{2+} (b)

Thus, we propose that two major mechanisms are operating for the quenching of fluorescence emission of CdTe@3-MIBA during its interaction with Hg^{2+}. One of the major mechanisms that operate at lower concentrations of Hg^{2+} can be a dynamic electron transfer. In addition to this, due to the favorable interaction of Hg^{2+} with the S of ligand, we are anticipating the removal of ligand from the surface of QDs as well. At higher concentrations, due to the removal of majority of the ligands, we can observe aggregation of QDs, which further reduces the fluorescence intensity of CdTe@3-MIBA.

3.2.4 Selectivity of CdTe@3-MIBA to Hg^{2+}

In order to investigate the interference of various coexistence ions, which influences the performance of fluorescent sensor for practical applications, the selective interaction of the fluorescence probe with Hg^{2+} ions were studied. To study the selectivity of CdTe@3-MIBA QD probe towards Hg^{2+}, luminescence of the QD was recorded in the presence of several interferants including metal ions such as Co^{2+}, Fe^{2+}, Fe^{3+}, K^{+}, Na^{+}, Ba^{2+}, Ca^{2+}, Mn^{2+}, Mg^{2+}, Zn^{2+}, Cu^{2+}, Ni^{2+}, Al^{3+}, Pb^{2+}, Sn^{2+}, Ag^{+} and Cd^{2+}, biologically relevant molecules such as dopamine, Vit. C and amino acids. From Figure

3.16, it is observed that CdTe@3-MIBA QDs did not show significant fluorescent quenching by any of these interferant ions/molecules. This result suggests that the interferant metal ions only slightly quench the photoluminescent intensity due to the weak affinity of these interferant ions towards the thiol groups of the capping agent and have small influence on the interaction between the Hg^{2+} ions and the thiol ligands from 3-MIBA.

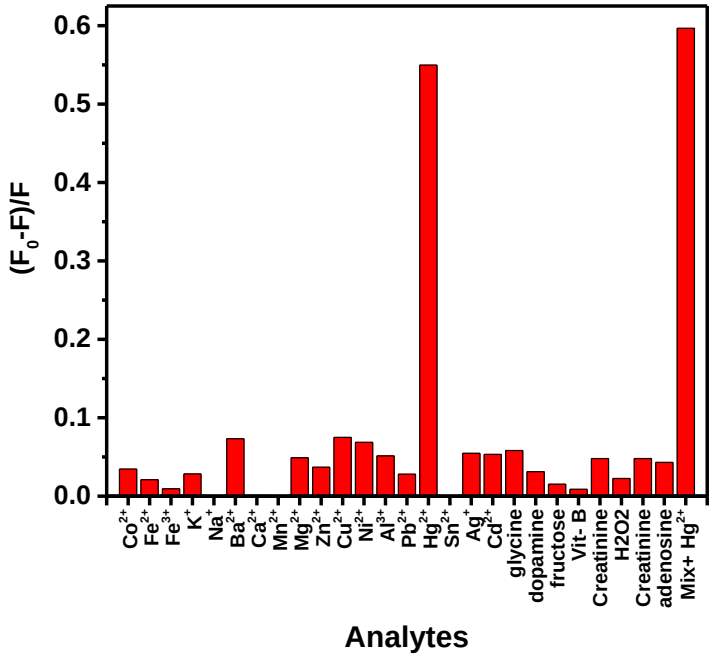

Figure 3.16. Effect of different metal ions on the fluorescence intensity of CdTe@3-MIBA QDs.

3.2.5 Visual detection and real sample analysis

A qualitative recognition of Hg^{2+} using a solid substrate was performed in order to check the utility of the present sensor for visual detection platform. For this purpose, we used thin layer chromatographic (TLC) plate where several CdTe@3-MIBA QD spots were drop-casted and dried. Three different concentrations of Hg^{2+} (50 nM, 100 nM, and 200 nM) were deposited on to these dried sensor spots and illuminated under UV radiation (365 nm). As is evident in Figure 3.17, an easy

qualitative detection of Hg^{2+} can be realized using CdTe@3-MIBA QD without the use of any sophisticated instruments.

To verify the feasibility of the present sensor for the detection of Hg^{2+} in real samples, we have analyzed the response of CdTe@3-MIBA QDs in tap water and pond water samples spiked with different concentrations of Hg^{2+}. Table 3.4 summarizes the result obtained. A recovery of 102.35, 101.70 and 100.12 % were obtained for tap water samples for the spiked concentrations of 10, 20, and 30 nM with % relative standard deviation (% RSD) of 1.3, 1.6 and 0.9 respectively. A percentage recovery of 105.92, 104.96, and 103.72 % were observed for pond water sample, with % RSD of 0.4, 1.4 and 1.2 respectively. All experiments were repeated three times and a mean value is reported.

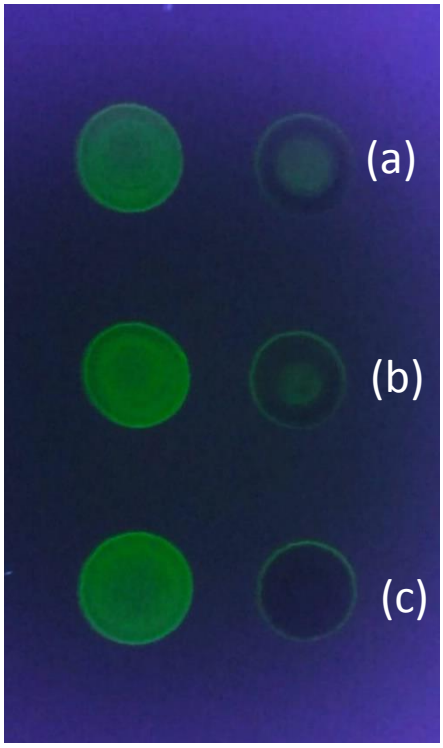

Figure 3.17. Photographs of TLC plate-based sensor platform. The first column represents CdTe@3-MIBA QD drop casted on TLC under UV light (green dots), second column represent QDs treated with a) 50 nM b) 100 nM and c) 200 nM concentrations of Hg^{2+}.

Table 3.4. Table showing the results obtained for real sample analysis.

Sample	Spiked (nM)	Found (Mean; nM)	Recovery	% RSD
Tap water	10	10.24±0.02	102.35 %	1.3
	20	20.34±0.06	101.70 %	1.6
	30	30.04±0.10	100.12 %	0.9
Pond water	20	21.19±0.03	105.92 %	0.4
	50	52.48±0.06	104.96 %	1.4
	100	103.72±0.11	103.72 %	1.2

3. 3 Conclusion

In this work, we have demonstrated a turn off fluorescent sensor for mercury ions at the nanomolar concentration using branched mercapto acid capped CdTe QDs with a linear range of 1.5–100 nM with limit of detection of 1.5 ± 0.5 nM. Time resolved fluorescence decay, UV–Vis absorption spectroscopy, XPS and CV analysis along with TEM studies evidence the multiple quenching mechanisms namely electron transfer, removal of ligands and aggregation induced quenching involved in Hg^{2+} sensor using 3-MIBA capped CdTe QDs.

CHAPTER 4

ETHYL-2-MERCAPTOPROPIONATE AS A STABILIZER FOR CdTe QUANTUM DOTS AND ITS USE AS A Cu^{2+} IONS PROBE IN AQUEOUS MEDIUM

In this chapter, we explored the possibility of using a novel stabilizing ligand namely ethyl-2-mercaptopropionate (E2MP) for the synthesis of CdTe quantum dots (QDs) with high fluorescent emission centered around 560 nm. Extensive microscopic and photo physical characterization have been carried out in order to unearth the nature of the QDs synthesized. Interestingly it has been observed that, the PL emission of as synthesized QDs is getting quenched linearly in the presence of Cu^{2+}, which prompts us to make use of these QDs for the detection of Cu^{2+} ions in aqueous media. A detailed mechanism of quenching is also proposed. The linear range over which the QDs was selective to Cu^{2+} ions was from 0.5 nM to 129.5 nM with a detection limit (LOD) of 0.5 nM providing a pathway for the QDs based Cu^{2+} probe.

4.1 Introduction

Copper ion (Cu^{2+}), recognized as one of the most toxic pollutants to eco-systems, is released into the environment by industries, mines, waste dumps, smelters, combustion of fuels and other wastes, and natural sources like volcanoes, decaying vegetation, forest fire etc. Copper ion plays a pivotal role in bone formation, cellular respiration, connective tissue development etc (McDowell, 2003). However, exposure to high levels of copper can cause nausea, vomiting, and abdominal pain, while chronic over exposure to copper can cause damage to kidney, liver and central nervous system leading to neurogenerative diseases like Alzheimer, Parkinson and Wilson (Gaggelli et al., 2006; Waggoner et al., 1999; Kumar & Dutta, 2017). Also, deficiency of copper can cause damage to the blood cells resulting in anemia, neutropenia and bone abnormalities (Georgopoulos et al., 2001; Uriu-Adams & Keen, 2005; Yahui Wang et al., 2016). Therefore, specific and accurate determination of copper ion in the

ecosystems is of great importance. The U.S. Environmental Protection Agency (EPA) has set a maximum permissible limit of copper in drinking water to be 1.3 ppm (~20 μM). The available detection strategies for the sensors such as electrochemical methods, inductively coupled plasma mass spectrometry (ICP-MS), atomic absorption spectroscopy (AAS), chromatography, etc. offer precision level detection, but are expensive, complicated and time consuming, thus limiting its usage in normal day to day scenarios for sensing. Fluorescence based sensing, on the contrary, is more popular for analytes of diverse categories such as metal ions, biologically significant molecules, and environmentally harmful compounds due to its noteworthy advantages such as easy sample preparation, high sensitivity and selectivity, low-cost detection, wide dynamic linear range, etc. Various reports are available, on detection of Cu^{2+} by exploiting the photoluminescence behavior of several moieties such as simple organic molecules, semiconductor-based quantum dots (QDs), metal organic frameworks etc. (Dong et al., 2012; Yu-zhen Chen & Jiang, 2016; Sivaraman et al., 2018; B. Zhang et al., 2017; Gu & Zhang, 2018; Gu et al., 2018; J. F. Zhao et al., 2012). For example, a fluorescence turn-off detection of Cu^{2+} in river water was demonstrated using blue emitting branched poly(ethylenimine) (BPEI)-functionalized carbon quantum dots (CQDs) (Dong et al., 2012). The amino groups at the surface of CQDs can bind with Cu^{2+}, forming cupric amine and quench the emission of fluorophore via inner filter effect. A turn-on sensing of Cu^{2+} using Pd(II)-porphyrinic metal-organic framework was also demonstrated, taking advantage of stronger binding affinity of Cu^{2+} over Pd (II) to the nitrogen atoms in porphyrin (Yu-zhen Chen & Jiang, 2016). Fluorescent turn-off probe based on quinoline and benzimidazole groups (QLBM) was utilized for the simultaneous detection of Cu^{2+} and Fe^{3+}. The reduction ability difference between Cu^{2+} and Fe^{3+} towards ascorbic acid were exploited for the discrimination of Cu^{2+} from Fe^{3+} (B. Zhang et al., 2017).

Nonetheless, of these fluorophores, semiconductor based QDs show several significant optical properties. Based on the understanding of photoluminescence quenching of QDs by various analytes which can alter the surface states of QDs, several

sensors have been designed for the detection of Cu^{2+} (Elmizadeh et al., 2017; S. Yang et al., 2018). In this regard, the selection of suitable surface capping ligands is of paramount importance for the detection of specific analyte, as it can further improve the selectivity of the sensor. In this chapter, we have demonstrated the application of CdTe QDs capped with ethyl-2-mercaptopropionate (CdTe@E2MP) synthesized using one pot colloidal synthetic strategy as a highly selective and sensitive turn off chemo-sensor for Cu^{2+} ions detection in aqueous media. A plausible mechanism of quenching of photoluminescence emission of CdTe@E2MP by Cu^{2+} is also proposed.

4.2 Results and Discussions

4.2.1 Characterization of CdTe@E2MP

The QDs were prepared by colloidal synthesis route in a vacuum Erlenmeyer flask. The morphology of CdTe@E2MP QDs was unveiled by TEM analysis. The geometry of the QDs was observed to be spherical, with the size of the quantum dots to be around 3.46 nm (Figure 4.1). The inset to Figure 4.1a shows the HRTEM image of a single QD formed. The fringes in the image reveal its crystalline nature. In selected area electron diffraction (SAED), the pattern of dots suggests the polycrystalline nature of the sample. The first ring in SAED correspond to (200) plane of zincblende (ZB) structure, whereas the next three rings corresponding to wurtzite structures (W) of CdTe QDs. We surmise that during the formation of QDs, CdTe adopt both the crystalline structures.

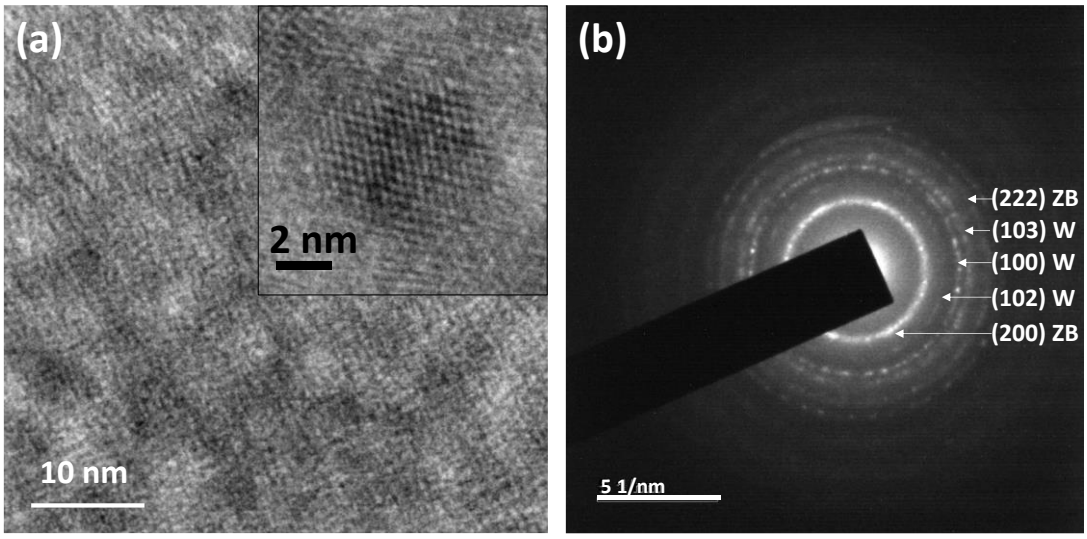

Figure 4.1. (a) TEM image of CdTe@E2MP QDs (inset shows the HRTEM image of a single QD), (b) SAED pattern of CdTe@E2MP QDs.

The X ray diffraction is performed on CdTe@E2MP sample (Figure 4.2, Table 4.1). Usually, in the case of QDs, due to the size restrictions of QDs it will be difficult to observe peaks in XRD spectra. So, fast scan will not result in any significant peak due to the dominating noise level. Hence, a slow scan of 0.5 degrees per second was performed on the sample and the peaks were spotted exhibiting the crystalline nature of the sample (Grandhi et al., 2016). The XRD pattern further corroborate with the result obtained from SAED indexing, showing two phase mixing of zinc blende (ZB) and wurtzite structures (W). The diffraction peaks indexed by comparing the data obtained with the JCPDS pattern no - 03-065-1046 demonstrate face centered cubic lattice. The indexed peaks were (111), (200), (220), (311), (222) and (400). The dominance of the diffraction peak from the crystal plane (200) over other planes could be easily seen from the Figure 4.2. Additionally, peaks corresponding to wurtzite stacking can also be seen at positions 23.25, 34.16, 38.8, 43.17 and 57° corresponding to (002), (102), (100), (103) and (203) planes respectively (JCPDS card No. 00-19-0193). The relative intensities of wurtzite peaks are less comparable to that of ZB, indicating the dominance of ZB phase.

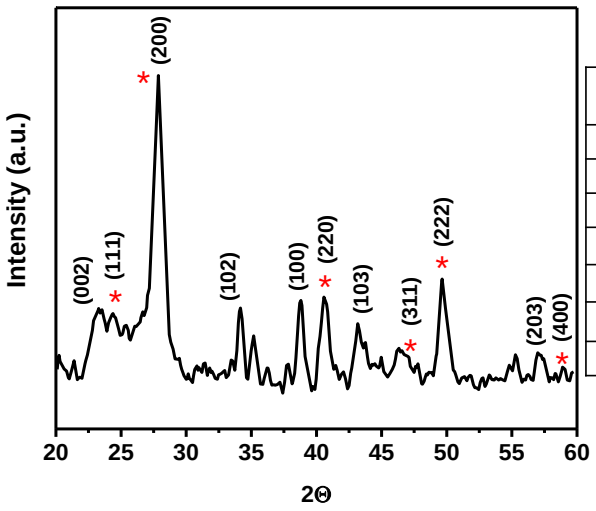

2 theta peaks (Crystal Planes)	
Zinc blende	Wurtzite
24.38° (111)	23.25° (002)
27.86° (200)	34.16° (102)
40.57° (220)	38.8° (100)
47.10° (311)	43.17° (103)
49.65° (222)	57.0° (203)
58.89° (400)	

Figure 4.2. XRD spectra of CdTe@E2MP. Peaks from ZB stacking are distinguished with an asterisk (*).

Table 4.1. 2 theta vs FWHM for CdTe@E2MP QDs

2 Theta (Degree)	FWHM (Degree)
27.8	0.58
38.7	0.48
40.5	0.76
34.1	0.42
35.1	0.43
36.2	0.28

To notice the structural changes and the molecular interactions between the CdTe QDs and the ligand E2MP, FTIR spectra were analyzed (Figure 4.3). In the case of E2MP ligand, a sharp peak was observed at 1731 cm^{-1}, which can be assigned to C=O stretching. The sharp peak at 1177 cm^{-1} corresponds to C-O stretching vibrations of C-C(C=O)-O group (Inácio et al., 2018). The C-H stretching vibrations were observed at 2983 and 2936 cm^{-1}. However, when CdTe@E2MP QDs were analyzed, the C=O stretching peak from the ligand was observed to be shifted to a lower

wavenumber of 1549 cm^{-1}. Also, C-H peaks observed for the ligand was noticed to be shifted to a slightly lower wavenumbers of 2967 and 2925 cm^{-1}. We are anticipating the conformational changes upon the interaction of QDs with ligands and the redistribution of electron density are responsible for this shift in vibrational position, as explained elsewhere (Abuelela et al., 2012). One of the significant information obtained from FTIR studies is the binding site of ligand with the QDs. A small and sharp peak was observed at 2565 cm^{-1} for E2MP ligand, which corresponds to the S-H vibrations. Absence of this signature peak in the case of QDs substantiate that the bonding of ligand with QD surface is through thiol functional group. The presence of vibrations corresponding to Cd-S at 1645 and 671 cm^{-1} is another direct evidence for this (Pandian et al., 2011; Yogamalar et al., 2015). Further, the peaks at 1549 and 1446 cm^{-1} correspond to asymmetric and symmetric vibrations of carboxylate group respectively (Yao et al., 2014; Zheng et al., 2017) and a broad peak from 3320 to 3200 cm^{-1} can be assigned to O-H stretching vibrations in the QDs.

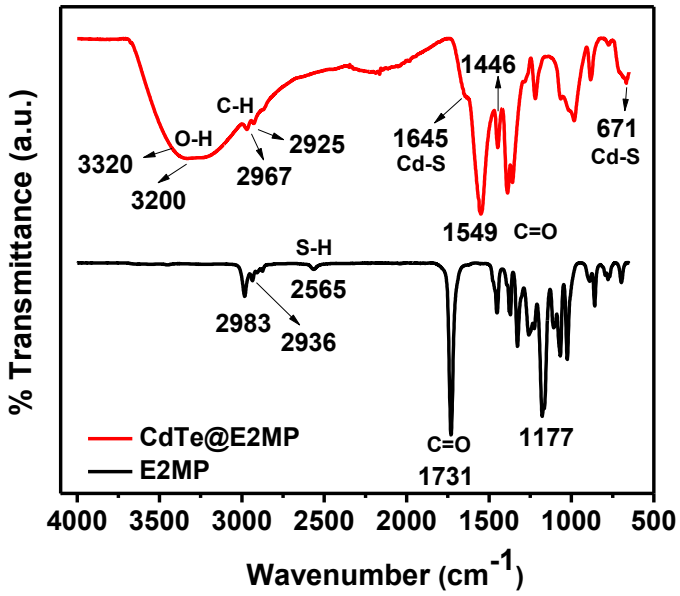

Figure 4.3. FTIR spectra of the ligand E2MP and CdTe@E2MP QDs

Further structural properties were evaluated using Raman spectral analysis which shed light to the phase, phonon mode, even crystallinity of the QDs synthesized.

Figure 4.4 shows the Raman spectra of the sample, recorded using an excitation source of 514 nm laser. As reported, Raman peak corresponding to the longitudinal optical (LO) and its second order mode (2LO) were obtained at 162 and 324 cm^{-1}, respectively. A rigorous study correlating the extend of crystallinity with the intensity of 2LO peaks of CdTe were performed by Moure-Flores et. al. (2014) The higher the intensity of 2LO Raman peak, the more will be its crystallinity. The distinct 2LO peak in the present case, corroborate with the results obtained from SAED and XRD studies. Also, the peaks correspond to the A1 and E1 mode of Te and the fundamental transverse optical mode of CdTe were obtained at 127 and 141 cm^{-1}.

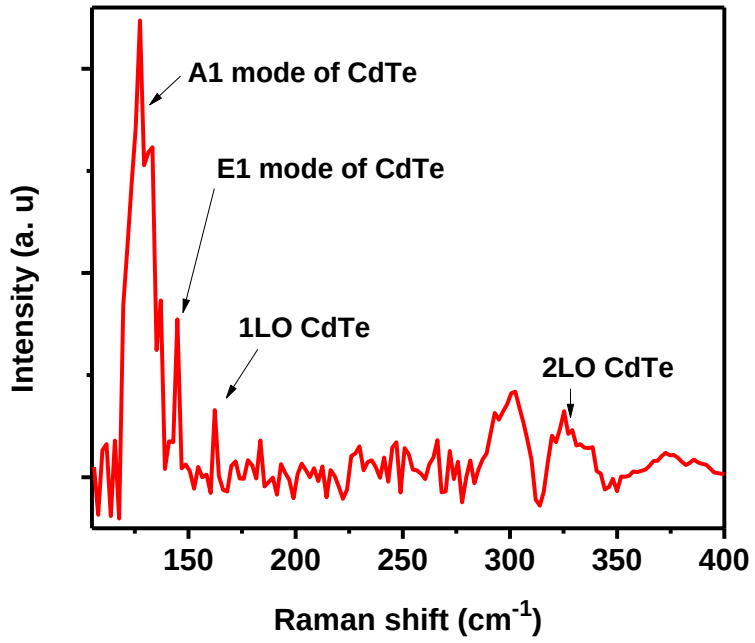

Figure 4.4. Raman spectra of CdTe@E2MP QDs

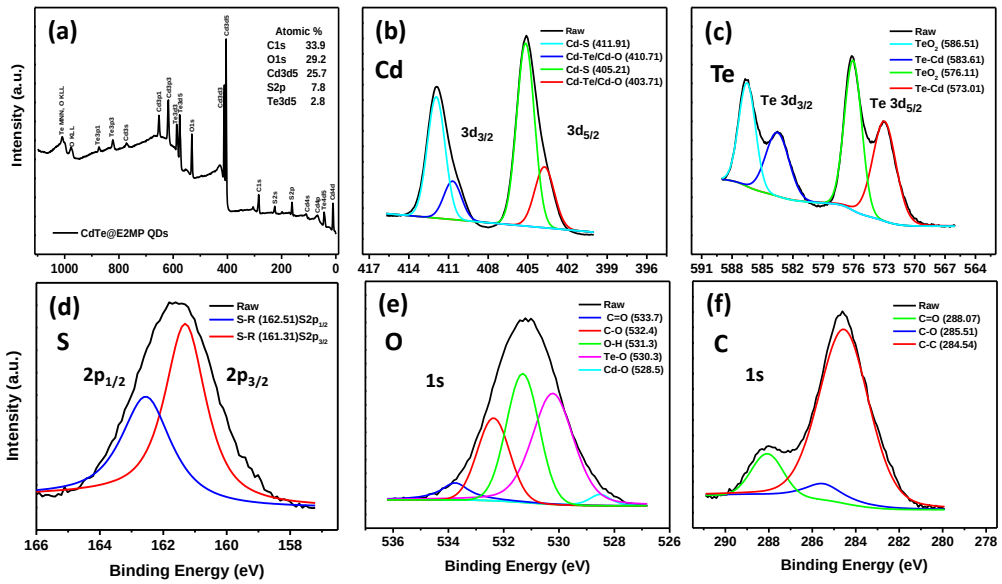

Figure 4.5. (a) Survey scan X-ray photoelectron spectra (XPS) of CdTe@E2MP QDs (b-f) High resolution X-ray photoelectron spectra (HRXPS) of Cd, Te, S, O and C of CdTe@E2MP QDs

XPS was used to further confirm the chemical state and composition of the QDs formed. The survey spectrum for powdered sample formed by drying of CdTe@E2MP solution displayed in Figure 4.5a, reveals peaks corresponding to Cd, Te, S, O and C. The corresponding deconvoluted high resolution X-ray photoelectron spectra (HRXPS) are also shown in the Figure 4.5b-f. HRXPS peaks for Cd 3d are deconvoluted into 4 peaks, where the majority of intensified signals were observed at 411.91 and 405.21 eV, which correspond to $Cd_{3/2}$ and $Cd_{5/2}$ respectively. These two peaks could be assigned to surface Cd-S (Bag et al., 2017; L. Zhao et al., 2017; Yan et al., 2016). The difference between these binding energies of Cd $3d_{3/2}$ and Cd $3d_{5/2}$ was observed to be around 6.7 eV, which corresponds to the +2 oxidation state of Cd 3d at the QDs surface (G. Yang et al., 2013; Kundu et al., 2011). The binding energies of Cd 3d peaks in CdTe and CdO lies in proximity of each other, making it difficult to identify the formation of oxide form of Cd (Schneider et al., 2009). The other two peaks at 410.71 and 403.71 can be assigned to Cd-Te/Cd-O corresponding to Cd $3d_{3/2}$ and Cd $3d_{5/2}$ respectively (Zeng et al., 2015).

The atomic ratio of Cd and Te obtained from XPS was more than 1 indicating that Te is not sufficient to stabilize the complete Cd present in the sample and hence the excess of Cd present in the sample may be getting stabilized by thiol ligands instead of Te atoms. A total of four peaks were noticed for Te, out of which, two peaks at 583.6 ($3d_{3/2}$) and 573 ($3d_{5/2}$) eV, belong to Cd-Te bond, whereas, other two peaks found at higher energies of 586.5 and 576.1 eV (Figure 4.5c) were due to the formation of oxide form of Te (TeO_2) (Hongbo Li et al., 2013; Shen et al., 2013). This partial oxidation of Te is a very common phenomenon as per reports (X. Zhang et al., 2011; Y. Liu et al., 2006; Y. J. Chen & Yan, 2009). The S2p spectrum of CdTe@E2MP is deconvoluted into two peaks, corresponding to $S2p_{1/2}$ at 162.5 eV and $S2p_{3/2}$ at 161.3 eV, with an energy difference of 1.2 eV as reported earlier (H. Peng et al., 2007). These binding energies represent the existence of chemical bonds between cadmium ions and thiols on the surface of CdTe@E2MP QDs (Cd–S-$CH(CH_3)COOC_2H_5$) (H. Peng et al., 2007). The oxygen spectrum O1s was deconvoluted into 5 peaks corresponding to C=O, C-O, O-H, Te-O and Cd-O situated at 533.7, 532.4, 531.3, 530.3 and 528.5 eV respectively (X. Zhang et al., 2011; Ying Wang et al., 2017; Ghazzal et al., 2014; King et al., 2009; Hammond et al., 1975). The C1s spectra observed around 284 eV in survey scan is deconvoluted into 3 peaks. The intensified peak at 284.5 eV corresponds to C-C bond while the oxidized form of carbon C=O and C-O is visible at 288.07 and 285.5 eV respectively (Ghazzal et al., 2014).

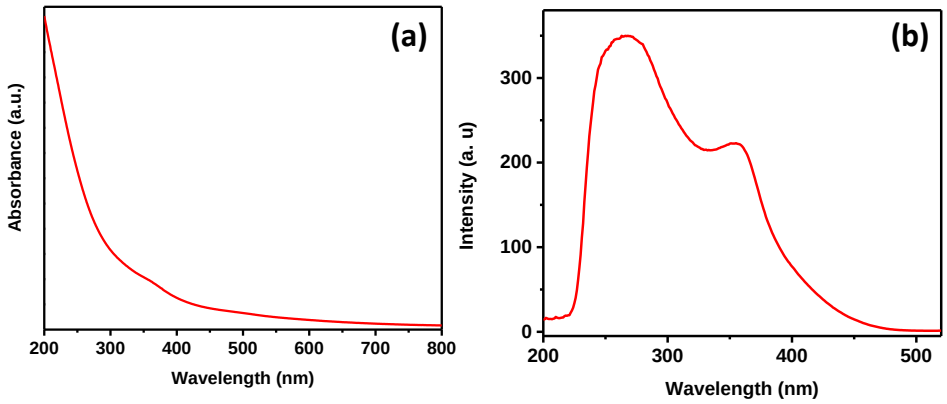

Figure 4.6. a) Absorption spectra of CdTe@E2MP b) excitation spectra of CdTe@E2MP

Thorough optical characterization of CdTe@E2MP QDs was performed using UV-visible and photoluminescence spectroscopy. The UV-visible absorption spectra were recorded after washing and purifying CdTe@E2MP QDs to elucidate the absorption features of the material. A small absorption feature was observed at 360 nm (Figure 4.6a), along with shoulder peaks around 500-550 nm region which confirms the formation of CdTe QDs having small size. The observed peak was very small and narrow, indicating the possible homogeneous size distribution of QDs formed. The excitation spectra of CdTe@E2MP were also recorded, at emission position of 560 nm, showing a prominent peak near to 360 nm corresponding to the absorption features of the QDs, around same wavelength (Figure 4.6b).

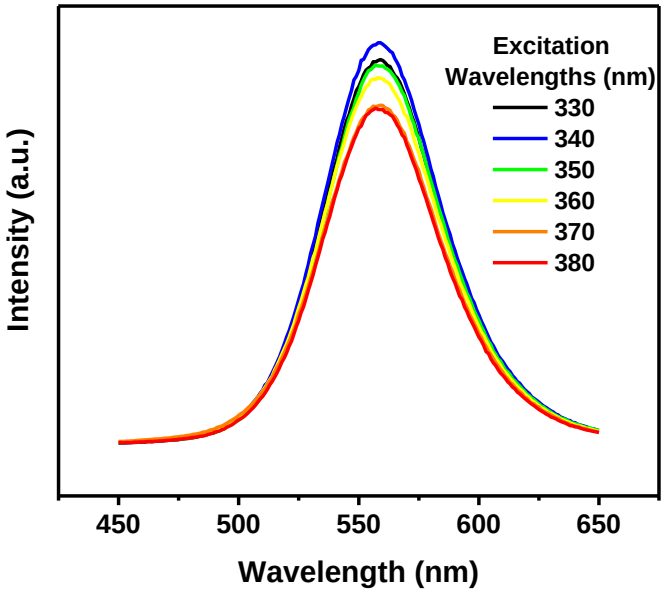

Figure 4.7. Photoluminescence spectra of CdTe@E2MP.

The steady state photoluminescence spectra of CdTe@E2MP QDs provide the information regarding the luminescence properties of the materials. The QDs were subjected to the photoluminescence studies, and it was found that CdTe@E2MP shows high yellow-green emission centered around 560 nm, when excited with a xenon lamp or illuminated under UV radiation. Maximum photoluminescence intensity was

obtained at an excitation wavelength of 340 nm. CdTe@E2MP QDs scanned with different excitation wavelength shows no observable peak shift in the emission spectrum (Figure 4.7). Hence, the emission peak is excitation independent, which further exhibits the size homogeneity of the QDs. Also, the full width at half maximum (FWHM) of the emission peak was noted to be around 45 nm. The narrow FWHM further suggests that the synthesized sample is quite monodisperse and homogeneous.

In order to calculate the band energy gap of the QDs, we have generated a Tauc plot from UV-Vis absorption spectra (Figure 4.8a). The band gap of the CdTe@E2MP QDs was calculated to be a lower value of 2.36 eV, compared to CdTe@3-MIBA (2.56 eV). The difference in the bandgap must be due to the increased average size of the CdTe@E2MP QDs (3.5 nm) compared to QDs passivated with 3-MIBA (2.3 nm). We have also calculated the VB level of the dots using cyclic voltammetric study employing ferrocene/ferrocenium couple as internal standard (Figure 4.8b) and illustrated an electronic band structure diagram of CdTe@E2MP, as shown in Figure 4.8a inset.

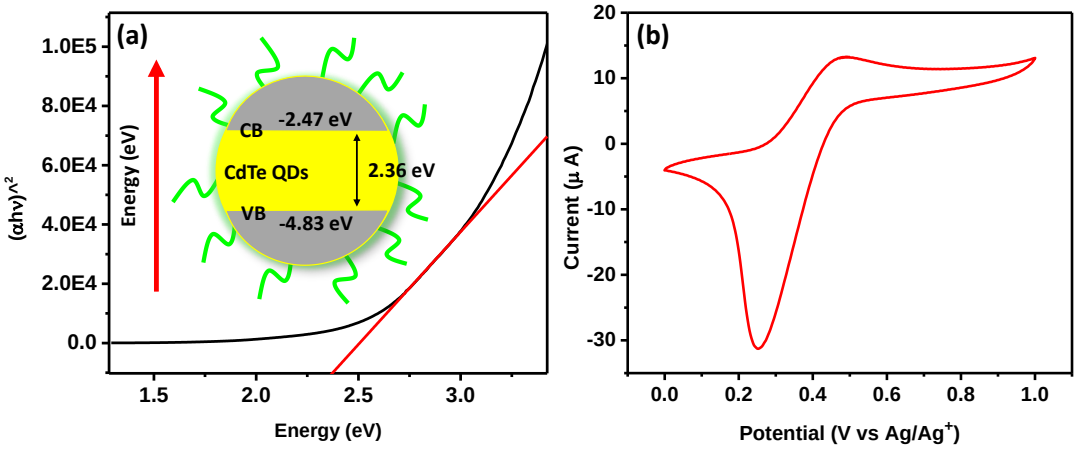

Figure 4.8. a) Tauc plot of CdTe@E2MP QDs. Inset shows electronic band structure diagram of CdTe@E2MP QDs b) The cyclic voltammogram of acetonitrile solution of ferrocene/ferrocenium couple as internal standard and CdTe@E2MP QDs deposited glassy carbon electrode as working electrode.

We have checked the temporal as well as photostability of QDs as well, since highly stable fluorophores were preferred for their applications in various fields like,

bioimaging, chemical sensing, photocatalysis, light emitting devices etc. As is visible from Figure 4.9a, CdTe@E2MP QDs, possess phenomenal temporal stability as 93 % of the original intensity is maintained even after seven months of preparation keeping at 4 °C. Therefore, the QDs can be made use for various fluorescence based applications. For photostability studies, an aqueous solution of CdTe@E2MP QDs was irradiated with UV light (365 nm, Power: 16 W) for different time intervals and the PL intensity was subsequently recorded. 50% of intensity was remaining after 150 min of continuous irradiation, showing the better photostability of CdTe@E2MP QDs compared to CdTe@3-MIBA.

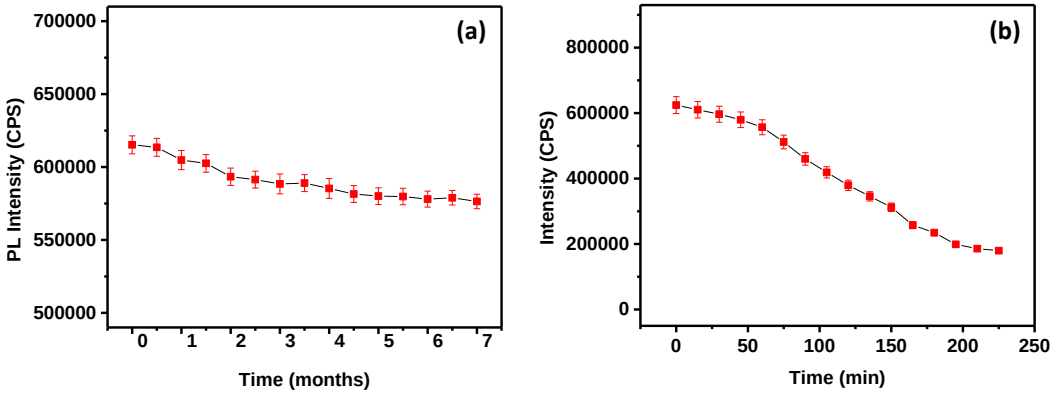

Figure 4.9. a) Temporal stability of CdTe@E2MP QDs under ambient conditions and b) photostability study under UV light.

4.2.2 Fluorescence quenching of CdTe@E2MP QDs by Cu^{2+}

Copper is an essential trace element, present in biological system, and regulation of its concentration is crucial as it can lead to undesirable health conditions. Hence detection and quantification of copper ions in biological fluids are vital. Various reports are available, where the quenching of fluorescent emission of QDs by Cu^{2+} ions was exploited for their detection (Zheng et al., 2017; Yilin Wang et al., 2009). Encouraged by these studies, we speculate that, Cu^{2+} ions can exhibit excellent quenching efficiency towards the fluorescent emission of CdTe@E2MP. The titration experiments were carried out in the presence of different concentration of Cu^{2+} ions in order to demonstrate the utility of CdTe@E2MP as a sensor for Cu^{2+}. As can be seen

in Figure 4.10, the fluorescent emission of CdTe@E2MP is found to be quenched linearly with respect to the concentration of Cu^{2+}. The sensitivity studies were performed and the Stern-Volmer plot was obtained. The linearity is noted to be from 0.5 nM to 129.5 nM with an LOD of 0.5 nM. Hence, the present sensor could be easily used for nanomolar detection of copper.

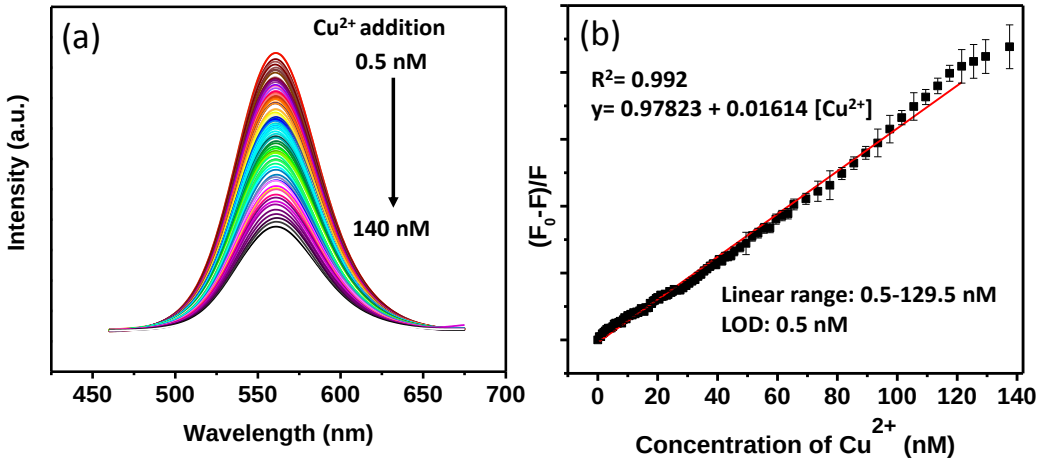

Figure 4.10. (a) Fluorescence emission spectra of CdTe@E2MP QDs with increasing concentration of Cu^{2+} ions, (b) $(F_0-F)/F$ vs concentration of Cu^{2+}.

A comprehensive study on the performance of CdTe@E2MP sensor among other CdTe QDs based sensors is performed and the results are tabulated in Table 4.2. The CdTe@E2MP sensor is comparable with other CdTe QDs based sensors capped with different capping ligands like TGA, MPA, GSH etc (Yahui Wang et al., 2016; Zheng et al., 2017; Yilin Wang et al., 2009; Yunsheng Xia & Zhu, 2008; Sha et al., 2015; Bian et al., 2015; Durán-Toro et al., 2014; A. Wang et al., 2015; Nurerk et al., 2016).

Table 4.2. Comparison of performance of CdTe@E2MP sensor with other reported works.

QDs	Capping agent	Linear range	LOD	Reference
CdTe	MPA	0 to 100 nM	0.36 nM	(Yahui Wang et al., 2016)

CdTe	MPA	$1x10^{-7}$ to $1x10^{-6}$ M	$1x10^{-8}$ M	(Zheng et al., 2017)
CdTe/CdSe	MPA	0.05 to 50 × 10^{-6} M	$2x10^{-8}$ M	(Yunsheng Xia & Zhu, 2008)
PPV@MSN @CdTe	MPA	3 $x10^{-8}$ to $1.6x10^{-7}$ M	31.2 nM	(Sha et al., 2015)
CdTe/ZnS	MPA	$2.5x10^{-9}$ to $17.5x10^{-7}$ M	$1.5x10^{-9}$ M	(Bian et al., 2015)
CdTe	GSH	10^{-9} to 10^{-8} M	$1.2x10^{-10}$ M	(Durán-Toro et al., 2014)
CdTe	L-cysteine	20 to 300 μgL^{-1}	9.3 μgL^{-1}	(Yilin Wang et al., 2009)
CdTe	TGA	0.25 – 617.53 nM	0.04 nM	(A. Wang et al., 2015)
CdTe	GSH	0.10 – 4.0 μg/mL	0.06 μg/mL	(Nurerk et al., 2016)
CdTe	E2MP	0.5 to 129.5 nM	0.5 nM	Present work

4.2.3 Selectivity of CdTe@E2MP to Cu^{2+}

The changes in the intensity of the QDs were recorded after the addition of the several metal ions and biologically relevant molecules. The largest intensity change was noted for Cu^{2+} ions as compared to the other metal ions considered in the experiment. Figure 4.11 gives a clear insight into the same. If the quenching due to Cu^{2+} ions was taken as 100% then the quenching due to all the remaining metal ions considered in the experiment was less than 25% exhibiting a very good selectivity for the Cu^{2+} ions. The remaining interfering metal ions considered for the selectivity study are Fe^{2+}, Co^{2+}, K^{+}, Na^{+}, Au^{+}, Pb^{2+}, Hg^{2+}, Fe^{3+}, Ag^{+}, Mg^{2+}, Sn^{2+}, Mn^{2+}, Al^{3+}, Ba^{2+}, Cd^{2+}, Zn^{2+}, Ca^{2+} and Ni^{2+}, biologically relevant molecules like creatinine, dopamine, amino

acids etc. From the selectivity graph, it is clear that almost all the metal ions and molecules are having more or less similar quenching intensities except Cu^{2+}. No significant interference could be observed from the investigated metal ions. Interestingly, Ag^{+} was not observed as an interferent as reported elsewhere, using TGA and MPA as ligands (Nurerk et al., 2016). Therefore, the present sensor acts as a potential candidate for the sensing of Cu^{2+} without the need for separation of interferents.

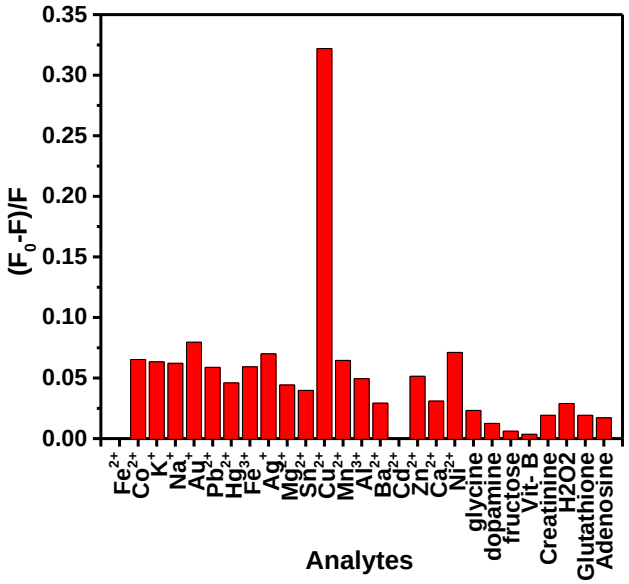

Figure 4.11. Effect of different metal ions and small molecules on the fluorescence intensity of CdTe@E2MP QDs.

4.2.4 Mechanism of Fluorescence Quenching

The interaction of the metal ions with QDs surface depends on several parameters. Hence, exploring the proper mechanism of the quenching is a critical task as metals usually tend to bind to the QDs surface. Reports are available which showcase the aggregation induced quenching, electron transfer, ground state complex formation and Förster resonance energy transfer (FRET) as major mechanism of fluorescence quenching by copper ions (Zheng et al., 2017; Sha et al., 2015; Sutter et al., 2012; Ribeiro et al., 2019). We executed various morphological and spectroscopic analysis in order to throw light into the mechanism involved during the interaction of Cu^{2+} ions with the CdTe@E2MP. As mentioned earlier, TEM results suggested the formation of

spherically shaped CdTe@E2MP QDs with good dispersibility (Figure 4.1a). The addition of Cu^{2+} ions failed to show any significant morphological changes in the QDs' structure (Figure 4.12a), which clearly indicates that the quenching is not due to aggregation of QDs upon interaction with Cu^{2+}. Though, its average size was found to be increased to 3.7 nm from 3.5 nm while retaining its crystallinity as evidenced from Figure 4.12b.

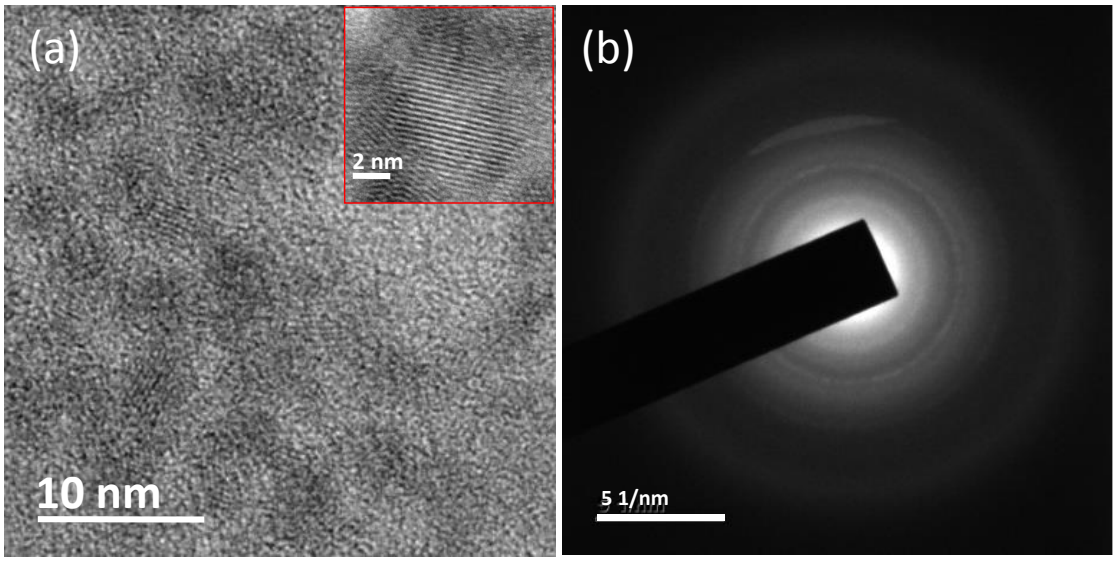

Figure 4.12. (a) TEM image of CdTe@E2MP QDs (inset shows the HRTEM image of a single QD) after the addition of Cu^{2+} ions, (b) corresponding SAED pattern

Energy-dispersive X-ray spectroscopy (EDS) was performed to identify the elemental composition of QDs. To notice the changes taking place in the sample with the addition of Cu^{2+} ions, EDS was taken for the samples, without and with addition of analyte (Cu^{2+}), and, in both the samples, we could easily locate the presence of Cd, Te, O, S and Cu (Figure 4.13a-b). The existence of Cu in QDs might be due to usage of copper grid for drop-casting the sample. Hence, the changes in the elemental composition of sensor due the addition of analyte (Cu^{2+}), could not be properly quantified using EDS. The presence of Cd and Te gives an additional layer of proof for the existence of CdTe QDs in the sample. O and S are representing the elements present in ligand, but their atomic ratios could not be relied upon since the Cu^{2+} ions were added in the QDs solution in the form of copper sulphate pentahydrate.

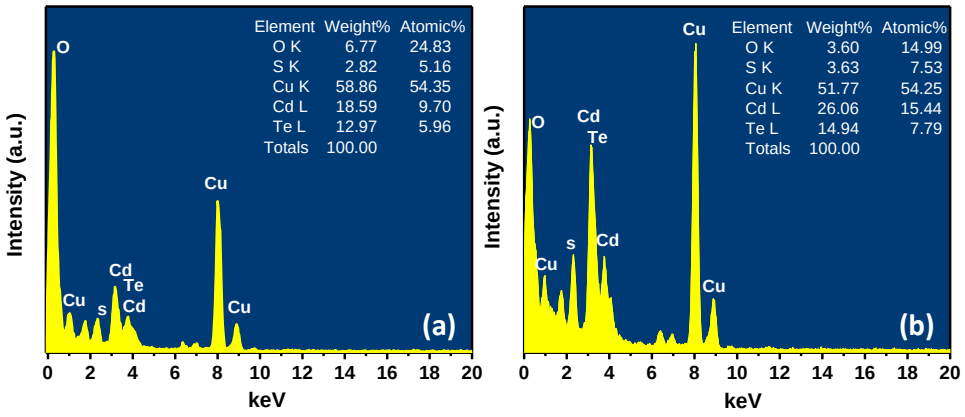

Figure 4.13. (a) EDS before addition of analyte b) EDS after addition of analyte (Cu^{2+} ions).

To discover the possibility of changes in the structure of QDs after the Cu^{2+} addition, FTIR spectrum was recorded for QDs, before and after addition of Cu^{2+}. By carefully analyzing the spectra, we could infer that, Cu^{2+} ions are not responsible for carrying out any structural changes in the QDs and is restricted to carry through only intensity changes (especially in the fingerprint region) in the vibrations (Figure 4.14). Though, no structural changes could be observed, the zeta potential mark towards the existence of possible interaction of QDs with Cu^{2+} ions. As, upon addition of 120 nM of Cu^{2+} ions, the zeta potential value of QDs was changed from -26.6 mV to -17.5 mV (see Table 4.3), which shows the destabilizing action of Cu^{2+} on the overall stability of CdTe@E2MP QDs. Further, the peaks at 1645 and 671 cm^{-1} which correspond to the Cd-S vibrations (Pandian et al., 2011; Yogamalar et al., 2015) are present even after the addition of Cu^{2+} ions; ruling out the possibility of removal of ligand E2MP by Cu^{2+}. Hence this further corroborate the hypothesis that there is no aggregation of QDs due to the removal of ligands.

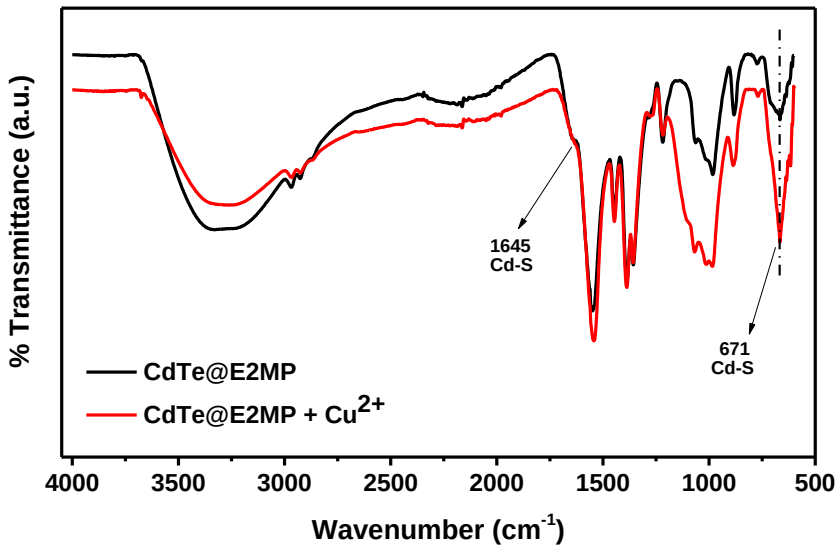

Figure 4.14. FTIR of CdTe@E2MP QDs before and after Cu^{2+} addition.

Table 4.3. Sequential decrease in the zeta values of the QDs system with successive addition of Cu^{2+} ions.

Sample	Zeta Value (mV)
CdTe QDs	-26.6
CdTe QDs + 10 nM Cu^{2+}	-24.4
CdTe QDs + 20 nM Cu^{2+}	-24.1
CdTe QDs + 40 nM Cu^{2+}	-23.2
CdTe QDs + 60 nM Cu^{2+}	-21.9
CdTe QDs + 80 nM Cu^{2+}	-20.9
CdTe QDs + 100 nM Cu^{2+}	-18.4
CdTe QDs + 120 nM Cu^{2+}	-17.5

When CdTe@E2MP QDs mixed with the copper ions was subjected to UV-visible spectroscopy, it was found that the excitonic peak intensity was going down with increasing concentration of Cu^{2+} ions (Figure 4.15a). Also, there was no

emergence of any new peak in the spectra, pointing that the addition of Cu^{2+} ions to QDs solution does not result in any ground state complex formation.

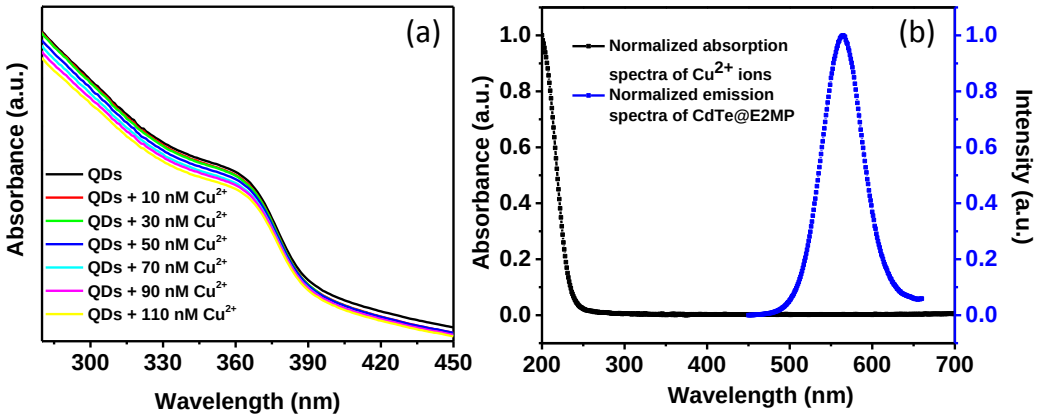

Figure 4.15. (a) Absorption spectra of CdTe@E2MP with sequential addition of Cu^{2+} ions. (b) Spectra showing the emission of CdTe@E2MP QDs and absorption of Cu^{2+}.

To identify the possibility of existence of FRET, absorbance of acceptor (Cu^{2+} ions) was taken and plotted against the fluorescence emission of the donor (CdTe@E2MP QDs), as the spectral overlap between these is a pre-requisite for FRET to happen (Zu et al., 2017). But, in the present study, such spectral overlap was not observed (Figure 4.15b). Thus, the possibility of the existence of the FRET is nullified.

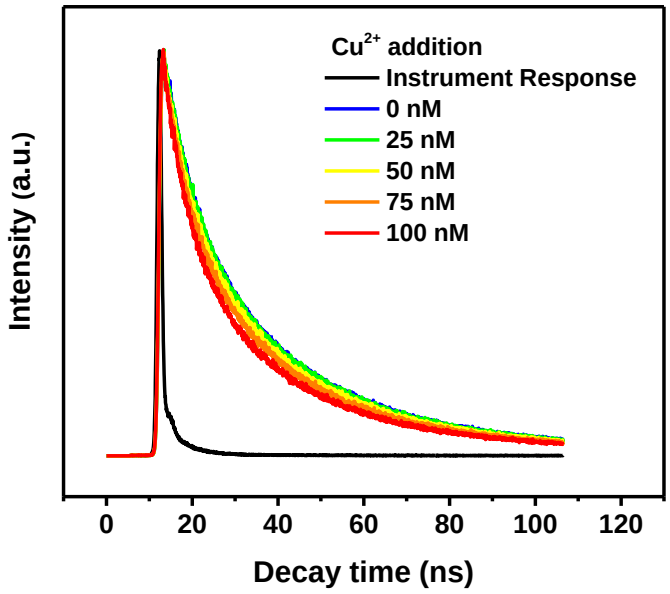

Figure 4.16. Decay curve of CdTe@E2MP QDs with sequential addition of Cu^{2+} ions

The analysis of the decay curves obtained from time resolved fluorescence spectroscopy gives an indication about the possible interactions happening in the system at the excited state providing a pathway for exploring the hidden mechanism. Hence, lifetime measurements were performed on QDs using time-correlated single-photon counting (TCSPC) by using nanosecond LED (NanoLED) as an excitation source. The NanoLED used is a pulsed diode light source having an excitation wavelength of 344 nm and a pulse duration of <1ns. The decay was recorded at different concentrations of Cu^{2+} that comes within the linear range of the sensor (Figure 4.16). The obtained lifetime profiles were fitted bi-exponentially using DAS software by maintaining χ^2 value around 1 for obtaining the best fit and the corresponding decay parameters were noted. It was observed that as the concentration of the copper ions was increased, there is a regular decrease in the decay time of QDs (refer Table 4.4). This could be possibly attributed to the electron transfer between the quencher and donor, at the excited state.

Table 4.4. Time-resolved fluorescence decay of CdTe@E2MP QDs with increasing concentration of Cu^{2+} ions (τ_1 and τ_2 are lifetime components, A_1 and A_2 are corresponding amplitude, χ^2 represents the fitting parameter and τ is the average lifetime).

Sample	τ_1(ns)	A_1	τ_2(ns)	A_2	χ^2	Average τ(ns)
QDs	6.93	12.82	27.45	87.18	1.06	26.72
QDs+25 nM Cu^{2+}	6.89	13.43	27.45	86.57	1.05	26.68
QDs+50 nM Cu^{2+}	6.4	13.29	26.66	86.71	1.08	25.94
QDs+75 nM Cu^{2+}	6.12	14.62	26.26	85.38	0.99	25.48
QDs+100 nM Cu^{2+}	5.58	15.89	25.03	84.11	1.11	24.24

Further proof for the transfer of electrons from CdTe@E2MP QDs to Cu^{2+} can be obtained from XPS analysis. Figure 4.17 shows the HRXPS peaks for Cd, Te, S and Cu. One of the major observations while comparing with the corresponding HRXPS peaks of these elements of CdTe@E2MP QDs is the presence of intense peaks at the higher energy region, probably due to the formation of oxides. The intensity of higher energy peaks of Cd and Te has increased, whereas two new peaks were emerged at 164.23 and 163.03 eV corresponding to $S2p_{1/2}$ and $S2p_{3/2}$ peaks of S-O bonds. Along with the oxidation of these elements, the HRXPS peaks of Cu found to be split into four peaks corresponding to $Cu2p_{1/2}$, $Cu2p_{3/2}$ of +2 (953.13, 933.33 eV) and 0 (952.63, 932.73 eV) oxidation states respectively. The analyte we add for the quenching studies was $CuSO_4$, having +2 oxidation state. The presence of 0 oxidation state, along with the +2 oxidation state explicitly demonstrate the electron transfer of QDs to the Cu ions, during the interaction.

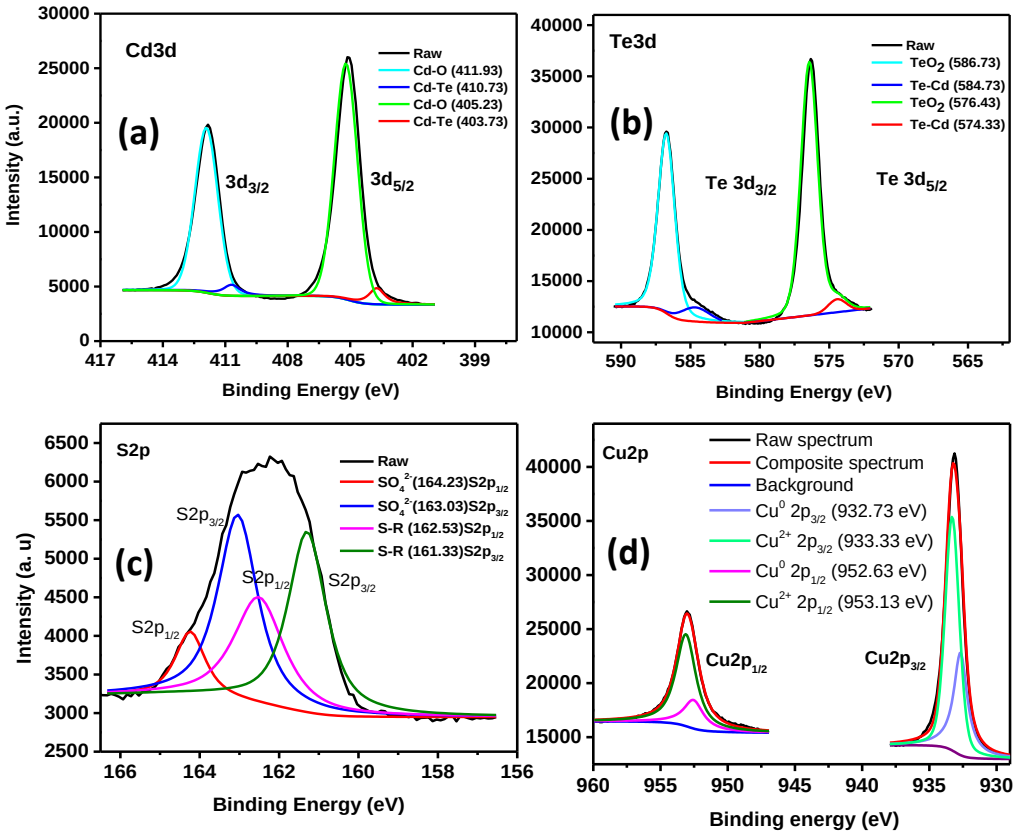

Figure 4.17. HRXPS peaks of Cd (a), Te (b), S (c) and Cu (d) of CdTe@E2MP QDs after interaction with Cu^{2+}.

The ease of electron transfer was further deciphered by cyclic voltammetric analysis of CdTe@E2MP QDs, using a three-electrode setup, with Ag/AgCl as reference electrode, Pt wire as counter electrode and CdTe@E2MP QDs deposited on glassy carbon as working electrode. A buffer of 9.2 pH was used as electrolyte solution for checking the electro-activity of CdTe@E2MP QDs. Emergence of oxidation and reduction peaks at -0.771 and -1.0078 V respectively, shows the redox nature of the QDs. The difference between the anodic and cathodic peak potentials; called peak-to-peak separation (ΔEp) of CdTe@E2MP QDs is found to be 0.2368 V. We have conducted the experiments, upon addition of Cu^{2+} ions into the electrolytic solution also. The oxidation and reduction are found to be respectively at -0.7925 and -0.9927 V, with a ΔEp of 0.2002 V. We assume that this reduction in ΔEp is owing to the less

barrier for electron transfer in the presence of Cu^{2+} ions. The results are depicted in Figure 4.18.

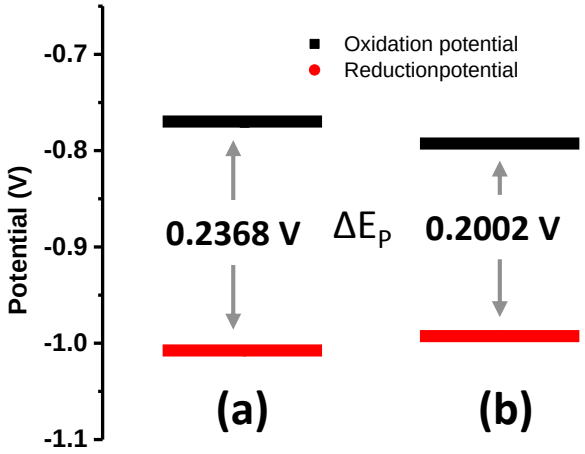

Figure 4.18. Alignment of the oxidation reduction potential of CdTe@E2MP QDs alone (a) and with Cu^{2+} (b)

Thus, we speculate that, the quenching of photoluminescence emission from highly fluorescent CdTe@E2MP by Cu^{2+} ions are due to the electron transfer from the fluorophore to quencher. The scheme of detection of Cu^{2+} using CdTe@E2MP can be schematically represented as given in Scheme 4.1

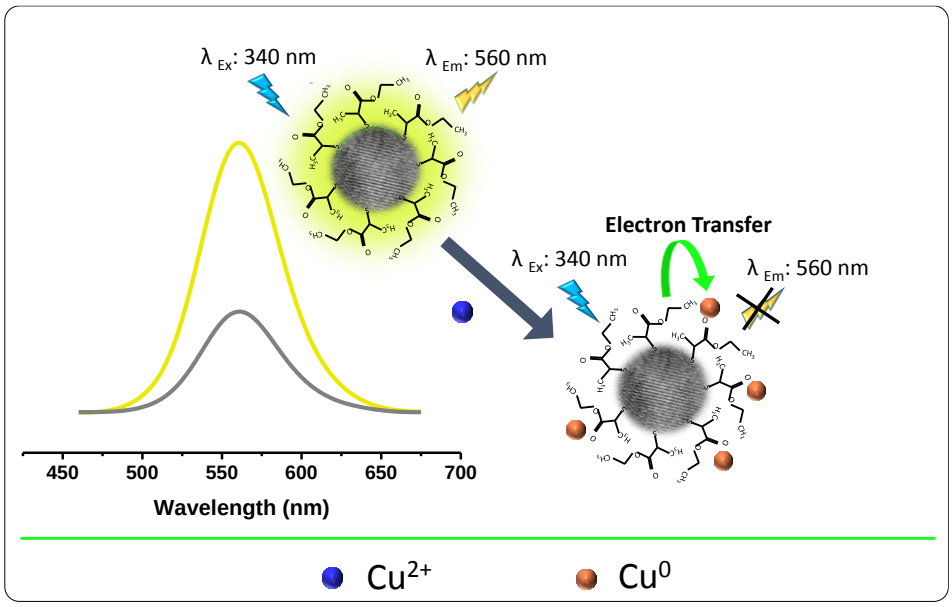

Scheme 4.1. Quenching mechanism of CdTe@E2MP QDs by Cu^{2+}

4.2.5 Visual detection and real sample analysis

Evaluation of the utility of CdTe@E2MP QDs as a sensor for Cu^{2+} in real sample analysis was performed using tap water, pond water and rainwater samples. The samples were then spiked with known concentrations of Cu^{2+} and introduced into 2.5 mL of CdTe@E2MP QD solutions. The PL intensity of the solution was recorded after the addition of the Cu^{2+} solutions and the amount of Cu^{2+} recovered was calculated. Each experiment was repeated three times and the average values with the corresponding percentage recovery are summarized in Table 4.5. The present detection strategy was found to be superior, as it can detect the amount of spiked Cu^{2+} concentration with relatively good accuracy, and good % RSD.

Table 4.5. Detection of Cu^{2+} in the real samples.

Sample	Spiked (nM)	Found (Mean; nM)	Recovery	% RSD
Tap water	0	0.2194±0.69	-	2.5
	20	20.228±0.16	100.5- 101.1 %	2.8
	30	31.6246±1.14	102.7- 105.4 %	2.9
Pond water	10	12.41±0.49	123.1- 123.6 %	0.4

	20	22.43±0.31	110.4- 113.3 %	1.4
	30	32.98±0.39	109.0 -110.8 %	1.2
Rainwater	10	10.61±0.24	104.4-107.9 %	2.3
	20	20.99±0.26	104.1-105.9 %	1.2
	30	30.44±0.33	100.7-102.2 %	1.1

A solid substrate-based detection of Cu^{2+} was demonstrated in order to check the utility of the present sensor for the practical application scenario. The sensor material was initially drop-casted onto TLC plate and dried. Different concentrations of Cu^{2+} (50 nM, 100 nM, and 200 nM) were deposited on to these dried sensor spots and illuminated under UV radiation (365 nm). As is evident in Figure 4.19, an easy qualitative detection of Cu^{2+} can be realized using CdTe@E2MP QDs using a handy substrate.

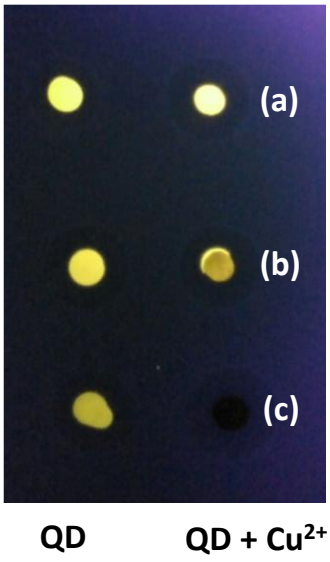

Figure 4.19. Photographs of TLC plate based sensor platform. The first column represents CdTe@E2MP QD drop casted on TLC under UV light (yellow-green dots), other rows represent QDs treated with a) 50 nM b) 100 nM and c) 200 nM concentrations of Cu^{2+}

4. 3 Conclusion

Highly stable CdTe QDs synthesized by one pot synthetic strategy using the ligand E2MP were characterized by the commonly used spectroscopic and microscopic techniques and its properties were explored. The synthesized QDs were used for sensing heavy metals and found to be highly selective towards Cu^{2+} ions. LOD and linear range of the sensor were identified to be 0.5 nM and 0.5 nM–129.5 nM respectively. The sensor was further studied for unveiling the quenching mechanism. Hence, an effective nanomolar Cu^{2+} sensor was established using CdTe QDs stabilized by a novel bio ligand E2MP.

CHAPTER 5

SYNTHESIS AND CHARACTERIZATION OF CdTe QDs CAPPED WITH BRANCHED 3MB3MP LIGAND AND FLUORESCENT SWITCHING DETECTION OF H_2O_2

Owing to the possibility for modification with various multifunctional ligand groups, and thereby attaining selective and sensitive detection; water soluble quantum dots (QDs) always attract scientific attention, in the realm of fluorescence based sensing. Herein, we describe the synthesis of highly fluorescent water soluble CdTe QDs using a novel branched ligand 3-Methoxybutyl 3-mercaptopropionate (3MB3MP), by facile colloidal synthesis method. The synthesized QDs shows excitation independent high fluorescent emission at 590 nm wavelength with excellent temporal stability and an atypical phenomenon of photo-enhancement effect. A novel label free fluorescence based detection of H_2O_2 has also been demonstrated using CdTe@3MB3MP QDs. The fluorescent emission of CdTe@3MB3MP QDs were found to be enhanced in linear fashion in the presence of H_2O_2, within a linear range of 10-250 nM concentration, which then found to plummet significantly upon concentrations higher than 300 nM. A thorough photophysical and microscopic characterizations have been carried out in order to unveil the mechanism of photo-enhancement as well as H_2O_2 detection.

5.1 Introduction

In the realm of chemical sensors, optical sensors are prominent owing to its inherent characteristics where light-matter interactions are continuously monitored. These include detection and quantification of analytes with high detection sensitivity, non-contact or long distance monitoring, lack of analyte consumption as well as electrical interference, wavelength selectivity etc. (Orellana, 2006). Of these,

fluorescence based sensors have their own advantages such as high sensitivity, facile and easy mode of operation, availability of numerous parameters to serve as analytical information etc. (Wolfbeis, 2005). Therefore, discoveries of novel sensitive fluorophore materials with exotic properties always catch significant attention. Semiconductor based Quantum dots (QDs) are such a new class of fluorescent materials with unique and superior optical properties such as high photo-bleaching threshold compared to organic fluorophores, good chemical stability, broad absorption and size-tunable photoluminescence with narrow emission wavelengths.

The choice of surface capping agents of semiconductor quantum dots is crucial, as it can advocate their optical properties such as fluorescence, quantum yield (QY) and can determine stability and solubility in a major extend. The fluorescence emission of QDs is prone to changes in its micro-environment as well, such as changes in pH of the solution, presence of interacting species etc. which makes QDs a versatile probe for fluorescent based sensors. The surface imperfections or the dangling bonds on the surface of QDs are found to be seats for exciton recombination, which in turn favor non-radiative emission, and thereby creating quenching of fluorescence emission (Reiss et al., 2009). Many analytes are capable of quenching the fluorescence of QDs (turn-off sensors), attributed to the formation of these non-radiative recombination centers. Surface modification is the key for restricting such trap states, concurrently which enhance the fluorescence emission of the QDs. For example, the emission efficiency and quantum yield of the MPA-capped CdTe quantum dots were improved by addition of reduced glutathione (GSH). This is due to the complexation of incompletely bounded cadmium ions on the QDs surface by GSH thiol group, thereby passivating the trap states at the surfaces (Rodrigues et al., 2014). In another report, Glyphosate (Glyp) ligand was utilized for the modification of the surface of thioglycolic acid (TGA) capped CdTe/CdS QDs, resulting in the fluorescence intensity enhancement, which is attributed to the passivation of trap states through the chelate bond between PO_3^{2-} group and Cd^{2+} also through the hydrogen bonds with TGA (Z. Liu et al., 2012). Recently Gong et al. (2017) reported improving the fluorescent intensity of CdTe QDs using hepatitis B core antibody labeled with horseradish

peroxidase (HBcAb-HRP). The mechanism is attributed to the sulfurs in the ligands having strong affinity towards Cd^{2+}, which create more radiative centers at CdTe/Cd-SR complex, ultimately improving the recombination fluorescence of CdTe QDs. Enhancement effect of (MPA)-capped CdTe nanocrystals by cysteine and homocysteine (Y. S. Xia & Zhu, 2009), N-Acetyl-l-cysteine (Frigerio et al., 2012), or doping with silver impurities (S. J. Ding et al., 2015) and effect of TGA-capped CdS QDs by melamine (G. L. Wang et al., 2012) are other examples of fluorescence enhancement by surface modification. Apart from ligands small analyte molecules also can enhance the fluorescence emission of the QDS. Such turn-on sensors are more preferable to turn-off sensors, owing to the less chance for false positives, and as such are rare as well.

The variation of luminescence intensity of QDs in response to exposure of light (photobleaching and photobrightening) is another common phenomenon, which yet need a better understanding. Both the enhancement and quenching of intensity has been reported. Of these, the increase of fluorescence intensity, which is commonly termed as photo-activation is more intriguing which is attributed to different mechanisms, such as surface modification of QDs by light-induced generation of heat, surface passivation by photoadsorbed molecules, e.g. adsorption of water molecules or reactive oxygen species or polar solvents, surface passivation by light induced rearrangement of capping agents, surface smoothening of QDs due to photo oxidation or photo corrosion etc. (Carrillo-Carrión et al., 2009; Patra & Samanta, 2014; Patra & Samanta, 2013; Pechstedt et al., 2010). Owing to the importance of photo-activation as its direct influence towards the optical attributes and other properties of QD, an ample understanding of the mechanism of the process is highly crucial.

Hydrogen peroxide, a stable member of reactive oxygen species (ROS), is generally renowned for its cytotoxic effects (usually at a concentration > 50 µM) and cautioned to regulate the amount produced in the cells by means of various antioxidant defense enzymes (Halliwell et al., 2000). Even though myriad reports are focusing on the cell death and cardiovascular events induced by H_2O_2, recent reports focus on its

remarkable role in physiological signaling mechanisms as inter- and intra-cellular signaling molecule (Chang et al., 2013; Wu et al., 2011; Yun & Yingqiu and Dorn, 2010). For example, role of H_2O_2 as a messenger in the stimulation of JAK2 activity, ERK2 activity, and activation of NFκB etc. has been reported (Sauer et al., 2001; Simon et al., 1998; True et al., 2000; Abe et al., 1998). Therefore, along with the amount of H_2O_2 formed, the type of cell, its physiological state, time period of exposure, as well as cell culture media of the studies determines its effects on the cell. Therefore, it is imperative to determine the concentration of H_2O_2 in the biomedical field. Our aim is to utilize the enhancement effect of fluorescent intensity of CdTe@3MB3MP QDs in the presence of H_2O_2 for its efficient detection.

In this chapter, we describe a highly selective and sensitive detection of H_2O_2, based on the principle of enhancement of fluorescent intensity of CdTe QDs capped by a novel branched ligand 3-methoxybutyl-3-mercaptopropionate (3MB3MP). We anticipate that, due to the steric effect/ bulkiness of the ligand, the initial ligand coverage of the QDs is very modest, and the surface passivation can be effective in the presence of small H_2O_2 molecules, which emerge as fluorescent enhancement. The analytical performance of the system is satisfactory in terms of selectivity and the lower detection limit value (10 nM).

5.2 Results and Discussions

5.2.1 Characterization of CdTe@3MB3MP

On account of practicability, efficiency and easiness of method, we have synthesized CdTe QDs passivated with a novel branched ligand, 3-Methoxybutyl 3-mercaptopropionate employing facile colloidal strategy using optimized reaction conditions. The as synthesized QDs were then characterized thoroughly using various microscopic as well as spectroscopic means.

The combination of TEM and SAED allow us to understand the morphology and crystalline nature of the nanomaterials formed. Figure 5.1, attest the successful synthesis of highly homogenous quantum dots of spherical morphology. The QDs are not aggregated and displayed well resolved individual particles. Statistical analysis of high resolution TEM images reveals the average size of QDs are 4.63 nm. Further, the selected area electron diffraction (SAED) pattern of QDs suggest the crystalline nature of the synthesized quantum dots. The SAED indexing reflects the formation of zinc blende as crystal structure.

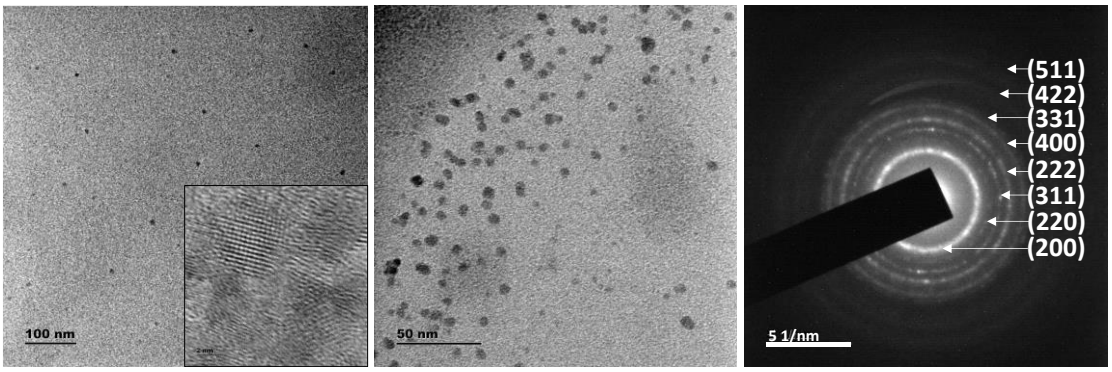

Figure 5.1. TEM and SAED pattern of CdTe@3MB3MP QDs

The typical XRD pattern of CdTe QDs is depicted in Figure 5.2, which further confirm the crystalline nature of the CdTe@3MB3MP QDs. The spectrum exhibits major diffraction peaks at 2θ= 23.7°, 39.6° and 45.8°, 57° etc. corresponding to the planes (111), (220), (311) and (400) respectively. These are attributable to the cubic (zinc blende) crystal structure, which matches with the JCPDS card number 03-065-1046; thus, confirming the formation of the CdTe quantum dots (Tenório et al., 2015).

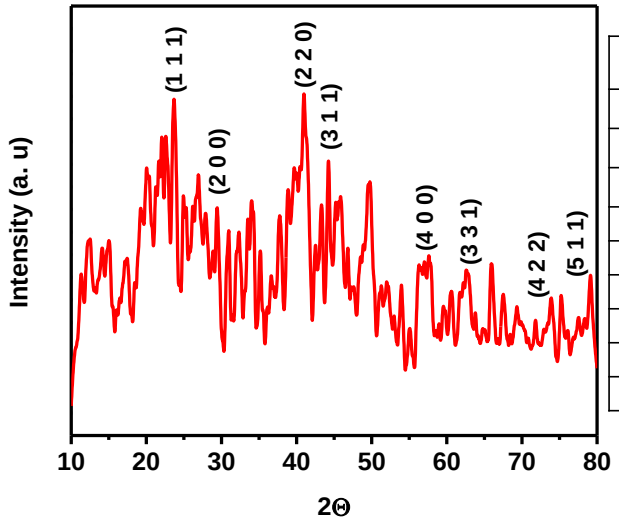

2 theta peaks	Crystal Planes
23.7°	(111)
28.9	(200)
39.6°	(220)
45.8°	(311)
49.4°	(222)
57.0	(400)
65.9	(331)
73.9	(422)
79.1	(511)

Figure 5.2. XRD pattern of CdTe@3MB3MP QDs

The structural properties of QDs were analyzed using FTIR and Raman spectroscopies. Figure 5.3a depicts the FTIR spectra of free ligand and ligand associated with QDs. The peaks observed for ligand alone and QDs located around 2900 cm^{-1} are corresponding to C-H asymmetric and symmetric stretching vibrations. Bands located around 3300 cm^{-1} for QDs are corresponding to –OH vibrations. Peaks observed at 1554 and 1302 cm^{-1} for QDs are the asymmetric and symmetric stretching of COO- group of the ester. One of the significant differences in the spectra of ligand and QDs are the peak corresponding to SH vibrations. For ligand, SH peaks are present at the 2568 cm^{-1}, which is absent in the case of QDs. This validates the successful binding of ligands to the surface of QDs through S bonding, and the intact COO- peaks preclude the possibility of binding through O (L. Li et al., 2017). Raman spectral analysis is well known non-destructive characterization technique, with which we can determine the phase, phonon mode, even crystallinity of the QDs synthesized. Figure 5.3b shows the Raman spectra of the sample, recorded using an excitation source of 514 nm laser. The longitudinal optical (LO) and its second order mode (2LO) at 327 cm^{-1} correlate to the Raman peak at 162 cm^{-1}. The intensity of 2LO Raman peak is an indirect way to check the crystallinity of the QDs, the more intensity, the better crystallinity. The intense peak in the present case, corroborate with the results obtained

from SAED and XRD studies. The peaks at 125 and 142 cm^{-1} correspond to A1 and E1 mode of Te and the fundamental transverse optical mode of CdTe (Kale et al., 2012; Frausto-Reyes et al., 2006).

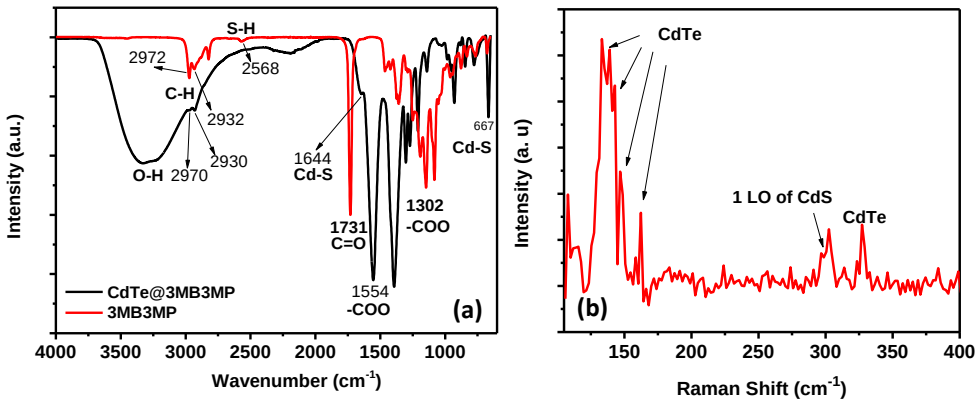

Figure 5.3. a) FTIR spectra of CdTe@3MB3MP QDs b) Raman spectra of CdTe@3MB3MP QDs

XPS analysis were carried out for determining the elemental composition and to identify the chemical states of the elements present in the QDs. Figure 5.4a shows the survey scan spectrum of CdTe QDs. Peaks corresponding to different Cd and Te core levels were visible, along with the peaks for C, S and O, which are present in the ligands. Of the core levels of Cd and Te, we consider peaks corresponding to 3d for HRXPS analysis. The binding energy of Cd $3d_{3/2}$ and $Cd3d_{5/2}$ are found to be at 411.6 and 404.6 eV respectively, which is in agreement with the values reported for Cd linked to Te in CdTe material (Shen et al., 2013). And the peak corresponding to 3d levels of Te are located at 571.9 ($3d_{5/2}$)and 582.4eV ($3d_{3/2}$) (Shen et al., 2013; H. Zhang et al., 2003). The existence of these peaks confirms the formation of CdTe QDs. The absence of any other peaks in the higher binding energy region of Cd or Te rules out the possibility of oxidation of QDs, or formation of oxide layer during the refluxing time. To investigate the possibility of formation of CdS nanoparticles, during the reaction, as S containing ligands were being added prior to the addition of Te precursor, HRXPS spectra of S is also analyzed. The spectrum shows peaks at 161.9 and 163.2 eV corresponding to $S2p_{3/2}$ and $S2p_{1/2}$ of organic stabilizer. The value for $S2p_{3/2}$ peak for CdS is reported to be below 161.7 eV, and the absence of multiple peaks for S HRXPS

justify the formation of CdTe QDs alone and no S is incorporated into CdTe lattice (Kakuta et al., 1985; Borchert et al., 2003; Shen et al., 2013).

.

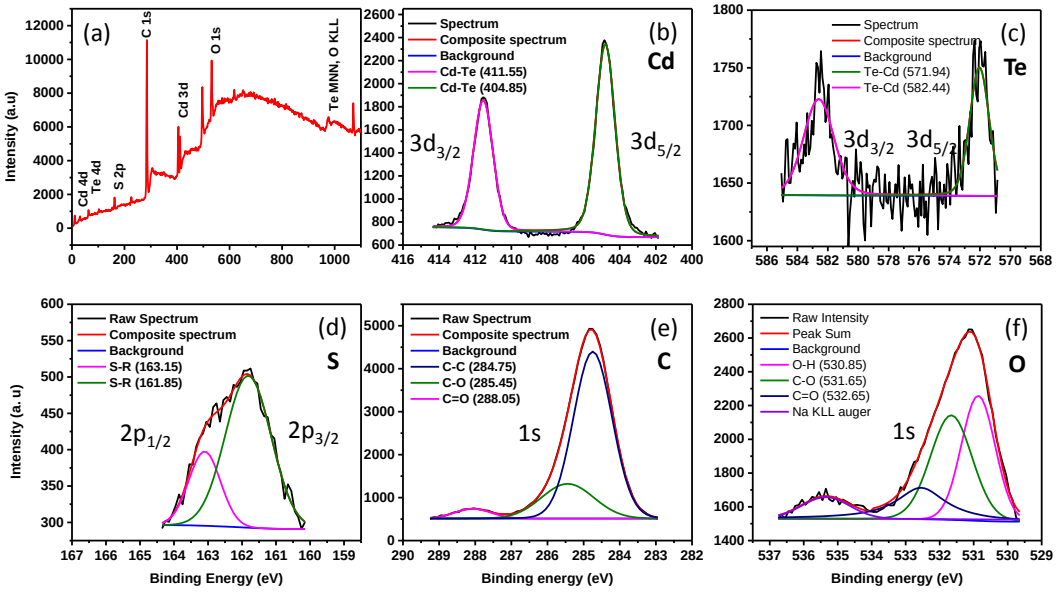

Figure 5.4. a) Survey scan spectra of CdTe@3MB3MP. b-f) HRXPS spectra of Cd, Te, S, C and O respectively

One of the unique attributes of semiconductor based QDs are their size dependent optical properties. As the size of the QDs shrinks, the absorption peak shifts to higher energy regions (lower wavelength) due to quantum confinement effect. Also, the peak intensity and nature of the peak (broad or narrow) depends on the size distribution of QDs. The reason behind this observation is that QDs absorb the energy, same as their bandgap, which invariably depends on the size of QDs (C. Xia et al., 2018). Figure 5.5 illustrates the ground-state electronic UV-Vis absorption spectra of CdTe QD@3MB3MP. A well resolved characteristic peak of QDs can be seen around 350 nm, along with small peaks around 500-600 nm region. Also, the narrow FWHM of the peak demonstrate the narrow size distribution of the QDs. The inset to Figure 5.5a shows the excitation spectra of the sample at an emission position of 590 nm. The multiple peaks reveal the possible energy levels of the QDs.

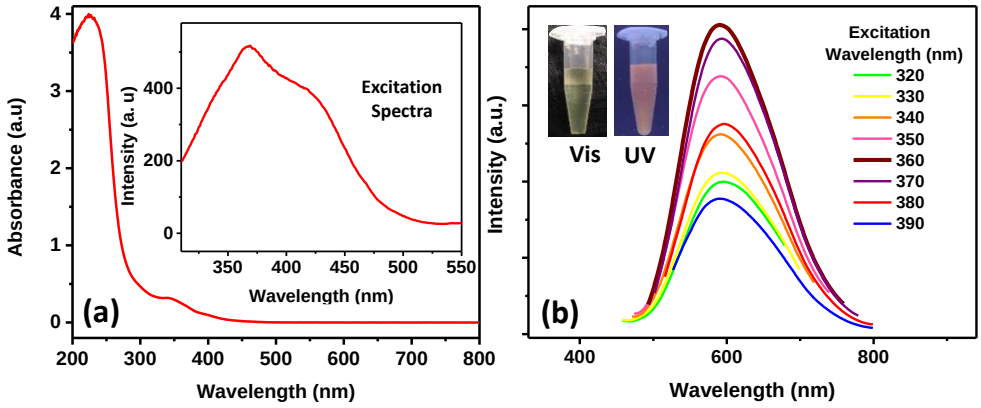

Figure 5.5. a) Absorption spectra of CdTe@3MB3MP. Inset shows the excitation spectra. b) Excitation independent emission spectra of CdTe@3MB3MP

Another salient feature of the CdTe@3MB3MP QDs is their photoluminescence emission, which also arise due to the quantum confinement effect. The reason for the emergence of fluorescence emission is due to the recombination of charge carriers (electron-hole pairs) upon excitation. Figure 5.5 b depicts the excitation independent emission spectra of the QDs. The maximum emission is found to be at 592 nm, upon excitation of 360 nm. The generation of high intense red light demonstrated the passivation capacity of the novel ligand. The quantum yield of the QDs is calculated to be 12 %.

5.2.2 Photo-enhancement effect of CdTe@3MB3MP

The surface chemistry of the QDs is known to have largely depend on the nature of the capping agent and medium of dispersion. The effect of continuous exposure of UV radiation (365 nm; power 16 W) on the emission spectra of the QDs is depicted in Figure 5.6. Nearly 26-fold enhancement of the fluorescence intensity is observed within a time duration of ~190 min along with a shift of the maximum emission peak from 592 to 528 nm. The quantum yield of this sample measured is 56.35%, which is around 5-fold increment from the QD synthesized. Whereas further illumination leads to a sudden decrease in emission intensity along with a small blue shift of emission maxima from 528 to 520 nm.

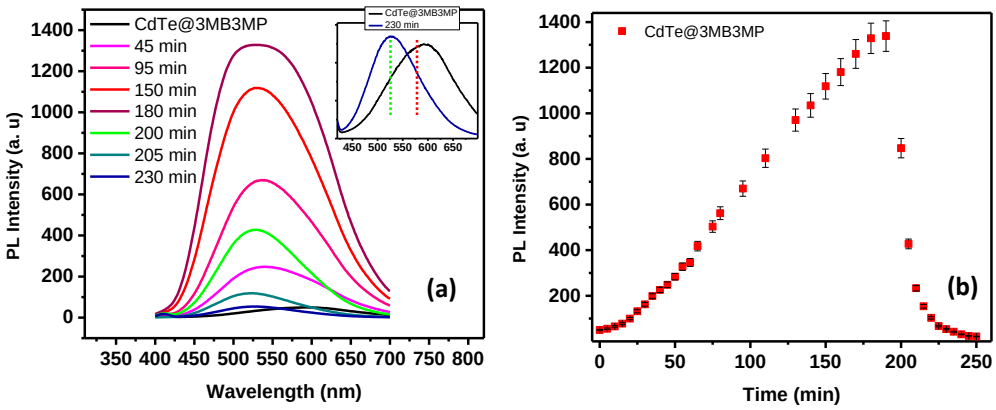

Figure 5.6. a) Photoactivation study: steady state spectra showing enhancement of fluorescence emission with blue shift b) photoactivation spectra of maximum emission intensity plotted against time

A thorough literature review has been carried out in order to unveil the mechanism of photo activation of the synthesized CdTe QDs. Apart from common mechanisms such as surface modification or surface passivation, there is a possibility for multiple mechanism acting simultaneously, as reported by Carrilio-Carrion et al. (2009) as the combination of photo-oxidation and photo-adsorption of water molecules for the photo activation of CdTe QDs. Therefore, ample control experiments were carried out in the present case, as discussed in the coming sections.

Being highly stable in aqueous media and solvent medium used for the studies being water, we consider the possibility of surface passivation of QDs by photo-adsorbed H_2O molecules, as our first hypothesis, for the initial enhancement of fluorescence intensity. As we have already discussed, the QDs taken in water as solvent shows huge enhancement in the emission with a blue shift of emission position. In addition to that, we have observed a drop of fluorescence intensity in the enhanced sample, upon keeping the solution in dark, which can recover again upon irradiation (Figure 5.7a). This clearly shows the photo-adsorption of water as a major mechanism of activation (Patra & Samanta, 2014). Also, the experiments were repeated with purified QDs, dissolved in methanol solution. As can be seen in Figure 5.7b, practically, there were no visible enhancement in the solution upon irradiation for a time duration

of 240 minutes. This large enhancement of emission of QDs in water, whereas, no visible changes in non-aqueous, solvents establishes the role of water in the enhancement mechanism. Thus, we anticipate that the surface trap states of QDs were efficiently passivated by the photo-adsorbed water molecules at the early stages of irradiation of the QDs with UV rays.

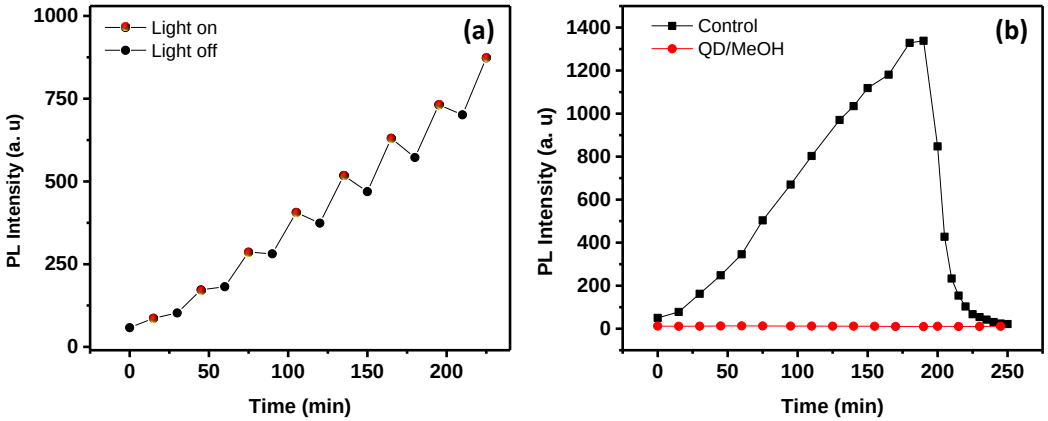

Figure 5.7. a) Photoactivation study with light on and off. b) Photoactivation study using methanol as solvent

A close observation of the variation of emission intensity with respect to time of irradiation further throw light into the possibilities of other mechanisms. As we can see, the initial increase of fluorescence intensity is slow and steady till 190 minutes of continuous irradiation with a large blue shift of emission maxima, which then decrease rapidly, with a small blue shift. This clearly indicate two competing processes, one which increases the intensity at the early stages, which later dominated by another process finally leading to the quenching of fluorescence emission (Patra & Samanta, 2014). In order to understand the role of dissolved oxygen, we carried out the irradiation experiments in aerated samples as well as de-aerated samples prepared under a nitrogen atmosphere (Figure 5.8). A steady increase in the fluorescence emission were observed, even in the absence of oxygen, which rule out the role of oxygen in the photoactivation process. However, the sample purged with N_2 shows no immediate quenching of fluorescence even after irradiation of 270 minutes, which conclusively prove the inevitable role of oxygen in the quenching of emission. Thus, we anticipate that, the

later quenching of emission may be due to the slow photo-oxidation or photo-corrosion process.

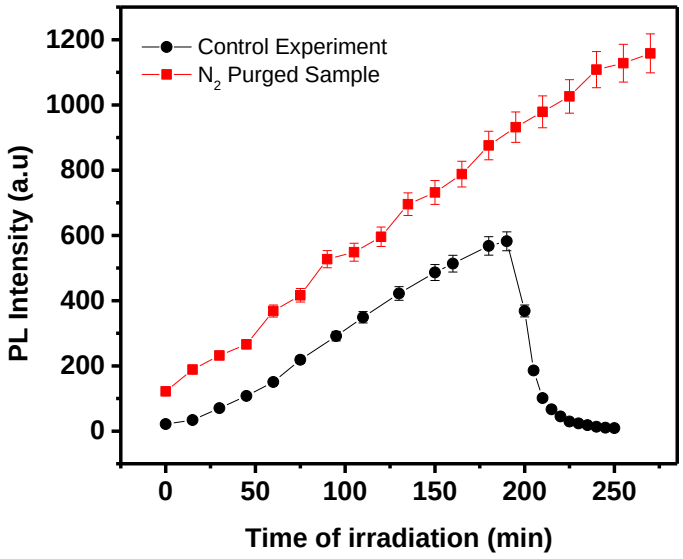

Figure 5.8. Photoactivation study of the nitrogen purged sample

In addition to that, the chemistry of formation of reactive oxygen species (ROS) from water are well known upon continuous irradiation of high energy UV radiation. Therefore, we cannot circumvent the possibility of the formation of such ROS in the present case as well. As a proof of concept, we carried out the photoexcitation experiments in the presence of an antioxidant, beta mercaptoethanol (BME). BME is capable of reducing free radicals, which ultimately can prevent the generation of any ROS formed in the sample mixture (Cooper et al., 2009). Very strikingly, we couldn't observe, any significant changes upon irradiation of QDs in the presence of BME (Figure 5.9a). We assume that the in-situ formed ROS might be getting reduced in the presence of BME, before they could encounter with the QDs in solution. This unambiguously prove the crucial role of ROS in the enhancement of PL emission of QDs upon irradiation. So as to confirm the formation of ROS and its effects on photobrightening, we conducted the experiments using green LEDs with lower power (Figure 5.9b). No enhancement was observed after irradiation of longer time duration, which confirms this assumption. Hence, we envisage that, with the exposure

of light, the electrons in the QDs are getting photoexcited to its conduction band, which can electrostatically attract reactive oxygen and other species in solution to the surface of the QDs. These moieties are highly capable of interacting with the trap states of QD surfaces. The better the interactions and bonding, the more complete can be the passivation, which ultimately brings about the brighter QDs (Y. F. Liu & Yu, 2010; Trotzky et al., 2008). The TEM analysis shows the QDs are intact during photobrightening, but with a small reduction in size to 3.35 nm, which explains the blue-shift of the emission position (Figure 5.10)

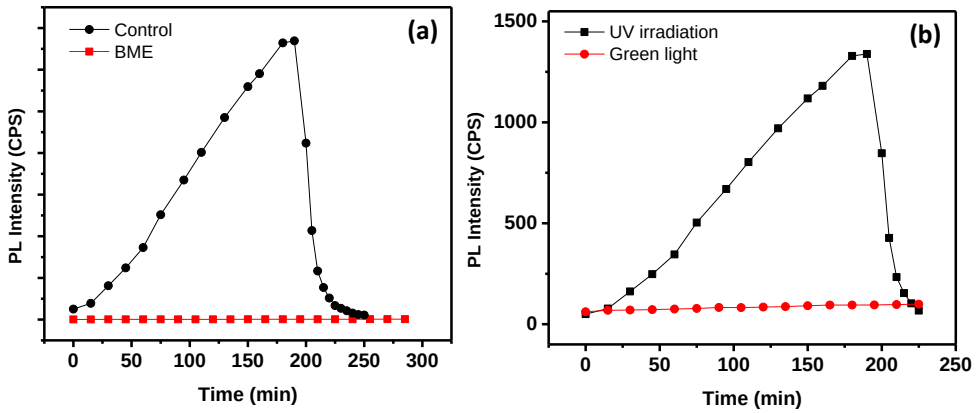

Figure 5.9. a) Photoactivation of QDs in the presence of beta mercapto ethanol b) photoactivation study using green light

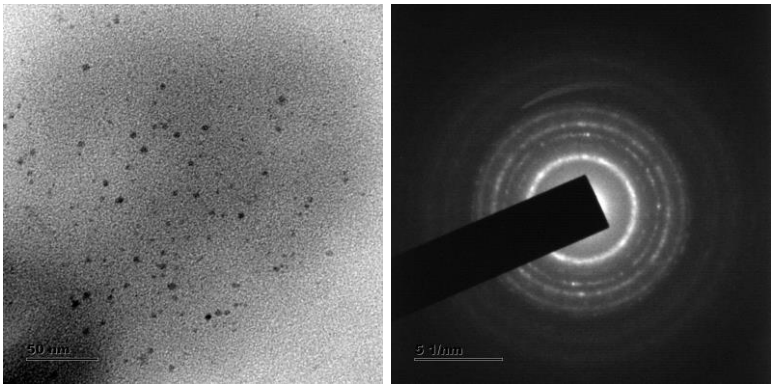

Figure 5.10. TEM images of CdTe@E2MP 3MB3MP after 150 minutes of UV irradiation

However, upon prolonged irradiation, there is a possibility for the detachment of nearly all the solubilizing groups from the surface of QDs, exposing the surface defects once again. This can finally lead to the formation of poorly soluble and less

fluorescing products (Cooper et al., 2009). Formation of a white precipitate after the irradiation experiments validate this phenomenon (inset to Figure 5.11).

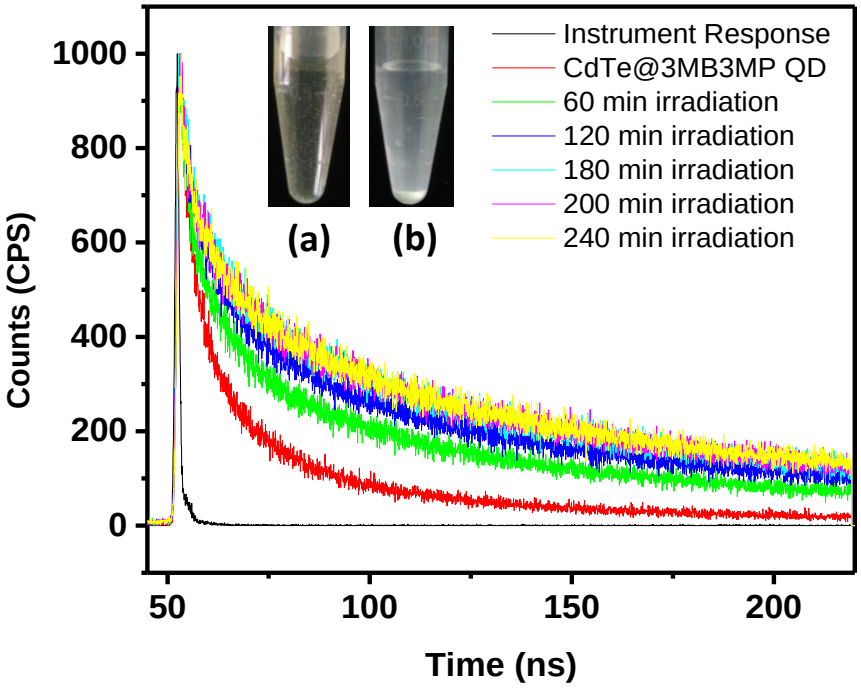

Figure 5.11. Time resolved fluorescence spectra of CdTe@3MB3MP QDs at different time of irradiation. Inset shows the QD solution before (a) and after (b) the irradiation experiment

Table 5.1. Table showing the lifetime analysis of CdTe@3MB3MP QDs at different time of UV irradiation

SYSTEM	τ_1 (ns)	a_1	τ_2 (ns)	a_2	τ_3 (ns)	a_3	$\langle\tau\rangle$ (ns)	χ^2
QD	75.25	55.85	13.78	33.78	1.81	10.37	68.85	1.08
60 min	110.59	80.47	15.46	14.44	1.76	5.09	108.16	1.12
120 min	124.26	83.88	16.76	12.24	1.85	3.88	122.10	1.13
180 min	137.36	86.57	18.51	10.29	1.94	3.14	135.42	1.09
200 min	129.25	87.56	16.51	9.51	1.68	2.93	127.65	1.09
240 min	78.94	92.02	10.59	7.28	1.45	0.70	78.21	1.02

These speculations were further clarified using time resolved fluorescence spectral analysis. The influence of UV radiation upon the lifetime of QDs are shown in

Figure 5.11 and Table 5.1. The lifetime decays at different time intervals were monitored at the emission maxima in the steady state spectra with an excitation wavelength of 344 nm. All the decay profiles were fitted into tri-exponential decay with best χ^2 value, revealing an exciton and trap radiation behavior. For CdTe QDs capped with 3MB3MP, the lifetime decay constitutes of three components, a fast component with an amplitude of around 10%, a medium component with amplitude around 30% and a longer lifetime component of around 50 % amplitude, with an average lifetime of 69 ns. The short lifetimes attributed to the intrinsic recombination of the CdTe QDs, whereas surface state recombination emerged as longer lifetime components (Liu et al., (2010). It is believed that the passivation of surface of QDs either by better ligands or through shell structure can increase the lifetimes, as this facilitates recombination from surface states, and eliminate nonradiative faster decays (Suffern et al., 2009). As the QDs getting exposed to UV radiation, it can be seen that, there is a significant increase in the average lifetime values of QDs, up to 135 ns, in accordance with the steady state observation of enhancement till 180 minutes, which then decreases to values near to that of original QDs (78 ns) with 240 min exposure. The variation of longer lifetime component also follows the same fashion of initial increase and subsequent decrease. Another notable point is variation of amplitude associated with these lifetime components. There is a regular increase in the amplitude associated with slowest component from 55 to 92 %, and a corresponding decrease in the amplitude of fast non-radiative component (from 10 % to nearly 1 %) probably resulted from the removal of surface states and thereby by quenching the non-radiative exciton recombination pathways, upon irradiation which corroborate with the results obtained from steady state measurements.

5.2.3 Fluorescence Switch of CdTe@3MB3MP for the Detection of H_2O_2

The enhancement effect on the PL emission spectra of CdTe@3MB3MP QDs upon UV irradiation due to the formation of ROS motivated us to investigate its response towards ROS under normal conditions. For this purpose, we have chosen a

comparatively stable ROS, hydrogen peroxide (H_2O_2). Most strikingly, we have observed that, like photobrightening, CdTe QDs respond positively towards the presence of H_2O_2. The response time of the sensor was checked by adding 50 nM concentration of H_2O_2 into 2 mL of sensor solution and recording the spectra at different time intervals. The sensor responds to the presence of H_2O_2 fast, and we can observe a steady increase in the emission for 5 minutes, which then become a plateau. Thus, we fixed the response time of the sensor as 5 minutes Figure 5. 12.

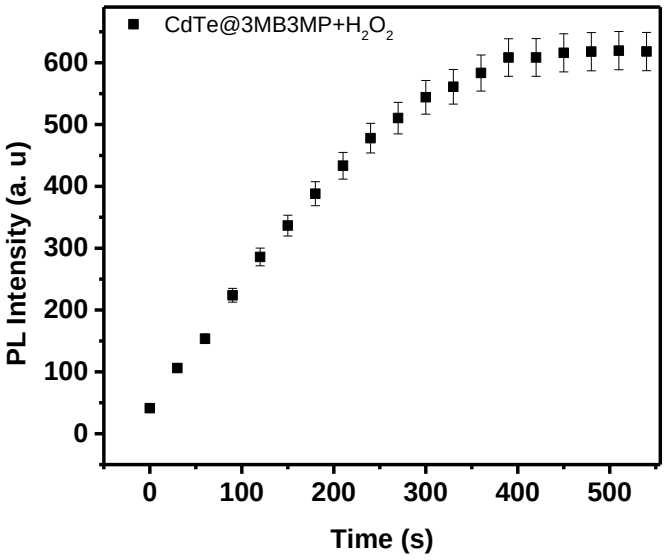

Figure 5. 12. Graph showing the response time of the sensor towards detection of H_2O_2

The fluorescence intensity of CdTe@3MB3MP QDs found to be enhanced initially in the presence of increasing concentration of H_2O_2, as can be seen in Figure 5. 13a, within a concentration range of 10 to 300 nM gradually, which then decrease in a much slower fashion. Thus, CdTe@3MB3MP QDs can be used as a sensitive turn-on fluorescence probe for the detection and quantification of H_2O_2. Figure 5.13b showcase the relative enhancement of PL emission of CdTe QDs ($F-F_0/F$; where F and F_0 are the fluorescent intensity with and without H_2O_2 molecules) plotted against the concentration of H_2O_2. Each trial is repeated three times and deviation from the mean value is represented as error bars. A linear relationship was observed between the extent

of enhancement and the concentration of H_2O_2, within a dynamic range of 10-250 nM. The experimental limit of detection of the sensor is a satisfactorily low value of 10 nM, which is comparable to the values reported so far (Table 5.2) The initial enhancement and subsequent quenching as well as presence of shift of emission maxima from 592 to 529 nm, upon addition of analyte molecules as in the case of photoactivation, open the possibility for the involvement of similar mechanism. The quantum yield of the enhanced sample upon treatment of H_2O_2 is found to be 44.40, which is around 4 times increase from the bare QDs.

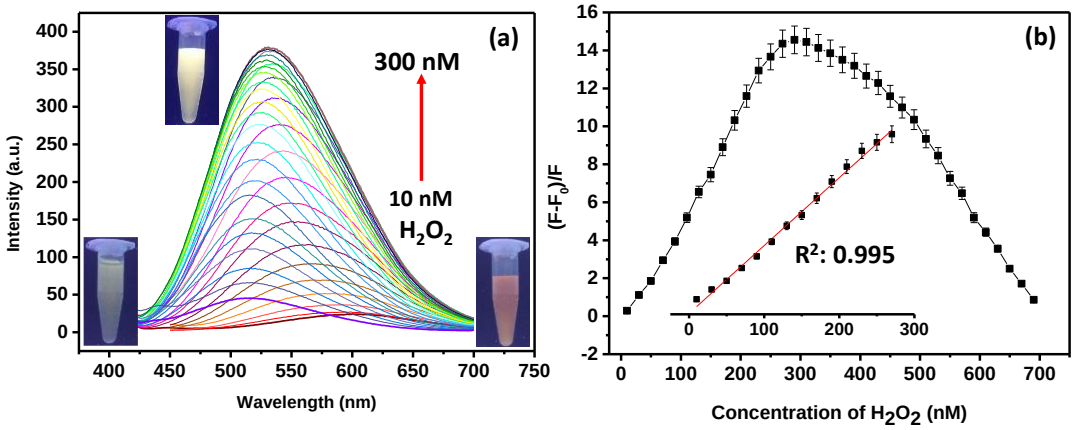

Figure 5.13. a) Fluorescence response of CdTe@3MB3MP QDs with various concentrations of H_2O_2. b) Dynamic range of the sensor.

Table 5.2. Comparison of analytical performance of CdTe@3MB3MP QDs as H_2O_2 sensor with other sensors

QDs	Capping agent	Linear range	LOD	Reference
CdTe	3-MPA	10-125 µM	0.3 µM	(Yongbo Wang et al., 2019)
SiO_2@CdTe	SH	0.005 mM to 0.1 mM	10 nM	(Ge et al., 2015)
CdTe@ZnS	Al-tetraamino-phthalocyanine	0–4.15×10−6 M	9.8 µM	(Adegoke et al., 2013)
CdTe/CDs	MPA	0.0100–0.2125% (w/w)	0.00793% (w/w)	(Castro et al., 2019)

CdTe	GSH	0.0025% - 0.040%	0.0012%	(Rodrigues et al., 2014)
CdTe/H2Q/HRP	MSA	1.0×10^{-6}-1.0×10^{-3} mol L^{-1}	1.0×10^{-7} mol L^{-1}	(Yuan et al., 2008)
CdTe	3MB3MP	10 to 250 nM	10 nM	Present work

5.2.4 Selectivity for H_2O_2 Detection

To scrutinize the activity of the QDs as a specific turn-on fluorescent sensor for H_2O_2, selectivity to various analyte moieties is compared. Figure 5.14 shows the changes in the relative fluorescence intensity of CdTe QDs towards the presence of different analytes, such as metal ions (Na^+, K^+, Mg^{2+}, Mn^{2+}, Sn^{2+}, Ca^{2+}, Al^{3+}, Co^{2+}, Ni^{2+}, Zn^{2+}, Ba^{2+}, Ag^+, Pb^{2+}, Fe^{2+}, Hg^{2+}, Cu^{2+}) aminoacids (glycine, lysine, valine, alanine, phenyl alanine, serine, proline, leucine, isoleucine, aspartic acid, glutamic acid, glutamine, tryptophan, arginine, histidine, aspargine, methionine, cysteine, threonine), carbohydrates, and biologically relevant other molecules (100 nM each). When most of the analyte quench the fluorescent emission, only H_2O_2, and two aminoacids are capable of enhancing the fluorescence emission. The extent of enhancement by aminoacids is negligible as compared to same concentration of H_2O_2 (12 times higher for H_2O_2, compared to methionine). Therefore, CdTe QDs capped with 3MB3MP can be used as a sensitive and selective biosensor for the detection of H_2O_2.

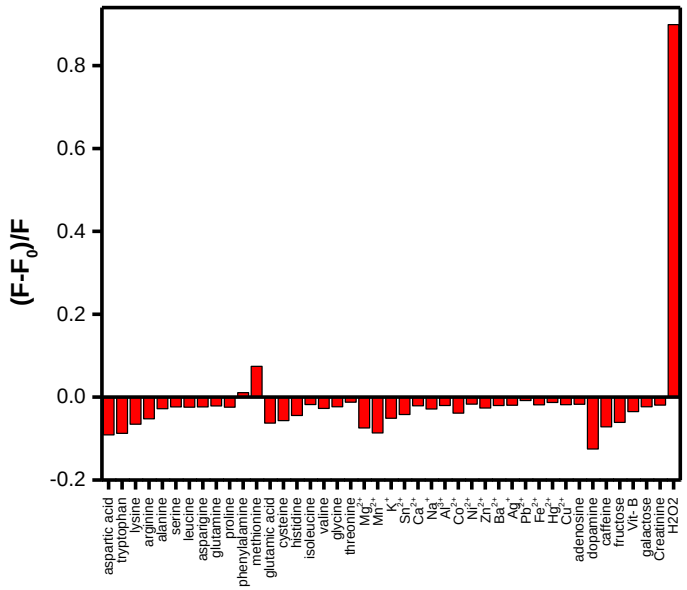

Figure 5.14. Selectivity profile of CdTe@3MB3MP QDs towards H_2O_2.

5.2.5 Mechanism of Sensing

Of the available reports on the sensing of H_2O_2 using CdTe, mostly rely on the fluorescence turn-off based sensors, utilizing the oxidative nature of H_2O_2. One of the reports which showcases the turn on sensor, is based on the shutting of Förster resonance energy transfer (FRET) between the fluorophore CdTe@ZnS QDs and a macrocylic compound; metal tetraamino-phthalocyanine by H_2O_2 (Adegoke et al., 2013). However, in the present case, we can circumvent the possibility for such conventional mechanisms. It is widely accepted that, the small size of 0-D QDs resulted in large surface/volume ratio, compared to other nanosystem, which render them enhanced surface activities. The surface of the QDs is usually passivated by organic ligands, which satisfies the dangling bonds, which otherwise would become seat for non-radiative recombination, and thus reduces the fluorescence intensity. The energy levels of such surface traps lie between the valence and conduction bands of QDs (Patra & Samanta, 2014). In the present case, we have made use of a bulky branched ligand for the passivation of CdTe QDs. The QY of the sample is 12 %, which is comparatively low for CdTe QDs. We presume that, the uncoordinated atoms on the surface of QDs might be the reason for these non-radiative recombination pathways which reduce the

QY. Upon addition of H_2O_2, the fluorescence is found to be enhanced. We assume that the passivation of surface states by small H_2O_2 molecules might be the reason for this unusual enhancement. Detailed photophysical characterizations such as UV-Vis absorption spectroscopy, Zeta potential studies, XPS analysis, steady state and time resolved fluorescence spectral analysis etc. have been carried out to unveil the mechanism of enhancement of emission upon interaction of CdTe QDs with H_2O_2.

UV-Vis absorption spectroscopy is highly sensitive towards any changes in the surface charge, morphology or functionality. Therefore, continuous monitoring of absorption features of QDs were carried out at different concentrations of H_2O_2 (Figure 5.15). Upon addition of H_2O_2 (100 nM; blue line), the peak become more distinct. Absence of emergence of any new peaks or disappearance of existing peaks circumvent the possibility of any ground state complex formation or the oxidation of QD surface, within linear range of the sensor (Pal et al., 2018). Another important observation is diminishing of the peaks upon increasing the concentration of H_2O_2 further at 500 nM (pink line) and fully gone for 750 nM (Yellow line).An ample explanation for this behavior would be the degradation of sensor material in the presence of higher concentrations of H_2O_2. The precipitate formed at 750 nM concentrations of H_2O_2, as shown in the inset photographic image (c) of Figure 5.15, is reasonable with this hypothesis. The TEM images at these concentrations (100 nM and 500 nM) manifest these speculations further (Figure 5.16). The QDs are intact at 100 nM concentrations of H_2O_2 (Figure 5.16 a) with retention of its crystallinity, while at 500 nM, the morphology of the QDs is different with loss of crystallinity.

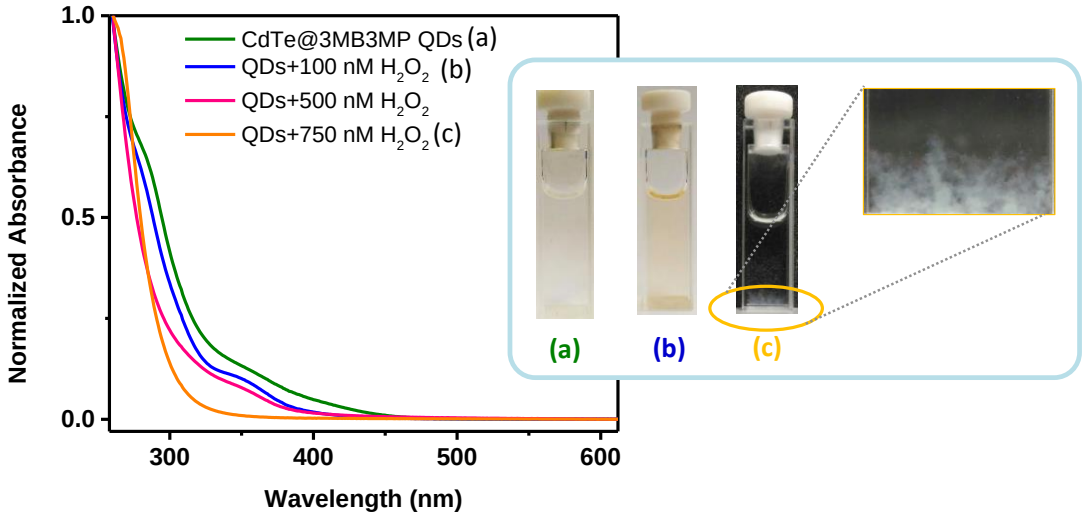

Figure 5.15. UV-visible absorption spectra of CdTe@3MB3MP QDs at different concentrations of H_2O_2

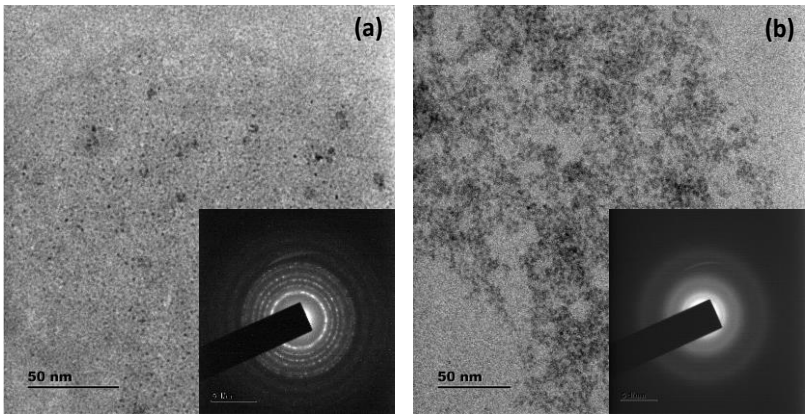

Figure 5.16. TEM images of CdTe@3MB3MP QDs at 100 nM (a) and 500 nM (b) concentrations of H_2O_2

A simple technique like zeta potential analysis can unveil a lot of information such as nature of interaction between different moieties, stability of the system etc. We have performed zeta potential studies of QDs with different concentrations of H_2O_2 for this purpose. As can be seen in the Table 5.3, zeta potential value of QD alone is -30.9 V, which demonstrates that QDs are negatively charged, having good stability and dispersibility. We can also notice that there is an H_2O_2 concentration dependent changes in the values of zeta potential. The highest value is found to be for a concentration of

250 nM, which denotes the maximum stability of the QDs. Thus, the addition of H_2O_2 renders an extra stability to the QDs initially, which then degrades after saturation point.

Table 5.3. Table showing Zeta potential values of CdTe@3MB3MP QDs at different concentrations of H_2O_2

Sample	**Zeta Value (mV)**
CdTe@3MB3MP QDs (QD)	-30.9
QDs + 50 nM of H_2O_2	-32.9
QDs + 100 nM of H_2O_2	-34.2
QDs + 150 nM of H_2O_2	-35.3
QDs + 200 nM of H_2O_2	-38.0
QDs + 250 nM of H_2O_2	-43.8
QDs + 300 nM of H_2O_2	-34.7
QDs + 350 nM of H_2O_2	-32.7
QDs + 400 nM of H_2O_2	-30.7
QDs + 450 nM of H_2O_2	-28.2

To better understand the mechanism of fluorescence sensor, we have carried out thorough XPS analysis, with two different concentrations of H_2O_2 (lower concentrations within dynamic range Figure 5.17, and very high concentration Figure 5.18, where the fluorescence of the system is quenched remarkably). Figure 5.17 shows a survey scan and HRXPS spectrum of the CdTe QDs. In both the survey scans, different Cd and Te core levels can be seen, as in the case of bare QD, along with the appearance of peaks corresponding to C, S and O, mainly stem from the ligand used. For unravelling the mechanism of interaction of fluorophore with the analyte, we compare the HRXPS peaks of Cd, Te, S and O of bare QD with that of QD associated with H_2O_2. It is clear that, the peak for Cd $3d_{5/2}$ has split into two components located at 404.8 and 406.1 eV (411.6 and 413.13 for $3d_{3/2}$), corresponding to Cd linked to Te as in the case of bare QD and a very small peak corresponding to Cd-O bonds (Zeng et al., 2015). Similarly, the peaks for Te also split into two (572.5 and 576.1 eV corresponding to Te $3d_{5/2}$ and 583.2 and 586.6 eV corresponding to Te $3d_{3/2}$), associated with Te-Cd and Te-O bonds respectively (Guillén-Cervantes et al., 2020; Masood et

al., 2017). The appearance of second peak at 576.1 eV binding energy value is significant, which endorse our speculation of surface passivation by reactive oxygen species. Whereas upon exposure to higher concentrations of H_2O_2, we can notice that there is a drastic change in the HRXPS peaks for Cd 3d and Te 3d. The intensity of Cd-O peak has increased, considerably which attest the increased oxidation of QD surface. The HRXPS of Te shows fully oxidized peak corresponding to TeO_2. Another noticeable changes in terms of peak position and number can be observed for sulphur peaks. The HRXPS of sulphur peak for bare QD contain two components of $S2p_{1/2}$ and $S2p_{3/2}$ at 163.15 and 161.85 eV respectively, which correspond to the peak of S present in the surface passivating ligand (S-R). Whereas a clear emergence of higher binding energy peaks can be observed even addition of lower concentrations of H_2O_2, which stipulates the possibility for the oxidation of some of the ligands or even ligand exchange reactions with analyte molecules (Vale et al., 2019). The complete disappearance of sulphur peaks corresponding to S-R and presence of high intense S-O peak for high H_2O_2 concentrated sample designate the complete removal of passivating ligands from the surface of QDs. Thus, we speculate that, the blue-shift of emission maximum position, along with the quenching of fluorescence indicate the possibility of surface etching of QD materials as well as removal of surface ligands and thus shrinking of size of the QDs. This can give rise to the formation of new non-radiative surface traps and dangling bonds, which can be further verified using time resolved fluorescence spectroscopy.

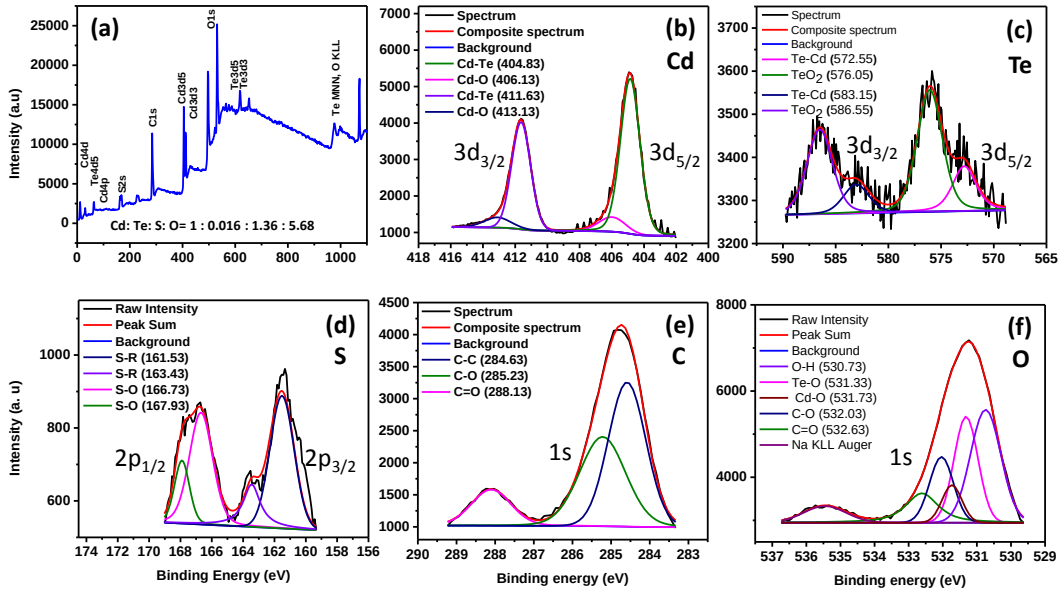

Figure 5.17. a) Survey scan spectrum of CdTe@3MB3MP QDs at lower concentrations of H_2O_2. b-f) Corresponding HRXPS spectra of Cd, Te, S, C and O respectively.

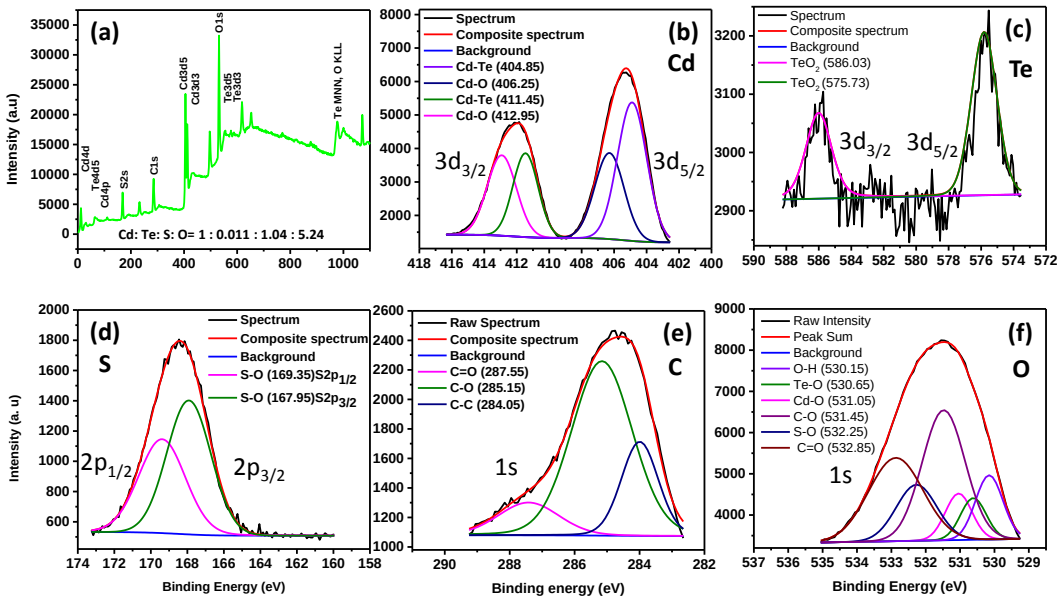

Figure 5.18. a) Survey scan spectrum of CdTe@3MB3MP QDs at higher concentrations of H_2O_2. b-f) Corresponding HRXPS spectra of Cd, Te, S, C and O respectively.

As we have already discussed, the lifetime decay profile of CdTe QDs can be fitted by triexponential fit, with a fast component (1.9 ns, 14 %), medium (14 ns, 29 %) and a slow radiative component (78 ns, 57 %), with an average lifetime of 72 ns. Upon

addition of increasing amount of H_2O_2, as in the case of photobrightening, there is a regular increase in the average lifetime from 72 to 97 ns, upon addition of up to 250 nM of H_2O_2. However, the average lifetime seems to decline, upon still higher concentrations of H_2O_2; 75 ns and 26 ns for 500 nM and 700 nM of H_2O_2 concentrations respectively. The same trend can be visible for longer and medium lifetime component as well, which is commensurate with the results obtained from steady state experiments. However, unlike in the case of photoexcitation studies, the amplitude of these components shows different behavior. We can see that, the amplitude of longer component increases initially, then decreases, as there is quenching in the steady state measurements. Whereas the amplitude of other two components show the opposite behavior. One assertion, we can make here is that, as the concentration of H_2O_2 increases initially, these small molecules can reach the surface of QDs easily and satisfy the dangling bonds present at the surface, which otherwise can act as seat for non-radiative decay. More concentration of H_2O_2, the better the surface passivation by these moieties. After saturation, being a strong oxidizing agent, H_2O_2 can oxidize the QDs as well, which can further lead to surface modifications and generation of new surface traps (Mani & Cyriac, 2019). The increase in the amplitude of fast component (44 % for 700 nM H_2O_2) and the significant reduction of longer and medium lifetime component values (to 31 and 5 ns respectively) attest the emergence of these non-radiative traps. We anticipate the etching of surface ligands as well as QDs, at this stage. The complete disappearance of fluorescence emission along with formation of white precipitate, upon addition of higher concentration of H_2O_2 can be regarded as a proof for this assertion (inset to Figure 5.15).

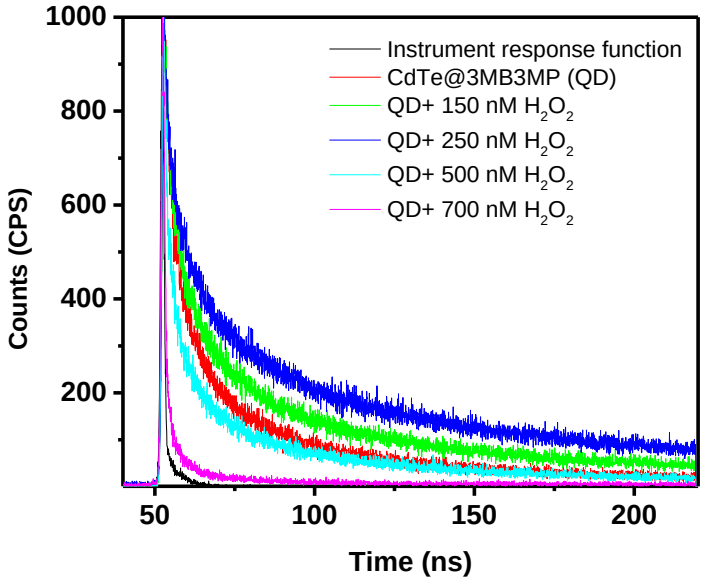

Figure 5.19. Time resolved fluorescence spectra of QDs at different concentrations of H_2O_2

Table 5.4. Table showing the lifetime analysis of CdTe@3MB3MP QDs at different concentrations of H_2O_2

SYSTEM	τ_1 (ns)	a_1	τ_2 (ns)	a_2	τ_3 (ns)	a_3	$<\tau>$ (ns)	χ^2
QD	77.66	57.52	13.89	28.83	1.89	13.65	72.04	1.2
QD+150 nM	86.81	70.84	14.18	23.40	1.49	5.76	82.98	1.04
QD+ 250 nM	99.62	79.22	15.51	15.86	0.91	4.92	97.02	1.01
QD+ 500 nM	78.24	58.89	13.13	18.04	0.64	23.07	74.83	1.07
QD+ 700 nM	31.27	26.86	5.17	29.58	0.76	43.56	26.39	1.2

5.2.6 Real sample analysis and solid substrate detection

Evaluation of the utility of CdTe@3MB3MP QDs as a sensor for H_2O_2 in real samples detection was performed using tap water and urine samples. The samples were prepared by spiking known concentration of H_2O_2 and fluorescence spectra were recorded after addition to CdTe QDs. The results obtained were shown in Table 5.5. The recovery and relative standard deviation (% RSD) were evaluated to check the accuracy of the method. For tap water sample, a recovery of 100.45, 101.65 and 100.7% were obtained with corresponding % RSD of 1.26, 1.59, and 1.14 whereas, for urine

sample, a recovery of 100.53, 100.33 and 100.30% were obtained with corresponding % RSD of 1.18, 0.94 and 1.17. The result obtained indicates the reliability of the sensor for analytical applications.

Facile qualitative recognition of H_2O_2 using a handy substrate was performed in order to check the utility of the present sensor as a solid substrate sensor platform. For this purpose, we used thin layer chromatographic plate (TLC plate) where several CdTe QD spots were drop-casted and dried. Three different concentrations of H_2O_2 (100 nM, 250 nM, and 750 nM) of H_2O_2 was drop-casted on to these dried sensor spots and illuminated under UV radiation (365 nm). The fluorescence intensity of the spots corresponding to 100 and 250 turn yellow with varying intensity, whereas 750 nM found to be quenched fully. Hence, an easy qualitative detection of H_2O_2 can be realized using CdTe QDs needless of any sophisticated instruments.

Table 5.5. Detection of H_2O_2 in real samples

Sample	**Spiked (nM)**	**Found (Mean; nM)**	**Recovery**	**% RSD**
Tap water	50.0	50.82±0.056	101.65	1.59
	62.5	62.78±0.053	100.45	1.26
	75.0	75.53±0.057	100.70	1.14
Urine Sample	75.0	75.40±0.024	100.53	1.18
	100.0	100.33±0.023	100.33	0.94
	112.50	112.84±0.032	100.30	1.17

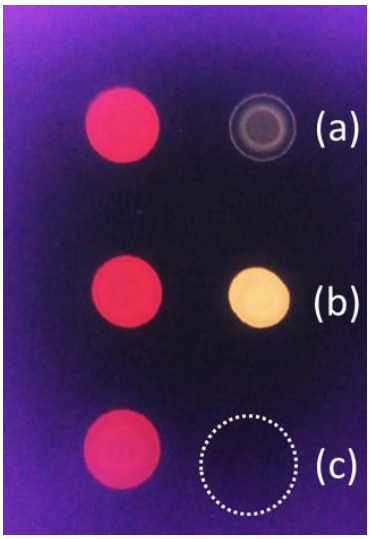

Figure 5.20. Photographs of TLC plate based sensor platform. The first column represents CdTe@3MB3MP QD drop casted on TLC under UV light (red dots) and the second column represent QDs treated with a) 50 nM b) 250 nM and c) 750 nM concentrations of H_2O_2.

5.3 Conclusion

In summary, we have successfully synthesized CdTe QDs passivated by a novel branched ligand viz. 3-methoxybutyl-3-mercaptopropionate for the first time. We have performed various morphological as well as photophysical characterization to unravel the nature and properties of the QDs synthesized. The quantum yield of the QDs were around 12 %, with excitation independent high emission in the red region. The QDs shows high temporal stability along with unusual photobrightening effects. With the help of spectroscopic analysis, the reason behind this enhancement of emission intensity in the presence of UV radiation has been investigated, in detail. We have also demonstrated its application as a turn-on fluorescence sensor for selective and sensitive detection of H_2O_2. The limit of detection of the sensor is found to be a low value of 10 nM, and sensor can act linearly within a concentration range of 10 to 250 nM. The sensor was demonstrated to be applicable for the detection of H_2O_2 in real samples also, with high accuracy and excellent recovery. The potential of CdTe QDs as a visual detection agent was also demonstrated by impregnating dried QD spots on a TLC plate.

CHAPTER 6

CONCLUSIONS AND FUTURE PERSPECTIVE

6.1 Conclusions

Fluorescent based sensors were catching enormous attention due to its facile nature, the simplicity of the procedures and instrumentation required, superior selectivity and sensitivity it can offer, better reproducibility and reliability of the results etc. The sensing parameters such as detection limit, dynamic range, possibility for multiplexed detection etc. rely hugely on the physicochemical properties of the fluorophore used. Therefore, choice and rational design of fluorescent probes demands considerable attention. Compared to conventional organic dyes, novel fluorescent quantum dots-inorganic nanocrystals, have manifold advantages. QDs are having symmetric and narrow emission profiles, high absorption efficient in UV region, high quantum yields especially in NIR region, exorbitant photo and temporal stability, very low photo- bleaching effect etc. The optical properties of QDs are defined largely by the nature of constituent materials, size and shape, surface chemistry, and nature of dangling bonds.

The applicability of CdTe QDs were limited in biological realm mainly due to the high toxic nature of its constituent materials. Use of benign ligand is one of the procedures to be adopted in order to overcome this impediment. Also, stability of the QDs warrant the limited bleaching of the material. Aqueous solubility of the material is another requirement to be satisfied. The functional groups in ligand also play significant role in determining the stability of QDs and utility of the QDs synthesized, as it can advocate the possibility of reactions and recognition of suitable analyte in sensing schemes. Present thesis is an attempt to address all these circumstances.

This thesis is an effort to understand the complex interactions of analytes which could take place with sulphur attached at the end of the ligands, using the available characterization techniques. As the number of molecules increases in the system, the complexity of the interactions between them increases further. Hence, we

tried to minimize the complexity in the interactions between various molecules by keeping the minimum possible molecules to get a clear picture of the necessary interactions taking place in the system. The usage of the quantum dots as such without any additional coating is one such attempt to keep the interactions between the molecules under control by not allowing the extra atoms to come into the picture. Another highlight of the thesis is the choice of ligands used. The quantum dots materials and the synthesis parameters are kept constant across different works to maintain the uniformity of the reactions for normalized comparison. The purpose in all the three works was same, to identify a novel ligand which can supplement or can be used in alternative to the present existing ligands, for the synthesis of QDs and which can be further implemented for the sensing of various analytes. We were successful in figuring out three ligands in the present study which can very well do the proposed work, with a side methyl chain in the mercapto ligand salt. The side methyl chain added several of the benefits for the QDs synthesis such as providing better stability of the QDs and in the sensing scenario as well.

Chapter 1 deals with introduction to quantum dots with a detailed literature review. It gives an overview of the present status of various synthetic routes, general properties and various applications of semiconductor based quantum dots in general with special emphasis on CdTe QDs capped with different ligands. The second part of Chapter 1 details about the basics of fluorescence such as different mechanisms of fluorescence quenching, general approaches to various fluorescence sensing using CdTe QDs with a few examples.

The material and methods, different characterization techniques used, detailed synthesis of CdTe QDs capped with three different branched ligands are well explained in chapter 2. Chapter 3 showcases detailed characterization of CdTe QDs synthesized by colloidal method surface passivated by 3-mercaptoisobutyric acid (3-MIBA). The high fluorescence of these QDs were utilized for the selective sensing of heavy metal ion pollutant Hg^{2+}. The strong affinity of Hg^{2+} towards S atom of ligand and possibility of electron transfer led to the fluorescent quenching of the QDs by Hg^{2+}, preferentially.

Chapter 4 demonstrated successful synthesis of CdTe QDs with ethyl-2-mercaptopropionate (E2MP) as surface ligand. We tried to perform all the possible photophysical and the spectroscopic characterizations to disclose the nature of the QDs formed and then to understand the mechanism behind it's sensing for copper ions in the aqueous phase at the room temperature with a very low detection limit. The CdTe@E2MP QDs shows better temporal as well as photostability compared to other two QDs.

In the 5th chapter a further attempt was made in the same direction where CdTe QDs were passivated with an altogether different ligand; 3-Methoxybutyl 3-mercaptopropionate (3MB3MP) to show the potential for the formation of the QDs and sensing capabilities. This ligand was chosen to be having a side methyl chain which was in line with our previous works. All the characterizations were performed to confirm the formation of the QDs. Then, attempts were directed towards its sensing capabilities as well, and it was found to be sensing H_2O_2 in a turn on fashion. To confirm the same, again several supporting characterization techniques were performed. The linear range for the analyte were noted along with LOD and it was found in well agreement with the other reported values with other ligands.

The thesis reported three different works with three different ligands used for the synthesis of the QDs. Each ligand is unique and different and offers various parameters and properties for tuning the size of the quantum dots which in turn is responsible for tuning the band gap of the synthesized QDs. Along with the change in the size of the QDs, the ligands played a significant role in the selectivity of the quantum dots towards specific analyte. As it is very clear from the literature that the surface of the QDs could be tuned easily by modifying the surface over it. Hence in the same manner we have noticed that by simply changing the surface of the QDs by different organic ligands, it could sense different analytes in each case. This also depends on the end groups attached to the ligands. The QDs with the ligand 3MB3MP was observed to be selective to H_2O_2 whereas the ligand 3MIBA was observed to be selective to Hg^{2+} and the ligand E2MP was observed to be selective to Cu^{2+}.

There are various other parameters which could be responsible for the specific selectivity. The bulkiness of the ligand is also crucial as the bulky ligand will have its own significance and will not allow to cover all the surface sites of the QDs resulting in more defect states. The same thing can be easily noticed in our third work, where the ligand 3MB3MP was bulky enough to leave free sites on the surface of the QDs, thereby creating enough defects in the system. This in turn also effects the selectivity and sensitivity of the sensor.

Along with the bulkiness, the position of the side methyl group may also play a role in the sensing process. As we can notice that in all our works, the methyl group is positioned at different carbon locations in the ligand.

6.2 Major Outcomes of the Thesis

The QDs used in the present work can be scaled up and used for fabricating any kind of devices. The similar kind of QDs can also be synthesized and fabricated and tested for the other visible spectrum like for near IR or IR.

Certain conclusions which can be derived from the thesis are listed below:

- The high quality QDs could be successfully synthesized using easy and facile colloidal method.
- All the QDs synthesized were found to be crystalline in structure as can be visualized from SAED and XRD studies. QDs capped with 3-MIBA and 3MB3MP are purely Zincblende structure and those capped with E2MP shows mixed Zincblende and Wurtzite structure.
- All the QDs irrespective of the ligands were found to be extremely stable for months that kept under 4 °C.
- The zeta potential of the QDs was observed to be around -30.
- All the QDs shows excitation independent emission with very narrow FWHM, suggesting narrow size range of nanoparticles suitable for various high end applications.

- The side methyl group coating over the QDs was found to be very much effective as the quantum yields are higher compared to QDs capped with conventional ligands.
- The QDs capped with 3-MIBA was found to be linearly and highly selective to the Hg^{2+} in the range of 1.5 nM to 100 nM due to quenching of fluorescence of QDs due to aggregation and electron transfer.
- CdTe QDs capped with E2MP was found to be sensing Cu ions with a limit of detection of 0.5 nM with a linear range of 0.5-129.5 nM.
- CdTe QDs capped with 3MB3MP was found to be sensing H_2O_2 in turn on manner.
- Even though the core of the QDs is the same, the response of the QDs towards various ions are different. We envisage, the reason behind this selectivity majorly depends on the ligands made use. The matching energy levels of Hg^{2+} and Cu^{2+} with the corresponding energy bands of QDs passivated with 3-MIBA and E2MP respectively can be another reason for the selectivity.
- Study mainly focuses on the effect of various branched ligands, and observed that, QDs with side methyl near to SH binding group (E2MP) gives more quantum yield, high temporal stability, better photostability (150 min than QD with 3-MIBA-60 min), more crystalline QDs, lower FWHM and surprisingly lower limit of detection as well.

6.3 Future Perspective

The growing interest in highly fluorescent semiconductor quantum dots as sensors or as imaging probes are evident from the considerable reports available in the literature. In this thesis, we have employed easy and facile colloidal synthetic procedures for ample time period for manipulating the size of QDs formed. Thanks to the increased stability, and enhanced fluorescence of these QDs, we are attempting to extend this strategy for the synthesis of similar QDs with different ligands. We also propose tuning of optical as well as electronic properties of QDs by functionalization

using suitable ligands, which can foster selectivity towards different analytes of interest. Any fluorophore can facilitate the sensitivity of the sensor having high quantum yield. Studies propelling to increase the quantum yield of as synthesized QDs is another area that can be focused on. A rigorous study for the calculation of HOMO and LUMO of the QDs using ultraviolet photoelectron spectroscopy (UPS), cyclic voltammetry and absorption spectroscopy can be adopted for better understanding the mechanism of quenching by various analytes. The leaching of heavy metal ions from QDs can be minimized by carefully designed core-shell type QDs which bear the prospective to become next generation bioimaging agents. These materials have the propensity to be modified for applications in the field of electronic and optoelectronic devices as well.

References

1. Abe, M. K., Kartha, S., Karpova, A. Y., Li, J., Liu, P. T., Kuo, W. L., & Hershenson, M. B. (1998). Hydrogen peroxide activates extracellular signal-regulated kinase via protein kinase C, Raf-1, and MEK1. *American Journal of Respiratory Cell and Molecular Biology*, *18*(4), 562–569. https://doi.org/10.1165/ajrcmb.18.4.2958

2. Abuelela, A. M., Mohamed, T. A., & Prezhdo, O. V. (2012). DFT simulation and vibrational analysis of the IR and Raman spectra of a CdSe quantum dot capped by methylamine and trimethylphosphine oxide ligands. *Journal of Physical Chemistry C*, *116*(27), 14674–14681. https://doi.org/10.1021/jp303275v

3. Adegoke, O., Khene, S., & Nyokong, T. (2013). Fluorescence "switch on" of conjugates of CdTe@ZnS quantum dots with Al, Ni and Zn tetraamino-phthalocyanines by hydrogen peroxide: Characterization and applications as luminescent nanosensors. *Journal of Fluorescence*, *23*(5), 963–974. https://doi.org/10.1007/s10895-013-1222-x

4. Ai, X., Niu, L., Li, Y., Yang, F., & Su, X. (2012). A novel β-Cyclodextrin-QDs optical biosensor for the determination of amantadine and its application in cell imaging. *Talanta*, *99*, 409–414. https://doi.org/10.1016/j.talanta.2012.05.072

5. Alivisatos, A. P. (1996). Semiconductor Clusters, nanocrystals, and Quantum Dots. *Science.*, *271*(5251), 933–937. https://doi.org/10.1126/science.271.5251.933

6. Amin, R. M., Elfeky, S. A., Verwanger, T., & Krammer, B. (2017). Fluorescence-based CdTe nanosensor for sensitive detection of cytochrome C. *Biosensors and Bioelectronics*, *98*, 415–420. https://doi.org/10.1016/j.bios.2017.07.020

7. Arachchige, I. U., & Brock, S. L. (2007). Sol-gel methods for the assembly of metal chalcogenide quantum dots. *Accounts of Chemical Research*, *40*(9), 801–809. https://doi.org/10.1021/ar600028s

8. Bacher, G., Ku¨mmell, T., Eisert, D., & Forchel, A. (1999). Buried single CdTe / CdMnTe quantum dots realized by focused ion beam lithography. *Applied Physics Letters*, *75*(7), 956. https://doi.org/10.1063/1.124565

9. Bag, P. P., Wang, X. S., Sahoo, P., Xiong, J., & Cao, R. (2017). Efficient photocatalytic hydrogen evolution under visible light by ternary composite CdS@NU-1000/RGO. *Catalysis Science and Technology*, *7*(21), 5113–5119. https://doi.org/10.1039/c7cy01254c

10. Bentzen, E. L., House, F., Utley, T. J., Crowe, J. E., & Wright, D. W. (2005).

Progression of respiratory syncytial virus infection monitored by fluorescent quantum dot probes. *Nano Letters*, *5*(4), 591–595. https://doi.org/10.1021/nl048073u

11. Bian, W., Wang, F., Zhang, H., Zhang, L., Wang, L., & Shuang, S. (2015). Fluorescent probe for detection of Cu^{2+} using core-shell CdTe/ZnS quantum dots. *Luminescence*, *30*(7), 1064–1070. https://doi.org/10.1002/bio.2859

12. Biswas, S., Brinkmann, F., Hirtz, M., & Fuchs, H. (2015). Patterning of Quantum Dots by Dip-Pen and Polymer Pen Nanolithography. *Nanofabrication*, *2*(1), 19–26. https://doi.org/10.1515/nanofab-2015-0002

13. Borchert, H., Talapin, D. V., Gaponik, N., McGinley, C., Adam, S., Lobo, A., Möller, T., & Weller, H. (2003). Relations between the Photoluminescence Efficiency of CdTe Nanocrystals and Their Surface Properties Revealed by Synchrotron XPS. *Journal of Physical Chemistry B*, *107*(36), 9662–9668. https://doi.org/10.1021/jp0352884

14. Borse, V., Sadawana, M., & Srivastava, R. (2016). CdTe quantum dots: aqueous phase synthesis, stability studies and protein conjugation for development of biosensors. *Proceedings of SPIE - The International Society for Optical Engineering*, *9884*, 988423. https://doi.org/10.1117/12.2225262

15. Brus, L. E. (1984). Electron–electron and electron-hole interactions in small semiconductor crystallites: The size dependence of the lowest excited electronic state. The Journal of chemical physics, 80(9), 4403-4409.) https://doi.org/10.1063/1.447218

16. Carrillo-Carrión, C., Cárdenas, S., Simonet, B. M., & Valcárcel, M. (2009). Quantum dots luminescence enhancement due to illumination with UV/Vis light. *Chemical Communications*, *35*, 5214–5226. https://doi.org/10.1039/b904381k

17. Castro, R. C., Soares, J. X., Ribeiro, D. S. M., & Santos, J. L. M. (2019). Dual-emission ratiometric probe combining carbon dots and CdTe quantum dots for fluorometric and visual determination of H_2O_2. *Sensors and Actuators, B: Chemical*, *296*(June), 126665. https://doi.org/10.1016/j.snb.2019.126665

18. Chakraborty, S., Mandal, I., Ray, I., Majumdar, S., Sen, A., & Maiti, H. S. (2007). Improvement of recovery time of nanostructured tin dioxide-based thick film gas sensors through surface modification. *Sensors and Actuators, B: Chemical*, *127*(2), 554–558. https://doi.org/10.1016/j.snb.2007.05.005

19. Chan, W. C. W., & Nie, S. (1998). Quantum dot bioconjugates for ultrasensitive nonisotopic detection. *Science.*, *281*(5385), 2016–2018. https://doi.org/10.1126/science.281.5385.2016

20. Chang, H., Wang, X., Shiu, K. K., Zhu, Y., Wang, J., Li, Q., Chen, B., & Jiang, H. (2013). Layer-by-layer assembly of graphene, Au and poly(toluidine blue O) films sensor for evaluation of oxidative stress of tumor cells elicited by hydrogen peroxide. *Biosensors and Bioelectronics*, *41*(1), 789–794. https://doi.org/10.1016/j.bios.2012.10.001

21. Chao, M. R., Chang, Y. Z., & Chen, J. L. (2013). Hydrophilic ionic liquid-passivated CdTe quantum dots for mercury ion detection. *Biosensors and Bioelectronics*, *42*(1), 397–402. https://doi.org/10.1016/j.bios.2012.10.065

22. Chen, Bin, Liu, J., Yang, T., Chen, L., Hou, J., Feng, C., & Huang, C. Z. (2019). Development of a portable device for Ag^{+} sensing using CdTe QDs as fluorescence probe via an electron transfer process. *Talanta*, *191*(August 2018), 357–363. https://doi.org/10.1016/j.talanta.2018.08.088

23. Chen, Bo, Yu, Y., Zhou, Z., & Zhong, P. (2004). Synthesis of Novel Nanocrystals as Fluorescent Sensors for Hg^{2+} Ions. *Chemistry Letters*, *33*(12), 1608–1609. https://doi.org/10.1246/cl.2004.1608

24. Chen, Y. J., & Yan, X. P. (2009). Chemical redox modulation of the surface chemistry of CdTe quantum dots for probing ascorbic acid in biological fluids. *Small*, *5*(17), 2012–2018. https://doi.org/10.1002/smll.200900291

25. Chen, Yongfen, & Rosenzweig, Z. (2002). Luminescent CdS quantum dots as selective ion probes. *Analytical Chemistry*, *74*(19), 5132–5138. https://doi.org/10.1021/ac0258251

26. Chen, Yu-zhen, & Jiang, H. (2016). Porphyrinic Metal-Organic Framework Catalyzed Heck- Reaction : Fluorescence " Turn-on " Sensing of Cu (II) Ion. *Chem. Mater.*, *28*(18), 6698–6704. https://doi.org/10.1021/acs.chemmater.6b03030

27. Cheng, L., Liu, X., Lei, J., & Ju, H. (2010). Low-potential electrochemiluminescent sensing based on surface unpassivation of CdTe quantum dots and competition of analyte cation to stabilizer. *Analytical Chemistry*, *82*(8), 3359–3364. https://doi.org/10.1021/ac100315a

28. Chizhov, A. S., Rumyantseva, M. N., Vasiliev, R. B., Filatova, D. G., Drozdov, K. A., Krylov, I. V., Abakumov, A. M., & Gaskov, A. M. (2014). Visible light activated room temperature gas sensors based on nanocrystalline ZnO sensitized with CdSe quantum dots. *Sensors and Actuators, B: Chemical*, *205*, 305–312. https://doi.org/10.1016/j.snb.2014.08.091

29. Choi, M. K., Yang, J., Kang, K., Kim, D. C., Choi, C., Park, C., Kim, S. J., Chae, S. I., Kim, T. H., Kim, J. H., Hyeon, T., & Kim, D. H. (2015). Wearable red-green-blue quantum dot light-emitting diode array using high-resolution intaglio

transfer printing. In *Nature Communications* (Vol. 6). https://doi.org/10.1038/ncomms8149

30. Choi, S. Y., Shim, J. P., Kim, D. S., Kim, T., & Suh, K. S. (2012). Aqueous synthesis of CdTe quantum dot using dithiol-functionalized ionic liquid. *Journal of Nanomaterials*, *2012*, 1–6. https://doi.org/10.1155/2012/519458

31. Choudhary, Y. S., & Nageswaran, G. (2019). Branched mercapto acid capped CdTe quantum dots as fluorescence probes for Hg^{2+} detection. *Sensing and Bio-Sensing Research*, *23*(March), 100278. https://doi.org/10.1016/j.sbsr.2019.100278

32. Clarkson, T. W., Magos, L., & Myers, G. J. (2003). The Toxicology of Mercury — Current Exposures and Clinical Manifestations. *New England Journal of Medicine*, *349*(18), 1731–1737. https://doi.org/10.1056/NEJMra022471

33. Coates, J. (2006). Interpretation of Infrared Spectra, A Practical Approach. *Encyclopedia of Analytical Chemistry*, 1–23. https://doi.org/10.1002/9780470027318.a5606

34. Coe, S., Woo, W. K., Bawendi, M., & Bulović, V. (2002). Electroluminescence from single monolayers of nanocrystals in molecular organic devices. *Nature*, *420*(6917), 800–803. https://doi.org/10.1038/nature01217

35. Cooper, D. R., Suffern, D., Carlini, L., Clarke, S. J., Parbhoo, R., Bradforth, S. E., & Nadeau, J. L. (2009). Photoenhancement of lifetimes in CdSe/ZnS and CdTe quantum dot-dopamine conjugates. *Physical Chemistry Chemical Physics*, *11*(21), 4298–4310. https://doi.org/10.1039/b820602c

36. de Moure-Flores, F., Quiñones-Galván, J.G., Guillén-Cervantes, A., Arias-Cerón, J.S., Hernández-Hernández, A., Santoyo-Salazar, J., Santos-Cruz, J., Mayén-Hernández, S.A., Olvera, M.D.L.L., Mendoza-Álvarez, J.G. and Meléndez-Lira, M., 2014. CdTe thin films grown by pulsed laser deposition using powder as target: Effect of substrate temperature. Journal of crystal growth, 386, pp.27-31. https://doi.org/10.1016/j.mssp.2018.07.004

37. Dennis, A. M., Rhee, W. J., Sotto, D., Dublin, S. N., & Bao, G. (2012). Quantum dot-fluorescent protein fret probes for sensing intracellular pH. *ACS Nano*, *6*(4), 2917–2924. https://doi.org/10.1021/nn2038077

38. Ding, L., Xu, B., Li, T., Huang, J., & Bai, W. (2018). A "turn-on" fluorescence copper biosensor based on DNA cleavage-dependent graphene oxide-dsDNA-CdTe quantum dots complex. *Sensors*, *18*(8), 2605. https://doi.org/10.3390/s18082605

39. Ding, S. J., Liang, S., Nan, F., Liu, X. L., Wang, J. H., Zhou, L., Yu, X. F., Hao,

Z. H., & Wang, Q. Q. (2015). Synthesis and enhanced fluorescence of Ag doped CdTe semiconductor quantum dots. *Nanoscale*, *7*(5), 1970–1976. https://doi.org/10.1039/c4nr05731g

40. Ding, X., Qu, L., Yang, R., Zhou, Y., & Li, J. (2015). A highly selective and simple fluorescent sensor for mercury (II) ion detection based on cysteamine-capped CdTe quantum dots synthesized by the reflux method. *Luminescence*, *30*(4), 465–471. https://doi.org/10.1002/bio.2761

41. Dong, Y., Wang, R., Li, G., Chen, C., Chi, Y., & Chen, G. (2012). Polyamine-Functionalized Carbon Quantum Dots as Fluorescent Probes for Selective and Sensitive Detection of Copper Ions. *Anal. Chem.*, *84*, 6220–6224. https://doi.org/10.1021/ac3012126

42. Duan, J., Song, L., & Zhan, J. (2009). One-Pot Synthesis of Highly Luminescent CdTe Quantum Dots by Microwave Irradiation Reduction and Their Hg^{2+}-Sensitive Properties. *Nano Research*, *2*, 61–68. https://doi.org/10.1007/s12274-009-9004-0

43. Durán-Toro, V., Gran-Scheuch, A., Órdenes-Aenishanslins, N., Monrás, J. P., Saona, L. A., Venegas, F. A., Chasteen, T. G., Bravo, D., & Pérez-Donoso, J. M. (2014). Quantum dot-based assay for Cu^{2+} quantification in bacterial cell culture. *Analytical Biochemistry*, *450*(1), 30–36. https://doi.org/10.1016/j.ab.2014.01.001

44. Dutta, P., Saikia, D., Adhikary, N. C., & Sarma, N. Sen. (2015). Macromolecular Systems with MSA-Capped CdTe and CdTe/ZnS Core/Shell Quantum Dots as Superselective and Ultrasensitive Optical Sensors for Picric Acid Explosive. *ACS Applied Materials and Interfaces*, *7*(44), 24778–24790. https://doi.org/10.1021/acsami.5b07660

45. Efros, A. L., & Efros, A. L. (1982). Interband absorption of light in a semiconductor sphere. Sov. Phys. Semicond, 16(7), 772-775.

46. Ekimov, A. I., & Onushchenko, A. A. (1981). Quantum size effect in three-dimensional microscopic semiconductor crystals. ZhETF Pisma Redaktsiiu, 34, 363.

47. Elizabeth, M., Mohan, J. C., Manzoor, K., Nair, S. V, Tamura, H., & Jayakumar, R. (2010). Folate conjugated carboxymethyl chitosan – manganese doped zinc sulphide nanoparticles for targeted drug delivery and imaging of cancer cells. *Carbohydrate Polymers*, *80*(2), 442–448. https://doi.org/10.1016/j.carbpol.2009.11.047

48. Elmizadeh, H., Soleimani, M., Faridbod, F., & Bardajee, G. R. (2017). Ligand-Capped CdTe Quantum Dots as a Fluorescent Nanosensor for Detection of Copper Ions in Environmental Water Sample. *Journal of Fluorescence*, *27*(6),

2323–2333. https://doi.org/10.1007/s10895-017-2174-3

49. Enright, B., & Fitzmaurice, D. (1996). Spectroscopic Determination of Electron and Hole Effective Masses in a Nanocrystalline Semiconductor Film. *Journal of Physical Chemistry*, *100*, 1027–1035. https://doi.org/10.1021/jp951142w

50. Ensafi, A. A., Kazemifard, N., & Rezaei, B. (2015). Label-free and turn-on fluorescent cyanide sensor based on CdTe quantum dots using silver nanoparticles. *RSC Advances*, *5*(50), 40088–40093. https://doi.org/10.1039/c5ra04585a

51. Fang, T., Ma, K., Ma, L., Bai, J., Li, X., Song, H., & Guo, H. (2012a). 3-mercaptobutyric acid as an effective capping agent for highly luminescent CdTe quantum dots: New insight into the selection of mercapto acids. *Journal of Physical Chemistry C*, *116*(22), 12346–12352. https://doi.org/10.1021/jp302820u

52. Fang, T., Ma, K., Ma, L., Bai, J., Li, X., Song, H., & Guo, H. (2012b). 3-Mercaptobutyric acid as an effective capping agent for highly luminescent CdTe quantum dots: New insight into the selection of mercapto acids. *Journal of Physical Chemistry C*, *116*(22), 12346–12352. https://doi.org/10.1021/jp302820u

53. Farkhani, S. M., & Valizadeh, A. (2014). Review: Three synthesis methods of CdX (X = Se, S or Te) quantum dots. *IET Nanobiotechnology*, *8*(2), 59–76. https://doi.org/10.1049/iet-nbt.2012.0028

54. Forleo, A., Francioso, L., Capone, S., Siciliano, P., Lommens, P., & Hens, Z. (2010). Synthesis and gas sensing properties of ZnO quantum dots. *Sensors & Actuators: B. Chemical*, *146*(1), 111–115. https://doi.org/10.1016/j.snb.2010.02.059

55. Frausto-Reyes, C., Molina-Contreras, J. R., Medina-Gutiérrez, C., & Calixto, S. (2006). CdTe surface roughness by Raman spectroscopy using the 830 nm wavelength. *Spectrochimica Acta - Part A: Molecular and Biomolecular Spectroscopy*, *65*(1), 51–55. https://doi.org/10.1016/j.saa.2005.07.082

56. Frigerio, C., Abreu, V. L. R. G., & Santos, J. L. M. (2012). Evaluation of acetylcysteine promoting effect on CdTe nanocrystals photoluminescence by using a multipumping flow system. *Talanta*, *96*, 55–61. https://doi.org/10.1016/j.talanta.2012.02.002

57. Gaggelli, E., Kozlowski, H., Valensin, D., & Valensin, G. (2006). Copper Homeostasis and Neurodegenerative Disorders (Alzheimer's , Prion, and Parkinson's Diseases and Amyotrophic Lateral Sclerosis). *Chem. Rev.*, *106*(6), 1995–2044. https://doi.org/10.1021/cr040410w.

58. Gaponenko, S. V., & Demir, H. V. (2018). Quantum confinement effects in

semiconductors. In *Applied Nanophotonics* (pp. 52–91). Cambridge University Press. https://doi.org/10.1017/9781316535868.004

59. Ge, J., Ren, X., Qiu, X., Shi, H., Meng, X., & Tang, F. (2015). Fast synthesis of fluorescent SiO2@CdTe nanoparticles with reusability in detection of H_2O_2. *Journal of Materials Chemistry B*, *3*(30), 6385–6390. https://doi.org/10.1039/c5tb00740b

60. Georgopoulos, P. G., Roy, A., Yonone-Lioy, M. J., Opiekun, R. E., & Lioy, P. E. (2001). Environmental Copper: Its Dynamics and Human Exposure Issues. *Journal of Toxicology and Environmental Health, Part B: Critical Reviews*, *4*(4), 341–394. https://doi.org/10.1080/109374001753146207.

61. Ghazzal, M. N., Wojcieszak, R., Raj, G., & Gaigneaux, E. M. (2014). Study of mesoporous CdS-quantum-dot-sensitized TiO2 films by using x-ray photoelectron spectroscopy and AFM. *Beilstein Journal of Nanotechnology*, *5*, 68–76. https://doi.org/10.3762/bjnano.5.6

62. Gipson, K., Stevens, K., Brown, P., & Ballato, J. (2015). Infrared spectroscopic characterization of photoluminescent polymer nanocomposites. *Journal of Spectroscopy*, *2015*. https://doi.org/10.1155/2015/489162

63. Gokarna, A., Lee, S. K., Hwang, J. S., Cho, Y. H., Lim, Y. T., Chung, B. H., & Lee, M. (2008). Fabrication of CdSe/ZnS quantum-dot-conjugated protein microarrays and nanoarrays. *Journal of the Korean Physical Society*, *53*(5), 3047–3050. https://doi.org/10.3938/jkps.53.3047

64. Gong, T., Liu, J., Wu, Y., Xiao, Y., Wang, X., & Yuan, S. (2017). Fluorescence enhancement of CdTe quantum dots by HBcAb-HRP for sensitive detection of H_2O_2 in human serum. *Biosensors and Bioelectronic*, *92*, 16–20. https://doi.org/10.1016/j.bios.2017.01.048

65. Gourgon, C., Eriksson, B., Dang, L. S., Mariette, H., & Vieu, C. (1994). Photoluminescence of CdTe / ZnTe semiconductor wires and dots. *Journal of Crystal Growth*, *138*, 590–594. https://doi.org/10.1016/0022-0248(94)90874-5

66. Grandhi, G. K., Arunkumar, M., & Viswanatha, R. (2016). Understanding the Role of Surface Capping Ligands in Passivating the Quantum Dots Using Copper Dopants as Internal Sensor. *Journal of Physical Chemistry C*, *120*(35), 19785–19795. https://doi.org/10.1021/acs.jpcc.6b04060

67. Green, M., Williamson, P., Samalova, M., Davis, J., Brovelli, S., Dobson, P., & Cacialli, F. (2009). Synthesis of type II/type I CdTe/CdS/ZnS quantum dots and their use in cellular imaging. *Journal of Materials Chemistry*, *19*(44), 8341. https://doi.org/10.1039/b913292a

68. Gu, B., Ye, M., Nie, L., Fang, Y., Wang, Z., Zhang, X., Zhang, H., Zhou, Y., & Zhang, Q. (2018). Organic-Dye-Modified Upconversion Nanoparticle as a Multichannel Probe to Detect Cu^{2+} in Living Cells. *ACS Applied Materials and Interfaces*, *10*(1), 1028–1032. https://doi.org/10.1021/acsami.7b13351

69. Gu, B., & Zhang, Q. (2018). Recent Advances on Functionalized Upconversion Nanoparticles for Detection of Small Molecules and Ions in Biosystems. *Advanced Science*, *5*(3), 1700609. https://doi.org/10.1002/advs.201700609

70. Guillén-Cervantes, A., Becerril-Silva, M., Silva-López, H. E., Arias-Cerón, J. S., Campos-González, E., Pérez-González, M., & Zelaya-Ángel, O. (2020). Structural and optical properties of CdTe + $CdTeO_3$ nanocomposite films with broad blueish photoluminescence. *Journal of Materials Science: Materials in Electronics*, *31*(9), 7133–7140. https://doi.org/10.1007/s10854-020-03284-z

71. Halliwell, B., Clement, M. V., & Long, L. H. (2000). Hydrogen peroxide in the human body. *FEBS Letters*, *486*(1), 10–13. https://doi.org/10.1016/S0014-5793(00)02197-9

72. Hammond, J. S., Gaarenstroom, S. W., & Winograd, N. (1975). X-Ray Photoelectron Spectroscopic Studies of Cadmium-and SiIver-Oxygen Surfaces. *Analytical Chemistry*, *47*(13), 2193–2199. https://doi.org/10.1021/ac60363a019

73. Han, B., Yuan, J., & Wang, E. (2009). Sensitive and selective sensor for biothiols in the cell based on the recovered fluorescence of the CdTe quantum dots-Hg(II) system. *Analytical Chemistry*, *81*(13), 5569–5573. https://doi.org/10.1021/ac900769h

74. Haotong Wei, Hao Zhang, Haizhu Sun, Weili Yu, Yi Liu, Zhaolai Chen, Liying Cui, W. T. and B. Y. (2012). *Aqueous-solution-processed PPV–$Cd_xHg_{1-x}Te$ hybrid solar cells with a significant near-infrared contribution*. 17827–17832. https://doi.org/10.1039/c2jm33958g

75. He, H., Qian, H., Dong, C., Wang, K., & Ren, J. (2006). Single nonblinking CdTe quantum dots synthesized in aqueous thiopropionic acid. *Angewandte Chemie - International Edition*, *45*, 7588–7591. https://doi.org/10.1002/anie.200602758

76. Hua, J., Yang, J., Zhu, Y., Zhao, C., & Yang, Y. (2017). Highly fluorescent carbon quantum dots as nanoprobes for sensitive and selective determination of mercury (II) in surface waters. *Spectrochimica Acta - Part A: Molecular and Biomolecular Spectroscopy*, *187*, 149–155. https://doi.org/10.1016/j.saa.2017.06.058

77. Iliuk, A. B., Hu, L., & Tao, W. A. (2011). Aptamer in bioanalytical applications. *Analytical Chemistry*, *83*(12), 4440–4452. https://doi.org/10.1021/ac201057w

78. Inácio, E. M., Lima, M. C. P., Souza, D. H. S., Sirelli, L., & Dias, M. L. (2018). Crystallization, thermal and mechanical behavior of oligosebacate plasticized poly(lactic acid) films. *Polímeros*, *28*(5), 381–388. https://doi.org/10.1590/0104-1428.04917

79. Jin, L., & Han, C. (2014). Ultrasensitive and Selective Fluorimetric Detection of Copper Ions Using Thiosulfate-Involved Quantum Dots. *Anal. Chem.*, *34*(15), 7209–7213.

80. Kakuta, N., White, J. M., Campion, A., Bard, A. J., Fox, M. A., & Webber, S. E. (1985). Surface analysis of semiconductor-incorporated polymer systems. 1. Nafion and CdS-Nafion. *Journal of Physical Chemistry*, *89*(1), 48–52. https://doi.org/10.1021/j100247a014

81. Kale, S., Kale, A., Gholap, H., Rana, A., Desai, R., Banpurkar, A., Ogale, S., & Shastry, P. (2012). Quantum dot bio-conjugate: As a western blot probe for highly sensitive detection of cellular proteins. *Journal of Nanoparticle Research*, *14*(3). https://doi.org/10.1007/s11051-012-0732-9

82. Kim, L. A., Anikeeva, P. O., Coe-Sullivan, S. A., Steckel, J. S., Bawendi, M. G., & Bulović, V. (2008). Contact printing of quantum dot light-emitting devices. *Nano Letters*, *8*(12), 4513–4517. https://doi.org/10.1021/nl8025218

83. Kim, T. H., Cho, K. S., Lee, E. K., Lee, S. J., Chae, J., Kim, J. W., Kim, D. H., Kwon, J. Y., Amaratunga, G., Lee, S. Y., Choi, B. L., Kuk, Y., Kim, J. M., & Kim, K. (2011). Full-colour quantum dot displays fabricated by transfer printing. *Nature Photonics*, *5*(3), 176–182. https://doi.org/10.1038/nphoton.2011.12

84. Kim, T. H., Chung, D. Y., Ku, J., Song, I., Sul, S., Kim, D. H., Cho, K. S., Choi, B. L., Min Kim, J., Hwang, S., & Kim, K. (2013). Heterogeneous stacking of nanodot monolayers by dry pick-and-place transfer and its applications in quantum dot light-emitting diodes. *Nature Communications*, *4*, 1–9. https://doi.org/10.1038/ncomms3637

85. King, P. D. C., Veal, T. D., Schleife, A., Zúñiga-Pérez, J., Martel, B., Jefferson, P. H., Fuchs, F., Muñoz-Sanjosé, V., Bechstedt, F., & McConville, C. F. (2009). Valence-band electronic structure of CdO, ZnO, and MgO from x-ray photoemission spectroscopy and quasi-particle-corrected density-functional theory calculations. *Physical Review B*, *79*(20), 205205. https://doi.org/10.1103/PhysRevB.79.205205

86. Koh, W. K., Saudari, S. R., Fafarman, A. T., Kagan, C. R., & Murray, C. B. (2011). Thiocyanate-capped PbS nanocubes: Ambipolar transport enables quantum dot based circuits on a flexible substrate. *Nano Letters*, *11*(11), 4764–4767. https://doi.org/10.1021/nl202578g

87. Kramer, I. J., Minor, J. C., Moreno-Bautista, G., Rollny, L., Kanjanaboos, P., Kopilovic, D., Thon, S. M., Carey, G. H., Chou, K. W., Zhitomirsky, D., Amassian, A., & Sargent, E. H. (2015). Efficient spray-coated colloidal quantum dot solar cells. *Advanced Materials*, *27*(1), 116–121. https://doi.org/10.1002/adma.201403281

88. Kuddus, A., Ismail, A. B. M., & Hossain, J. (2021). Design of a highly efficient CdTe-based dual-heterojunction solar cell with 44% predicted efficiency. *Solar Energy*, *221*, 488–501. https://doi.org/10.1016/j.solener.2021.04.062

89. Kumar, A., & Dutta, R. K. (2017). Rapid Photoluminescence Quenching Based Detection of Cu^{2+} in Aqueous Medium by CdS Quantum Dots Surface Passivated by Thiourea. *Analytical Sciences*, *33*(5), 565–571. https://doi.org/10.2116/analsci.33.565

90. Kundu, P., Deshpande, P. A., Madras, G., & Ravishankar, N. (2011). Nanoscale ZnO/CdS heterostructures with engineered interfaces for high photocatalytic activity under solar radiation. *Journal of Materials Chemistry*, *21*(12), 4209–4216. https://doi.org/10.1039/c0jm03116j

91. Kurtz, E., Shen, J., Schmidt, M., Grün, M., Hong, S. K., Litvinov, D., Gerthsen, D., Oka, T., Yao, T., & Klingshirn, C. (2000). Formation and properties of self-organized II-VI quantum islands. *Thin Solid Films*, *367*(1–2), 68–74. https://doi.org/10.1016/S0040-6090(00)00665-9

92. Lakowicz, J. R. (2006). Quenching of Fluorescence. In *Principles of Fluorescence Spectroscopy* (pp. 277–330). https://doi.org/10.1007/978-0-387-46312-4_8

93. Lee, L. K., & Ku, P. C. (2012). Fabrication of site-controlled InGaN quantum dots using reactive-ion etching. *Physica Status Solidi C*, *9*(3–4), 609–612. https://doi.org/10.1002/pssc.201100428

94. Leonardi, K., Selke, H., Heinke, H., Ohkawa, K., Hommel, D., Gindele, F., & Woggon, U. (1998). Formation of self-assembling II–VI semiconductor nanostructures during migration enhanced epitaxy. *Journal of Crystal Growth*, *184–185*, 259–263. https://doi.org/10.1016/S0022-0248(98)80055-9

95. Li, Haibing, & Qu, F. (2007). Synthesis of CdTe Quantum Dots in Sol - Gel-Derived Composite Silica Spheres Coated with Calix [4] arene as Luminescent Probes for Pesticides. *Chem. Mater.*, *5*(4), 4148–4154. https://doi.org/10.1021/cm0700089

96. Li, Hongbo, Brescia, R., Povia, M., Prato, M., Bertoni, G., Manna, L., & Moreels, I. (2013). Synthesis of uniform disk-shaped copper telluride nanocrystals and cation exchange to cadmium telluride quantum disks with stable red emission.

Journal of the American Chemical Society, *135*(33), 12270–12278. https://doi.org/10.1021/ja404694k

97. Li, L., Liao, L., Ding, Y., & Zeng, H. (2017). Dithizone-etched CdTe nanoparticles-based fluorescence sensor for the off-on detection of cadmium ion in aqueous media. *RSC Advances*, *7*(17), 10361–10368. https://doi.org/10.1039/C6RA24971J

98. Li, T., Zhou, Y., Sun, J., Tang, D., Guo, S., & Ding, X. (2011). Ultrasensitive detection of mercury(II) ion using CdTe quantum dots in sol-gel-derived silica spheres coated with calix[6]arene as fluorescent probes. *Microchimica Acta*, *175*(1–2), 113–119. https://doi.org/10.1007/s00604-011-0655-7

99. Li, X., Zhou, Y., Zheng, Z., Yue, X., Dai, Z., Liu, S., & Tang, Z. (2009). Glucose biosensor based on nanocomposite films of CdTe quantum dots and glucose oxidase. *Langmuir*, *25*(11), 6580–6586. https://doi.org/10.1021/la900066z

100. Liang, S., Qi, L., Zhang, R., Jin, M., & Zhang, Z. (2017). Sensors and Actuators B : Chemical Ratiometric fluorescence biosensor based on CdTe quantum and carbon dots for double strand DNA detection. *Sensors & Actuators: B. Chemical*, *244*, 585–590. https://doi.org/10.1016/j.snb.2017.01.032

101. Liang, W., Liu, S., Liu, Z., Li, D., Wang, L., Hao, C., & He, Y. (2015). Electron transfer and fluorescence "turn-off" based CdTe quantum dots for vancomycin detection at nanogram level in aqueous serum media. *New Journal of Chemistry*, *39*(6), 4774-4782. https://doi.org/10.1039/C4NJ01764A

102. Lin, Y. W., Tseng, W. L., & Chang, H. T. (2006). Using a layer-by-layer assembly technique to fabricate multicolored-light- emitting films of CdSe@CdS and CdTe quantum dots. *Advanced Materials*, *18*(11), 1381–1386. https://doi.org/10.1002/adma.200502515

103. Liu, H., Li, M., Jiang, L., Shen, F., Hu, Y., & Ren, X. (2017). Sensitive arginine sensing based on inner filter effect of Au nanoparticles on the fluorescence of CdTe quantum dots. *Spectrochimica Acta - Part A: Molecular and Biomolecular Spectroscopy*, *173*, 105–113. https://doi.org/10.1016/j.saa.2016.08.057

104. Liu, J., Raveendran, P., Shervani, Z., & Ikushima, Y. (2004). Synthesis of Ag_2S quantum dots in water-in-CO_2 microemulsions. *Chem. Commun.*, 2582–2583. https://doi.org/10.1039/b410700d

105. Liu, S., Pang, S., Na, W., & Su, X. (2014). Near-infrared fluorescence probe for the determination of alkaline phosphatase. *Biosensors and Bioelectronics*, *55*, 249–254. https://doi.org/10.1016/j.bios.2013.12.023

106. Liu, S., Shi, F., Zhao, X., Chen, L., & Su, X. (2013). 3-Aminophenyl boronic

acid-functionalized $CuInS_2$ quantum dots as a near-infrared fluorescence probe for the determination of dopamine. *Biosensors and Bioelectronics*, *47*, 379–384. https://doi.org/10.1016/j.bios.2013.03.055

107. Liu, X., Zhou, P., Zhan, H., Liu, H., Zhang, J., & Zhao, Y. (2017). Synthesis and characterization of near-infrared-emitting CdHgTe/CdS/ZnS quantum dots capped by N-acetyl-L-cysteine for in vitro and in vivo imaging. *RSC Adv.*, *7*(48), 29998–30007. https://doi.org/10.1039/C7RA02403G

108. Liu, Y., Chen, W., Joly, A. G., Wang, Y., Pope, C., Zhang, Y., Bovin, J., & Sherwood, P. (2006). Comparison of Water-Soluble CdTe Nanoparticles Synthesized in Air and in Nitrogen. *J. Phys. Chem. B*, *110*(34), 16992–17000. https://doi.org/10.1021/jp063085k

109. Liu, Y. F., & Yu, J. S. (2010). In situ synthesis of highly luminescent glutathione-capped CdTe/ZnS quantum dots with biocompatibility. *Journal of Colloid and Interface Science*, *351*(1), 1–9. https://doi.org/10.1016/j.jcis.2010.07.047

110. Liu, Z., Liu, S., Yin, P., & He, Y. (2012). Fluorescence enhancement of CdTe/CdS quantum dots by coupling of glyphosate and its application for sensitive detection of copper ion. *Analytica Chimica Acta*, *745*, 78–84. https://doi.org/10.1016/j.aca.2012.07.033

111. Lu, L. Q., Tan, T., Tian, X. K., Li, Y., & Deng, P. (2017). Visual and sensitive fluorescent sensing for ultratrace mercury ions by perovskite quantum dots. *Analytica Chimica Acta*, *986*, 109–114. https://doi.org/10.1016/j.aca.2017.07.014

112. Lu, S., Li, G., Lv, Z., Qiu, N., Kong, W., Gong, P., Chen, G., Xia, L., Guo, X., You, J., & Wu, Y. (2016). Facile and ultrasensitive fluorescence sensor platform for tumor invasive biomaker β-glucuronidase detection and inhibitor evaluation with carbon quantum dots based on inner-filter effect. *Biosensors and Bioelectronics*, *85*, 358–362. https://doi.org/10.1016/j.bios.2016.05.021

113. Luther, J. M., Law, M., Song, Q., Perkins, C. L., Beard, M. C., & Nozik, A. J. (2008). Structural, optical, and electrical properties of self-assembled films of PbSe nanocrystals treated with 1,2-ethanedithiol. *ACS Nano*, *2*(2), 271–280. https://doi.org/10.1021/nn7003348

114. Ma, K., Fang, T., Bai, J., & Guo, H. (2013a). Regulating properties of quantum dots: effect of methyl side groups of mercapto acids. *RSC Advances*, *3*(15), 4935. https://doi.org/10.1039/c3ra22877k

115. Ma, K., Fang, T., Bai, J., & Guo, H. (2013b). Regulating properties of quantum dots: effect of methyl side groups of mercapto acids. *RSC Advances*, *3*(15), 4935–4939. https://doi.org/10.1039/c3ra22877k

116. Ma, Q., Ha, E., Yang, F., & Su, X. (2011). Synchronous determination of mercury (II) and copper (II) based on quantum dots-multilayer film. *Analytica Chimica Acta*, *701*(1), 60–65. https://doi.org/10.1016/j.aca.2011.04.051

117. Ma, Q., & Su, X. (2011). Recent advances and applications in QDs-based sensors. *Analyst*, *136*(23), 4883–4893. https://doi.org/10.1039/c1an15741h

118. Majid, A., & Bibi, M. (2018). Wet Chemical Synthesis Methods. In *Cadmium based II-VI Semiconducting Nanomaterials, Topics in Mining, Metallurgy and Materials Engineering* (pp. 43–101). Springer International Publishing. https://doi.org/10.1007/978-3-319-68753-7_3

119. Manavi, P. N., & Mazumder, A. (2018). Potential risk of mercury to human health in three species of fish from the southern Caspian Sea. *Marine Pollution Bulletin*, *130*, 1–5. https://doi.org/10.1016/j.marpolbul.2018.03.004

120. Mani, N. P., & Cyriac, J. (2019). pH-sensitive response of a highly photoluminescent MoS_2 nanohybrid material and its application in the nonenzymatic detection of H_2O_2. *Analytical and Bioanalytical Chemistry*, *411*(21), 5481–5488. https://doi.org/10.1007/s00216-019-01923-x

121. Mao, G., Zhang, Q., Yang, Y., Ji, X., & He, Z. (2019). Facile synthesis of stable CdTe/CdS QDs using dithiol as surface ligand for alkaline phosphatase detection based on inner filter effect. *Analytica Chimica Acta*, *1047*, 208–213. https://doi.org/10.1016/j.aca.2018.10.009

122. Masood, H. T., Muhammad, Z., Habib, M., Wang, D. M., & Wang, D. L. (2017). Low temperature ferromagnetic properties of CdS and CdTe thin films. *Chinese Physics B*, *26*(6). https://doi.org/10.1088/1674-1056/26/6/067503

123. McCranor, B. J., Szmacinski, H., Zeng, H. H., Stoddard, A. K., Hurst, T., Fierke, C. A., Lakowicz, J. R., & Thompson, R. B. (2014). Fluorescence lifetime imaging of physiological free Cu(II) levels in live cells with a Cu(II)-selective carbonic anhydrase-based biosensor. *Metallomics*, *6*(5), 1034–1042. https://doi.org/10.1039/c3mt00305a

124. McDowell, L. R. (2003). *Minerals in Animal and Human Nutrition* (Second). Elsevier.

125. Moquin, A., Hutter, E., Choi, A. O., Khatchadourian, A., Castonguay, A., Winnik, F. M., & Maysinger, D. (2013). Caspase‐1 Activity in Microglia Stimulated by Pro-In fl ammagen. *ACS Nano*, *7*(11), 9585–9598. https://doi.org/10.1021/nn404473g

126. Murray, C. B., Norris, D. J., & Bawendi, M. G. (1993). Synthesis and Characterization of Nearly Monodisperse CdE (E = S, Se, Te) Semiconductor

Nanocrystallites. *Journal of the American Chemical Society*, *115*(19), 8706–8715. https://doi.org/10.1021/ja00072a025

127. Nath, S. S., Choudhury, M., Chakdar, D., Gope, G., & Nath, R. K. (2010). Sensors and Actuators B : Chemical Acetone sensing property of ZnO quantum dots embedded on PVP. *Sensors & Actuators: B. Chemical*, *148*(2), 353–357. https://doi.org/10.1016/j.snb.2010.06.001

128. Nazzal, A. Y., Qu, L., Peng, X., & Xiao, M. (2003). Photoactivated CdSe Nanocrystals as Nanosensors for Gases. *Nano Letters*, *3*(6), 819–822. https://doi.org/10.1021/nl0340935

129. Nsibande, S. A., & Forbes, P. B. C. (2016). Fluorescence detection of pesticides using quantum dot materials – A review. *Analytica Chimica Acta*, *945*, 9–22. https://doi.org/10.1016/j.aca.2016.10.002

130. Nurerk, P., Kanatharana, P., & Bunkoed, O. (2016). A selective determination of copper ions in water samples based on the fluorescence quenching of thiol-capped CdTe quantum dots. *Luminescence*, *31*, 515–522. https://doi.org/10.1002/bio.2990

131. Orellana, G. (2006). Fluorescence-Based Sensors. In *Optical Chemical Sensors* (pp. 99–116). https://doi.org/10.1007/1-4020-4611-1_6

132. Pal, A., Arora, B., Rani, D., Srivastava, S., Gupta, R., & Sapra, S. (2018). Fluorescence quenching of CdTe quantum dots with Co (III) complexes via electrostatic assembly formation. *Zeitschrift Fur Physikalische Chemie*, *232*(9–11), 1413–1430. https://doi.org/10.1515/zpch-2018-1138

133. Pandian, S. R. kumar, Deepak, V., Kalishwaralal, K., & Gurunathan, S. (2011). Biologically synthesized fluorescent CdS NPs encapsulated by PHB. *Enzyme and Microbial Technology*, *48*, 319–325. https://doi.org/10.1016/j.enzmictec.2011.01.005

134. Pankiewicz, C. G., De Assis, P. L., Filho, P. E. C., Chaves, C. R., De Araújo, E. N. D., Paniago, R., & Guimarães, P. S. S. (2015). Characterization of the dynamics of photoluminescence degradation in aqueous CdTe/CdS core-shell quantum dots. *Journal of Fluorescence*, *25*(5), 1389–1395. https://doi.org/10.1007/s10895-015-1629-7

135. Patra, S., & Samanta, A. (2013). A Fluorescence Correlation Spectroscopy, Steady-State, and Time-Resolved Fluorescence Study of the Modulation of Photophysical Properties of Mercaptopropionic Acid Capped CdTe Quantum Dots upon Exposure to Light. *Journal of Physical Chemistry C*, *117*(44), 23313–23321. https://doi.org/10.1021/jp407130e

136. Patra, S., & Samanta, A. (2014). Effect of capping agent and medium on light-induced variation of the luminescence properties of CdTe quantum dots: A study based on fluorescence correlation spectroscopy, steady state and time-resolved fluorescence techniques. *Journal of Physical Chemistry C*, *118*(31), 18187–18196. https://doi.org/10.1021/jp5048216

137. Pechstedt, K., Whittle, T., Baumberg, J., & Melvin, T. (2010). Photoluminescence of colloidal CdSe/ZnS quantum dots: The critical effect of water molecules. *Journal of Physical Chemistry C*, *114*(28), 12069–12077. https://doi.org/10.1021/jp100415k

138. Peng, H., Zhang, L., Soeller, C., & Travas-Sejdic, J. (2007). Preparation of water-soluble CdTe/CdS core/shell quantum dots with enhanced photostability. *Journal of Luminescence*, *127*(2), 721–726. https://doi.org/10.1016/j.jlumin.2007.04.007

139. Peng, L., Xie, T. F., Yang, M., Wang, P., Xu, D., Pang, S., & Wang, D. J. (2008). Light induced enhancing gas sensitivity of copper-doped zinc oxide at room temperature. *Sensors and Actuators, B: Chemical*, *131*(2), 660–664. https://doi.org/10.1016/j.snb.2007.12.060

140. Pottathara, Y. B., Grohens, Y., Kokol, V., Kalarikkal, N., & Thomas, S. (2019). Synthesis and processing of emerging two-dimensional nanomaterials. In *Nanomaterials Synthesis: Design, Fabrication and Applications* (pp. 1–25). Elsevier Inc. https://doi.org/10.1016/B978-0-12-815751-0.00001-8

141. Pourret, A., Guyot-Sionnest, P., & Elam, J. W. (2009). Atomic layer deposition of ZnO in quantum dot thin films. *Advanced Materials*, *21*(2), 232–235. https://doi.org/10.1002/adma.200801313

142. Priyam, A., Chatterjee, A., Bhattacharya, C., & Saha, A. (2009). Conformation and activity dependent interaction of glucose oxidase with CdTe quantum dots : towards developing a nanoparticle based enzymatic assay. *Photochemical & Photobiological Sciences*, *8*, 362–370. https://doi.org/10.1039/b815881a

143. Ramírez-Herrera, D. E., Tirado-Guízar, A., Paraguay-Delgado, F., & Pina-Luis, G. (2017). Ratiometric arginine assay based on FRET between CdTe quantum dots and Cresyl violet. *Microchimica Acta*, *184*(7), 1997–2005. https://doi.org/10.1007/s00604-017-2205-4

144. Reiss, P., Protière, M., & Li, L. (2009). Core/shell semiconductor nanocrystals. *Small*, *5*(2), 154–168. https://doi.org/10.1002/smll.200800841

145. Resch-Genger, U., Grabolle, M., Cavaliere-Jaricot, S., Nitschke, R., & Nann, T. (2008). Quantum dots versus organic dyes as fluorescent labels. *Nature Methods*, *5*(9), 763–775. https://doi.org/10.1038/nmeth.1248

146. Rezlescu, N., Iftimie, N., Rezlescu, E., Doroftei, C., & Popa, P. D. (2006). Semiconducting gas sensor for acetone based on the fine grained nickel ferrite. *Sensors and Actuators, B: Chemical*, *114*(1), 427–432. https://doi.org/10.1016/j.snb.2005.05.030

147. Ribeiro, D. S. M., Castro, R. C., Páscoa, R. N. M. J., Soares, J. X., Rodrigues, S. S. M., & Santos, J. L. M. (2019). Tuning CdTe quantum dots reactivity for multipoint detection of mercury(II), silver(I) and copper(II). *Journal of Luminescence*, *207*, 386–396. https://doi.org/10.1016/j.jlumin.2018.11.035

148. Rizzo, A., Mazzeo, M., Palumbo, M., Lerario, G., D'Amone, S., Cingolani, R., & Gigli, G. (2008). Hybrid light-emitting diodes from microcontact-printing double-transfer of colloidal semiconductor CdSe/ZnS quantum dots onto organic layers. *Advanced Materials*, *20*(10), 1886–1891. https://doi.org/10.1002/adma.200701480

149. Rodrigues, S. S. M., Ribeiro, D. S. M., Molina-Garcia, L., Ruiz Medina, A., Prior, J. A. V., & Santos, J. L. M. (2014). Fluorescence enhancement of CdTe MPA-capped quantum dots by glutathione for hydrogen peroxide determination. *Talanta*, *122*, 157–165. https://doi.org/10.1016/j.talanta.2014.01.031

150. Rogach, A. L., Franzl, T., Klar, T. A., Feldmann, J., Gaponik, N., Lesnyak, V., Shavel, A., Eychmüller, A., Rakovich, Y. P., & Donegan, J. F. (2007). Aqueous synthesis of thiol-capped CdTe nanocrystals: State-of-the-art. *Journal of Physical Chemistry C*, *111*(40), 14628–14637. https://doi.org/10.1021/jp072463y

151. Roy, D., Munz, M., Colombi, P., Bhattacharyya, S., Salvetat, J. P., Cumpson, P. J., & Saboungi, M. L. (2007). Directly writing with nanoparticles at the nanoscale using dip-pen nanolithography. *Applied Surface Science*, *254*(5), 1394–1398. https://doi.org/10.1016/j.apsusc.2007.06.058

152. S., K., B.F., D., & M.O., O. (2018). Structural, optical and luminescence properties of CdTe quantum dots: Investigation on the effect of capping ligand ratio. *Materials Research Express*. https://doi.org/10.1088/2053-1591/aac938

153. Sabet, F. S., Hosseini, M., Khabbaz, H., Dadmehr, M., & Ganjali, M. R. (2017). FRET-based aptamer biosensor for selective and sensitive detection of aflatoxin B1 in peanut and rice. Food Chemistry, 220, 527-532.) https://doi.org/10.1016/j.foodchem.2016.10.004

154. Saeedzadeh Amiri, N., & Milani Hosseini, M. R. (2019). Application of ratiometric fluorescence sensor-based microwave-assisted synthesized CdTe quantum dots and mesoporous structured epitope-imprinted polymers for highly efficient determination of tyrosine phosphopeptide. *Analytical Methods*, *12*(1), 63–72. https://doi.org/10.1039/c9ay00276f

155. Sahoo, S. K., Sharma, D., Ber, R. K., Crisponi, G., & Callan, J. F. (2012). Iron(III) selective molecular and supramolecular fluorescent probes. *Chemical Society Reviews*, *41*(21), 7195–7227. https://doi.org/10.1039/c2cs35152h

156. Sander F. Wuister, Ingmar Swart, Floris van Driel, Stephen G. Hickey, A., & Donegá, C. de M. (2003). Highly luminescent water-soluble CdTe quantum dots. *Nano Letters*, *3*(4), 503–507. https://doi.org/10.1021/NL034054T

157. Santhosh, K., Patra, S., Soumya, S., Khara, D. C., & Samanta, A. (2011). Fluorescence quenching of CdS quantum dots by 4-azetidinyl-7-nitrobenz-2-oxa-1,3-diazole: A mechanistic study. *ChemPhysChem*, *12*(15), 2735–2741. https://doi.org/10.1002/cphc.201100515

158. Saran, A. D., Sadawana, M. M., Srivastava, R., & Bellare, J. R. (2011). An optimized quantum dot-ligand system for biosensing applications: Evaluation as a glucose biosensor. *Colloids and Surfaces A: Physicochemical and Engineering Aspects*, *384*(1–3), 393–400. https://doi.org/10.1016/j.colsurfa.2011.04.022

159. Sauer, H., Wartenberg, M., & Hescheler, J. (2001). Reactive oxygen species as intracellular messengers during cell growth and differentiation. *Cellular Physiology and Biochemistry*, *11*(4), 173–186. https://doi.org/10.1159/000047804

160. Sawicki, K., Malinowski, F. K., Gałkowski, K., Jakubczyk, T., Kossacki, P., Pacuski, W., & Suffczyński, J. (2015). Single-color, in situ photolithography marking of individual CdTe/ZnTe quantum dots containing a single Mn^{2+} ion. *Applied Physics Letters*, *106*(1), 012101. https://doi.org/10.1063/1.4905306

161. Schneider, R., Wolpert, C., Guilloteau, H., Balan, L., Lambert, J., & Merlin, C. (2009). The exposure of bacteria to CdTe-core quantum dots: The importance of surface chemistry on cytotoxicity. *Nanotechnology*, *20*, 225101. https://doi.org/10.1088/0957-4484/20/22/225101

162. Sha, J., Tong, C., Zhang, H., Feng, L., Liu, B., & Lü, C. (2015). CdTe QDs functionalized mesoporous silica nanoparticles loaded with conjugated polymers: A facile sensing platform for cupric (II) ion detection in water through FRET. *Dyes and Pigments*, *113*, 102–109. https://doi.org/10.1016/j.dyepig.2014.07.040

163. Shamsipur, M., Nasirian, V., Barati, A., Rafienia, M., & Sheikh Arabi, M. (2019). Development of a sensitive B12 determination method based on inner filter effect on CdTe quantum dots. *Advances in Nanochemistry*, *1*(1), 1–5. https://doi.org/10.22126/anc.2019.3146.1002

164. Shanehsaz, M., Mohsenifar, A., Hasannia, S., Pirooznia, N., Samaei, Y., & Shamsipur, M. (2013). Detection of Helicobacter pylori with a nanobiosensor based on fluorescence resonance energy transfer using CdTe quantum dots.

Microchimica Acta, *180*(3–4), 195–202. https://doi.org/10.1007/s00604-012-0906-2

165. Shang, L., Zhang, L., & Dong, S. (2009). Turn-on fluorescent cyanide sensor based on copper ion-modified CdTe quantum dots. *Analyst*, *134*(1), 107–113. https://doi.org/10.1039/b812458b

166. Shen, M., Jia, W., You, Y., Hu, Y., Li, F., Tian, S., Li, J., Jin, Y., & Han, D. (2013). Luminescent properties of CdTe quantum dots synthesized using 3-mercaptopropionic acid reduction of tellurium dioxide directly. *Nanoscale Research Letters*, *8*(1), 253. https://doi.org/10.1186/1556-276X-8-253

167. Shi, J. J., Zhu, J. C., Zhao, M., Wang, Y., Yang, P., & He, J. (2018). Ultrasensitive photoelectrochemical aptasensor for lead ion detection based on sensitization effect of CdTe QDs on MoS2-CdS: Mn nanocomposites by the formation of G-quadruplex structure. Talanta, 183, 237-244. https://doi.org/10.1016/j.talanta.2018.02.087

168. Simon, A. R., Rai, U., Fanburg, B. L., & Cochran, B. H. (1998). Activation of the JAK-STAT pathway by reactive oxygen species. *American Journal of Physiology - Cell Physiology*, *275*(6 44-6), 1640–1652. https://doi.org/10.1152/ajpcell.1998.275.6.c1640

169. Singh, V. K., Mishra, H., Ali, R., Umrao, S., Srivastava, R., Abraham, S., Misra, A., Singh, V. N., Mishra, H., Tiwari, R. S., & Srivastava, A. (2019). In Situ Functionalized Fluorescent WS_2-QDs as Sensitive and Selective Probe for Fe^{3+} and a Detailed Study of Its Fluorescence Quenching. *ACS Applied Nano Materials*, *2*(1), 566–576. https://doi.org/10.1021/acsanm.8b02162

170. Sivaraman, G., Iniya, M., Anand, T., Kotla, N. G., Sunnapu, O., Singaravadivel, S., Gulyani, A., & Chellappa, D. (2018). Chemically diverse small molecule fluorescent chemosensors for copper ion. *Coordination Chemistry Reviews*, *357*, 50–104. https://doi.org/10.1016/j.ccr.2017.11.020

171. Song, K. W., Costi, R., & Bulovič, V. (2013). Electrophoretic deposition of CdSe/ZnS quantum dots for light-emitting devices. *Advanced Materials*, *25*(10), 1420–1423. https://doi.org/10.1002/adma.201203079

172. Suffern, D., Cooper, D., Carlini, L., Parbhoo, R., Bradforth, S., & Nadeau, J. (2009). Photoenhancement of quantum dots and conjugates measured by time-resolved spectroscopy. *Colloidal Quantum Dots for Biomedical Applications IV*, *7189*(July 2014), 718905. https://doi.org/10.1117/12.813863

173. Suriamoorthy, P., Zhang, X., Hao, G., Joly, A. G., Singh, S., Hossu, M., Sun, X., & Chen, W. (2010). Folic acid-CdTe quantum dot conjugates and their applications for cancer cell targeting. *Cancer Nanotechnology*, *1*, 19–28.

https://doi.org/10.1007/s12645-010-0003-3

174. Sutter, J. U., Birch, D. J. S., & Rolinski, O. J. (2012). CdSe/ZnS core/shell quantum dots as luminescence lifetime sensors for Cu^{2+}. *Measurement Science and Technology*, *23*(5), 055103. https://doi.org/10.1088/0957-0233/23/5/055103

175. Tabaraki, R., & Sadeghinejad, N. (2018). Microwave assisted synthesis of doped carbon dots and their application as green and simple turn off–on fluorescent sensor for mercury (II) and iodide in environmental samples. *Ecotoxicology and Environmental Safety*, *153*(January 2017), 101–106. https://doi.org/10.1016/j.ecoenv.2018.01.059

176. Tan, X., Li, Q., Zhang, X., Shen, Y., & Yang, J. (2015). A novel and sensitive turn-on fluorescent biosensor for the determination of thioctic acid based on Cu^{2+}-modulated N-acetyl-l-cysteine capped CdTe quantum dots. *RSC Advances*, *5*(55), 44173–44182. https://doi.org/10.1039/c5ra05087a

177. Tang, B., Cao, L., Xu, K., Zhuo, L., Ge, J., Li, Q., & Yu, L. (2008). A New Nanobiosensor for Glucose with High Sensitivity and Selectivity in Serum Based on Fluorescence Resonance Energy Transfer (FRET) between CdTe Quantum Dots and Au Nanoparticles. *Chem. Eur. J*, *14*, 3637–3644. https://doi.org/10.1002/chem.200701871

178. Tang, B., Niu, J., Yu, C., Zhuo, L., & Ge, J. (2005). Highly luminescent water-soluble CdTe nanowires as fluorescent probe to detect copper(II). *Chemical Communications*, *33*, 4184–4186. https://doi.org/10.1039/b502978c

179. Tantama, M., Hung, Y. P., & Yellen, G. (2011). Imaging intracellular pH in live cells with a genetically encoded red fluorescent protein sensor. *Journal of the American Chemical Society*, *133*(26), 10034–10037. https://doi.org/10.1021/ja202902d

180. Tawfik, S. M., Shim, J., Biechele-Speziale, D., Sharipov, M., & Lee, Y. I. (2018). Novel "turn off-on" sensors for highly selective and sensitive detection of spermine based on heparin-quenching of fluorescence CdTe quantum dots-coated amphiphilic thiophene copolymers. *Sensors and Actuators, B: Chemical*, *257*, 734–744. https://doi.org/10.1016/j.snb.2017.10.172

181. Tenório, D. P. L. A., Andrade, C. G., Cabral Filho, P. E., Sabino, C. P., Kato, I. T., Carvalho, L. B., Alves, S., Ribeiro, M. S., Fontes, A., & Santos, B. S. (2015). CdTe quantum dots conjugated to concanavalin A as potential fluorescent molecular probes for saccharides detection in Candida albicans. *Journal of Photochemistry and Photobiology B: Biology*, *142*, 237–243. https://doi.org/10.1016/j.jphotobiol.2014.11.010

182. Trotzky, S., Kolny-Olesiak, J., Falke, S. M., Hoyer, T., Lienau, C., Tuszynski,

W., & Parisi, J. (2008). Ligand removal from soluble CdTe nanocrystals evidenced by time-resolved photoluminescence spectroscopy. *Journal of Physics D: Applied Physics*, *41*(10). https://doi.org/10.1088/0022-3727/41/10/102004

183. True, A. L., Rahman, A., & Malik, A. B. (2000). Activation of NF-κB induced by H_2O_2 and TNF-α and its effects on ICAM-1 expression in endothelial cells. *American Journal of Physiology - Lung Cellular and Molecular Physiology*, *279*(2 23-2), 302–311. https://doi.org/10.1152/ajplung.2000.279.2.l302

184. Ung, T. D. T., Tran, T. K. C., Pham, T. N., Nguyen, D. N., Dinh, D. K., & Nguyen, Q. L. (2012). CdTe and CdSe quantum dots: Synthesis, characterizations and applications in agriculture. *Advances in Natural Sciences: Nanoscience and Nanotechnology*, *3*(4). https://doi.org/10.1088/2043-6262/3/4/043001

185. Uriu-Adams, J. Y., & Keen, C. L. (2005). Copper, oxidative stress, and human health. *Molecular Aspects of Medicine*, *26*, 268–298. https://doi.org/10.1016/j.mam.2005.07.001

186. Vale, B. R. C., Mourão, R. S., Bettini, J., Sousa, J. C. L., Ferrari, J. L., Reiss, P., Aldakov, D., & Schiavon, M. A. (2019). Ligand induced switching of the band alignment in aqueous synthesized CdTe/CdS core/shell nanocrystals. *Scientific Reports*, *9*(1), 1–12. https://doi.org/10.1038/s41598-019-44787-y

187. Waggoner, D. J., Bartnikas, T. B., & Gitlin, J. D. (1999). The Role of Copper in Neurodegenerative Disease. *Neurobiology of Disease*, *6*, 221–230. https://doi.org/10.1006/nbdi.1999.0250.

188. Wang, A., Fu, L., Rao, T., Cai, W., Yuen, M.-F., & Zhong, J. (2015). Effect of metal ions on the quenching of photoluminescent CdTe QDs and their recovery. *Optical Materials*, *42*, 548–552. https://doi.org/10.1016/j.optmat.2015.01.010

189. Wang, G. L., Jiao, H. J., Zhu, X. Y., Dong, Y. M., & Li, Z. J. (2012). Enhanced fluorescence sensing of melamine based on thioglycolic acid-capped CdS quantum dots. *Talanta*, *93*, 398–403. https://doi.org/10.1016/j.talanta.2012.02.062

190. Wang, L. G., Pennycook, S. J., & Pantelides, S. T. (2002). The Role of the Nanoscale in Surface Reactions: CO_2 on CdSe. *Physical Review Letters*, *89*(7), 2–5. https://doi.org/10.1103/PhysRevLett.89.075506

191. Wang, S., Mamedova, N., Kotov, N. A., Chen, W., & Studer, J. (2002). Antigen/Antibody Immunocomplex from CdTe Nanoparticle Bioconjugates. *Nano Letters*, *2*(8), 817–822. https://doi.org/10.1021/nl0255193

192. Wang, S. N., Zhu, J., Li, X., Li, J. J., & Zhao, J. W. (2018). Fluorescence turn-on sensing of trace cadmium ions based on EDTA-etched CdTe@CdS quantum dot.

Spectrochimica Acta - Part A: Molecular and Biomolecular Spectroscopy, *201*, 119–127. https://doi.org/10.1016/j.saa.2018.04.065

193. Wang, X. Z., Zhang, Z. Q., Guo, R., Zhang, Y. Y., Zhu, N. J., Wang, K., Sun, P. P., Mao, X. Y., Liu, J. J., Huo, J. Z., Wang, X. R., & Ding, B. (2020). Dual-emission CdTe quantum dot@ZIF-365 ratiometric fluorescent sensor and application for highly sensitive detection of L-histidine and Cu^{2+}. *Talanta*, *217*, 121010. https://doi.org/10.1016/j.talanta.2020.121010

194. Wang, Y. Q., Liu, Y., He, X. W., Li, W. Y., & Zhang, Y. K. (2012). Highly sensitive synchronous fluorescence determination of mercury (II) based on the denatured ovalbumin coated CdTe QDs. *Talanta*, *99*, 69–74. https://doi.org/10.1016/j.talanta.2012.04.064

195. Wang, Yahui, Zhang, C., Chen, X., Yang, B., Yang, L., Jiang, C., & Zhang, Z. (2016). Ratiometric fluorescent paper sensor utilizing hybrid carbon dots-quantum dots for the visual determination of copper ions. *Nanoscale*, *8*(11), 5977–5984. https://doi.org/10.1039/c6nr00430j

196. Wang, Yilin, Lu, J., Tong, Z., & Huang, H. (2009). A fluorescence quenching method for determination of copper ions with CdTe quantum dots. *Journal of the Chilean Chemical Society*, *54*(3), 274–277. https://doi.org/10.4067/S0717-97072009000300015

197. Wang, Ying, Li, L., Dai, P., Yan, L., Cao, L., Gu, X., & Zhao, X. (2017). Missing-node directed synthesis of hierarchical pores on a zirconium metal-organic framework with tunable porosity and enhanced surface acidity via a microdroplet flow reaction. *Journal of Materials Chemistry A*, *5*(42), 22372–22379. https://doi.org/10.1039/c7ta06060b

198. Wang, Y., Si, B., Lu, S., Liu, E., Hu, X., & Fan, J. (2017). Near-infrared excitation of CdTe quantum dots based on fluorescence resonance energy transfer and their use as fluorescent sensors. Sensors and Actuators B: Chemical, 246, 127-135. https://doi.org/10.1016/j.snb.2017.02.069

199. Wang, Yongbo, Yang, M., Ren, Y., & Fan, J. (2019). Ratiometric determination of hydrogen peroxide based on the size-dependent green and red fluorescence of CdTe quantum dots capped with 3-mercaptopropionic acid. *Microchimica Acta*, *186*(5). https://doi.org/10.1007/s00604-019-3390-0

200. Weidman, M. C., Nguyen, Q., Smilgies, D. M., & Tisdale, W. A. (2018). Impact of Size Dispersity, Ligand Coverage, and Ligand Length on the Structure of PbS Nanocrystal Superlattices. *Chemistry of Materials*, *30*(3), 807–816. https://doi.org/10.1021/acs.chemmater.7b04322

201. Wen, G., Wen, X., Choi, M. M. F., & Shuang, S. (2015). Photoelectrochemical

sensor for detecting Hg^{2+} based on exciton trapping. *Sensors and Actuators, B: Chemical*, *221*, 1449–1454. https://doi.org/10.1016/j.snb.2015.07.103

202. Wolfbeis, O. S. (2005). Materials for fluorescence-based optical chemical sensors. *Journal of Materials Chemistry*, *15*(27–28), 2657. https://doi.org/10.1039/b501536g

203. Wood, V., Panzer, M. J., Chen, J., Bradley, M. S., Halpert, J. E., Bawendi, M. C., & Bulović, V. (2009). Inkjet-printed quantum dot-polymer composites for full-color AC-driven displays. *Advanced Materials*, *21*(21), 2151–2155. https://doi.org/10.1002/adma.200803256

204. Wu, P., Cai, Z., Gao, Y., Zhang, H., & Cai, C. (2011). Enhancing the electrochemical reduction of hydrogen peroxide based on nitrogen-doped graphene for measurement of its releasing process from living cells. *Chemical Communications*, *47*(40), 11327–11329. https://doi.org/10.1039/c1cc14419g

205. Xi, L. L., Ma, H. B., & Tao, G. H. (2016). Thiourea functionalized CdSe/CdS quantum dots as a fluorescent sensor for mercury ion detection. *Chinese Chemical Letters*, *27*(9), 1531–1536. https://doi.org/10.1016/j.cclet.2016.03.002

206. Xia, C., Wu, W., Yu, T., Xie, X., Van Oversteeg, C., Gerritsen, H. C., & De Mello Donega, C. (2018). Size-dependent band-gap and molar absorption coefficients of colloidal $CuInS_2$ quantum dots. *ACS Nano*, *12*(8), 8350–8361. https://doi.org/10.1021/acsnano.8b03641

207. Xia, N., Zhou, B., Huang, N., Jiang, M., Zhang, J., & Liu, L. (2016). Visual and fluorescent assays for selective detection of beta-amyloid oligomers based on the inner filter effect of gold nanoparticles on the fluorescence of CdTe quantum dots. Biosensors and Bioelectronics, 85, 625-632. https://doi.org/10.1016/j.bios.2016.05.066

208. Xia, Y. S., & Zhu, C. Q. (2009). Interaction of CdTe nanocrystals with thiol-containing amino acids at different pH: A fluorimetric study. *Microchimica Acta*, *164*(1–2), 29–34. https://doi.org/10.1007/s00604-008-0025-2

209. Xia, Yun-sheng, & Zhu, C. (2008). Use of surface-modified CdTe quantum dots as fluorescent probes in sensing mercury (II). *Talanta*, *75*, 215–221. https://doi.org/10.1016/j.talanta.2007.11.008

210. Xia, Yunsheng, & Zhu, C. (2008). Aqueous synthesis of type-II core/shell CdTe/CdSe quantum dots for near-infrared fluorescent sensing of copper(II). *Analyst*, *133*(7), 928–932. https://doi.org/10.1039/b801963k

211. Xin, S. H., Wang, P. D., Yin, A., Kim, C., Dobrowolska, M., Merz, J. L., & Furdyna, J. K. (1996). Formation of self-assembling CdSe quantum dots on ZnSe

by molecular beam epitaxy. *Applied Physics Letters*, *69*(25), 3884–3886. https://doi.org/10.1063/1.117558

212. Yan, S., Xu, X., Jiang, C., Pan, L., Shi, Y., Hu, D., & Cao, Z. (2016). Easy Preparation and Photoelectrochemical Properties of CdS Nanoparticle/Graphene Nanosheet Nanocomposites Using Supercritical Carbon Dioxide. *Journal of Nanoscience and Nanotechnology*, *16*(3), 2742–2751. https://doi.org/10.1166/jnn.2016.10838

213. Yang, F., Ma, Q., Yu, W., & Su, X. (2011). Naked-eye colorimetric analysis of $Hg^{2+}$with bi-color CdTe quantum dots multilayer films. *Talanta*, *84*(2), 411–415. https://doi.org/10.1016/j.talanta.2011.01.054

214. Yang, G., Yang, B., Xiao, T., & Yan, Z. (2013). Applied Surface Science One-step solvothermal synthesis of hierarchically porous nanostructured CdS / TiO_2 heterojunction with higher visible light photocatalytic activity. *Applied Surface Science*, *283*, 402–410. https://doi.org/10.1016/j.apsusc.2013.06.122

215. Yang, S., Guo, W., & Sun, X. (2018). Electrostatic association complex of a polymer capped CdTe(S) quantum dot and a small molecule dye as a robust ratiometric fluorescence probe of copper ions. *Dyes and Pigments*, *158*(May), 114–120. https://doi.org/10.1016/j.dyepig.2018.05.031

216. Yang, T., He, Q., Liu, Y., Zhu, C., & Zhao, D. (2013). Water-Soluble N-Acetyl-L-cysteine-Capped CdTe Quantum Dots Application for Hg(II) Detection. *J Anal Methods Chem*, *2013*, 902951. https://doi.org/10.1155/2013/902951

217. Yao, J., Yang, M., & Duan, Y. (2014). Highly fluorescent CdTe nanocrystals: Synthesis, characterization, property, mechanism, and application as a sensor for biomolecule analysis. *Journal of Materials Research*, *29*(05), 633–640. https://doi.org/10.1557/jmr.2014.25

218. Yogamalar, N. R., Sadhanandam, K., Bose, A. C., & Jayavel, R. (2015). Quantum confined CdS inclusion in graphene oxide for improved electrical conductivity and facile charge transfer in hetero-junction solar cell. *RSC Advances*, *5*(22), 16856–16869. https://doi.org/10.1039/C4RA13061H

219. Yuan, J., Guo, W., & Wang, E. (2008). Utilizing a CdTe quantum dots-enzyme hybrid system for the determination of both phenolic compounds and hydrogen peroxide. *Analytical Chemistry*, *80*(4), 1141–1145. https://doi.org/10.1021/ac0713048

220. Yun, G. 2011 C., & Yingqiu and Dorn, L. (2010). Voltammetric Detection of Hydrogen Peroxide at Carbon Fiber Microelectrodes. *Anal. Chem.*, *82*(12), 1–7. https://doi.org/10.1021/ac100536s

221. Zeng, C., Ramos-ruiz, A., Field, J. A., & Sierra-alvarez, R. (2015). Cadmium telluride (CdTe) and cadmium selenide (CdSe) leaching behavior and surface chemistry in response to pH and O_2. *Journal of Environmental Management*, *154*, 78–85. https://doi.org/10.1016/j.jenvman.2015.02.033

222. Zhang, B., Liu, H., Wu, F., Hao, G., Chen, Y., Tan, C., Tan, Y., & Jiang, Y. (2017). A dual-response quinoline-based fluorescent sensor for the detection of Copper (II) and Iron (III) ions in aqueous medium. *Sensors & Actuators: B. Chemical*, *243*, 765–774. https://doi.org/10.1016/j.snb.2016.12.067

223. Zhang, H., Zhou, Z., Yang, B., & Gao, M. (2003). The influence of carboxyl groups on the photoluminescence of mercaptocarboxylic acid-stabilized CdTe nanoparticles. *Journal of Physical Chemistry B*, *107*(1), 8–13. https://doi.org/10.1021/jp025910c

224. Zhang, X., Liu, Z., Ma, L., Hossu, M., & Chen, W. (2011). Interaction of porphyrins with CdTe quantum dots. *Nanotechnology*, *22*(19), 195501. https://doi.org/10.1088/0957-4484/22/19/195501

225. Zhang, Yanjie, & Clapp, A. (2011). Overview of stabilizing ligands for biocompatible quantum dot nanocrystals. *Sensors*, *11*(12), 11036–11055. https://doi.org/10.3390/s111211036

226. Zhang, Yi, Liu, K. J., Wang, T. L., Shih, I. M., & Wang, T. H. (2012). Mapping DNA quantity into electrophoretic mobility through quantum dot nanotethers for high-resolution genetic and epigenetic analysis. *ACS Nano*, *6*(1), 858–864. https://doi.org/10.1021/nn204377k

227. Zhao, J. F., Liu, Y., Soh, J. B., Li, Y. X., Ganguly, R., Ye, K. Q., Huo, F., Huang, L., Tok, A. I. Y., Loo, J. S. C., & Zhang, Q. (2012). One stone kills four birds: A novel diazaperinone 12H-pyrazino[2′, 3′:3,4]pyrrolo[1,2-a]perimidin-12-one recognizes four different metal ions. *Tetrahedron Letters*, *53*(45), 6044–6047. https://doi.org/10.1016/j.tetlet.2012.08.106

228. Zhao, Jialong, Bardecker, J. A., Munro, A. M., Liu, M. S., Niu, Y., Ding, I. K., Luo, J., Chen, B., Jen, A. K. Y., & Ginger, D. S. (2006). Efficient CdSe/CdS quantum dot light-emitting diodes using a thermally polymerized hole transport layer. *Nano Letters*, *6*(3), 463–467. https://doi.org/10.1021/nl052417e

229. Zhao, Jingjin, Wu, H., Jiang, J., & Zhao, S. (2014). Label-free fluorescence turn-on sensing for melamine based on fluorescence resonance energy transfer between CdTe/CdS quantum dots and gold nanoparticles. *RSC Advances*, *4*(106), 61667–61672. https://doi.org/10.1039/c4ra08776c

230. Zhao, L., Jia, J., Yang, Z., Yu, J., Wang, A., Sang, Y., Zhou, W., & Liu, H. (2017). One-step synthesis of CdS nanoparticles/MoS_2 nanosheets heterostructure on

porous molybdenum sheet for enhanced photocatalytic H_2 evolution. *Applied Catalysis B: Environmental*, *210*, 290–296. https://doi.org/10.1016/j.apcatb.2017.04.003

231. Zhao, Q., Rong, X., Ma, H., & Tao, G. (2013). Dithizone functionalized CdSe / CdS quantum dots as turn-on fluorescent probe for ultrasensitive detection of lead ion. *Journal of Hazardous Materials*, *250–251*, 45–52. https://doi.org/10.1016/j.jhazmat.2013.01.062

232. Zheng, Y., Tang, H., Wang, X., Di, Y., Lu, K., & Wang, J. (2017). Facile Synthesis and Properties of Aqueous CdTe Quantum Dots for High-Sensitive Copper (II) Ion Detection. *Nano*, *12*(12), 1750151. https://doi.org/10.1142/S179329201750151X

233. Zhou, D., Lin, M., Chen, Z., Sun, H., Zhang, H., Sun, H., & Yang, B. (2011). Simple synthesis of highly luminescent water-soluble CdTe quantum dots with controllable surface functionality. *Chemistry of Materials*, *23*(21), 4857–4862. https://doi.org/10.1021/cm202368w

234. Zhou, J., Zou, X., Song, S., & Chen, G. (2018). Quantum Dots Applied to Methodology on Detection of Pesticide and Veterinary Drug Residues. *J. Agric. Food Chem.*, *66*, 1307–1319. https://doi.org/10.1021/acs.jafc.7b05119

235. Zhu, Jian, Zhao, Z. J., Li, J. J., & Zhao, J. W. (2017). CdTe quantum dot-based fluorescent probes for selective detection of Hg (II): The effect of particle size. *Spectrochimica Acta - Part A: Molecular and Biomolecular Spectroscopy*, *177*, 140–146. https://doi.org/10.1016/j.saa.2017.01.043

236. Zhu, Junjie, Koltypin, Y., & Gedanken, A. (2000). General sonochemical method for the preparation of nanophasic selenides: Synthesis of ZnSe nanoparticles. *Chemistry of Materials*, *12*(1), 73–78. https://doi.org/10.1021/cm990380r

237. Zou, L., Gu, Z., & Sun, M. (2015). Review of the application of quantum dots in the heavy-metal detection. *Toxicological & Environmental Chemistry*, *97*(3–4), 477–490. https://doi.org/10.1080/02772248.2015.1050201

238. Zu, F., Yan, F., Bai, Z., Xu, J., Wang, Y., Huang, Y., & Zhou, X. (2017). The quenching of the fluorescence of carbon dots : A review on mechanisms and applications. *Microchimica Acta*, *184*, 1899–1914. https://doi.org/10.1007/s00604-017-2318-9

LIST OF PUBLICATIONS

Peer Reviewed Journals

1. "Branched mercapto acid capped CdTe quantum dots as fluorescence probes for Hg^{2+} detection" Yogesh S Choudhary, N Gomathi; *Sensing and Bio-Sensing Research*, 2019, 23, 100278, doi: 10.1016/j.sbsr.2019.100278.
2. "Branched Ligand Ethyl 2-Mercaptopropionate as a Stabilizer for CdTe Quantum Dots and its use as a Cu^{2+} Ions Probe in Aqueous Medium" Yogesh S Choudhary, N Gomathi; *ChemistrySelect*, 2020, 5 (1), 32-39, doi: 10.1002/slct.201903767.
3. "Synthesis and Characterization of CdTe QDs Capped with Branched 3MB3MP Ligand and Fluorescent Switching Detection of H_2O_2" Yogesh S Choudhary, N Gomathi; *New Journal of Chemistry*, 2022, doi: 10.1039/D1NJ05756A.

Book Chapters

1. Yogesh S. Choudhary, Lavanya Jothi and Gomathi Nageswaran. (2017). Electrochemical Characterization. In Sabu Thomas, Raju Thomas, Ajesh K. Zachariah, Raghvendra Kumar Mishra (Ed.), Spectroscopic Methods for Nanomaterials Characterization (pp. 19-51). Elsevier.

CONFERENCES ATTENDED

1. National Conference on Recent Trends in Materials Science and Technology- NCMST, Thiruvananthapuram, Kerala; December 2020 (Poster presentation).
2. International Conference on Functional Materials- ICFM 2020- IIT Kharagpur, West Bengal; January 2020 (Poster Presentation).
3. National Conference on Recent Trends in Material Science & Technology- NCMST, Thiruvananthapuram, Kerala; December 2019 (Oral Presentation).
4. Solid and Liquid State Fluorescent Sensor Using CdTe Quantum Dots for Mercury Detection, (abstract accepted in International Conference "233rd ECS meeting at Seattle, US, 13th-17th May 2018).